2019

Studies On Fractionalization And Topology In Strongly Correlated Systems From Zero To Two Dimensions

Yichen Hu
University of Pennsylvania, huyichen@gmail.com

Studies On Fractionalization And Topology In Strongly Correlated Systems From Zero To Two Dimensions

Abstract
The interplay among symmetry, topology and condensed matter systems has deepened our understandings of matter and lead to tremendous recent progresses in finding new topological phases of matter such as topological insulators, superconductors and semi-metals. Most examples of the aforementioned topological materials are free fermion systems, in this thesis, however, we focus on their strongly correlated counterparts where electron-electron interactions play a major role. With interactions, exotic topological phases and quantum critical points with fractionalized quantum degrees of freedom emerge. In the first part of this thesis, we study the problem of resonant tunneling through a quantum dot in a spinful Luttinger liquid. It provides the simplest example of a (0+1)d system with symmetry-protected phase transitions. We show that the problem is equivalent to a two channel SU(3) Kondo problem and can be mapped to a quantum Brownian motion model on a Kagome lattice. Utilizing boundary conformal field theory, we find the universal peak conductance and compute the scaling behavior of the resonance line-shape.

For the second part, we present a model of interacting Majorana fermions that describes a superconducting phase with a topological order characterized by the Fibonacci topological field theory. Our theory is based on a SO(7)1=SO(7)1/(G2)1 x (G2)1 coset construction and implemented by a solvable two-dimensional network model. In addition, we predict a closely related "anti-Fibonacci" phase, whose topological order is characterized by the tricritical Ising model. Finally, we propose an interferometer that generalizes the Z2 Majorana interferometer and directly probes the Fibonacci non-Abelian statistics.

For the third part, we argue that a correlated fluid of electrons and holes can exhibit fractional quantum Hall effects at zero magnetic field. We first show that a Chern insulator can be realized as a free fermion model with p-wave(m=1) excitonic pairing. Its ground state wavefunction is then worked out and generalized to m>1. We give several pieces of evidence that this conjectured wavefunction correctly describes a topological phase, dubbed "fractional excitonic insulator", within the same universality class as the corresponding Laughlin state at filling 1/m. We present physical arguments that gapless states with higher angular momentum pairing between energy bands are conducive to forming the fractional excitonic insulator in the presence of repulsive interactions. Without interactions, these gapless states appear at topological phase transitions which separate the trivial insulator from a Chern insulator with higher Chern number. Since the nonvanishing density of states at these higher angular momentum band inversion transitions can give rise to interesting many-body effects, we introduce a series of minimal lattice models realizations in two dimensions. We also study the effect of rotational symmetry broken electron-hole exciton condensation in our lattice models using mean field theory.

Degree Type
Dissertation

Degree Name
Doctor of Philosophy (PhD)

STUDIES ON FRACTIONALIZATION AND TOPOLOGY IN STRONGLY CORRELATED SYSTEMS FROM ZERO TO TWO DIMENSIONS

Yichen Hu

A DISSERTATION

in

Physics and Astronomy

Presented to the Faculties of the University of Pennsylvania in Partial Fulfillment of the Requirements for the Degree of Doctor of Philosophy

2019

Supervisor of Dissertation

_____

Charles L. Kane, Christopher H. Browne Distinguished Professor of Physics

Graduate Group Chairperson

_____

Joshua R. Klein, Edmund J. and Louise W. Kahn Professor

Dissertation Committee:
Randall D. Kamien, Vicki and William Abrams Professor in the Natural Science
Eugene J. Mele, Christopher H. Browne Distinguished Professor of Physics
Jonathan J. Heckman, Assistant Professor of Physics
Bo Zhen, Assistant Professor of Physics

STUDIES ON FRACTIONALIZATION AND TOPOLOGY IN STRONGLY CORRELATED SYSTEMS FROM ZERO TO TWO DIMENSIONS

Acknowledgments

Number is the law of the universe.

Pythagoras

This is a thesis dedicated to integer numbers and their fractionalizations in condensed matter physics.

I would like to begin by thanking my advisor Professor Charles Kane for his support and education during my six years at Penn. My happiest episodes in grad school are the countless afternoon discussions with Charlie about physics. No matter how busy he was, he would nevertheless patiently sat down to chat and share his passion for physics. His good taste in picking the right questions to ask and out-of-the-box ideas to attack them have greatly shaped the way I would approach physics problems.

I would like to thank Professor Randall Kamien, Eugene Mele, Jonathan Heckman and Bo Zhen for providing helping hands whenever I needed them. I have learned a lot from them outside my own research topics.

I am also fortunate to have made many friends along this journey. Representing

the frozen world of Midwest, Yuxuan Wang, Xiaoyu Wang, Jian Kang, Mengxing Ye, Xuzhe Ying, Chun Chen, Yuxiao Wu, Laimei Nie and Fnu Setiawan have all shown me the value of sincerity in doing good research. Friends I met at various workshops, Biao Lian, Juven Wang, Tianci Zhou, Xiao Chen and Shenghan Jiang, I enjoyed many intense discussions with them. Let me not forget my local pals who have always been friendly and supportive, Fan Zhang, Benjamin Wieder, Jörn Venderbos, Tatyana Gavrilchenko, Eric Horsley, Zachariah Addison, Andrew Li, Arjun Kar, Matthew Decross, Pok Man Tam, Jing Cai.

Most importantly, I would not have survived this tough PhD training without my family. My life trajectory could be completely altered without understandings from my parents, encouragements from my grandma and love from my wife. Although my mind is pondering mysteries of physics, my heart is always with you guys.

ABSTRACT

STUDIES ON FRACTIONALIZATION AND TOPOLOGY IN STRONGLY CORRELATED SYSTEMS FROM ZERO TO TWO DIMENSIONS

Yichen Hu

Charles L. Kane

The interplay among symmetry, topology and condensed matter systems has deepened our understandings of matter and lead to tremendous recent progresses in finding new topological phases of matter such as topological insulators, superconductors and semi-metals. Most examples of the aforementioned topological materials are free fermion systems, in this thesis, however, we focus on their strongly correlated counterparts where electron-electron interactions play a major role. With interactions, exotic topological phases and quantum critical points with fractionalized quantum degrees of freedom emerge. In the first part of this thesis, we study the problem of resonant tunneling through a quantum dot in a spinful Luttinger liquid. It provides the simplest example of a (0+1)d system with symmetry-protected phase transitions. We show that the problem is equivalent to a two channel $SU(3)$ Kondo problem and can be mapped to a quantum Brownian motion model on a Kagome lattice. Utilizing boundary conformal field theory, we find the universal peak conductance and compute the scaling behavior of the resonance line-shape.

For the second part, we present a model of interacting Majorana fermions that describes a superconducting phase with a topological order characterized by the Fi-

bonacci topological field theory. Our theory is based on a $SO(7)_1 = SO(7)_1/(G_2)_1 \times (G_2)_1$ coset construction and implemented by a solvable two-dimensional network model. In addition, we predict a closely related "anti-Fibonacci" phase, whose topological order is characterized by the tricritical Ising model. Finally, we propose an interferometer that generalizes the Z_2 Majorana interferometer and directly probes the Fibonacci non-Abelian statistics.

For the third part, we argue that a correlated fluid of electrons and holes can exhibit fractional quantum Hall effects at zero magnetic field. We first show that a Chern insulator can be realized as a free fermion model with p-wave($m = 1$) excitonic pairing. Its ground state wavefunction is then worked out and generalized to $m > 1$. We give several pieces of evidence that this conjectured wavefunction correctly describes a topological phase, dubbed "fractional excitonic insulator", within the same universality class as the corresponding Laughlin state at filling $1/m$. We present physical arguments that gapless states with higher angular momentum pairing between energy bands are conducive to forming the fractional excitonic insulator in the presence of repulsive interactions. Without interactions, these gapless states appear at topological phase transitions which separate the trivial insulator from a Chern insulator with higher Chern number. Since the nonvanishing density of states at these higher angular momentum band inversion transitions can give rise to interesting many-body effects, we introduce a series of minimal lattice models realizations in two dimensions. We also study the effect of rotational symmetry

broken electron-hole exciton condensation in our lattice models using mean field theory.

Contents

List of Tables

List of Figures

Chapter 1

Introduction

How does matter arrange itself? That is the ultimate puzzle that every condensed matter physicist would love to solve. Historically, symmetry has always been a fundamental principle underlying different phases of matter. One early success is Landau's approach where spontaneous symmetry breaking dictates phase transitions[1]. Then the discovery of integer quantum Hall effects[2] adds another layer - topology. Two distinct phases could possess the same symmetry, but there are robust physical quantities insensitive to smooth changes in material parameters that can tell them apart. Recent advancements in topological phases of matter, such as predictions and subsequently experimental realizations of topological materials[3, 4], are marvelous examples of the interplay of symmetry and topological in condensed matter physics. These topological materials can be modeled by free fermion band theory and are thus exactly solvable. On the other hand, many equally interest-

ing strongly correlated systems, such as fractional quantum Hall states[5], heavy fermion systems[6], and high T_c superconductors[7] where electron-electron interactions can not be ignored, fall out of the realm of band theory. Interactions are notoriously hard to analyze and traditionally treated with mean field approaches or diagrammatic perturbation theory, such as the BCS theory of superconductivity[8] and Landau's Fermi liquid theory[9, 10]. Our understandings of the role interactions played in many condensed matter systems are still far from complete. In this thesis, we take a stab at the question how interactions could bring novel phenomena to matter. We show that interactions can drive systems into exotic fixed points and can open up gaps which leads to highly non-trivial topological ordered phases.

This introduction is organized as follows. In 1.1, basic concepts of mesoscopic physics and Luttinger liquid are reviewed which is related to discussions in Chapter 2. In 1.2, we give a concise introduction to Majorana fermions in condensed matter systems which are the fundamental building blocks in Chapter 3. In 1.3, we study quantum Hall effects in crystal - Chern insulators. This serves as a warm-up for studies in Chapter 4 and 5.

1.1 Mesoscopic Quantum Wires and Luttinger Liquid

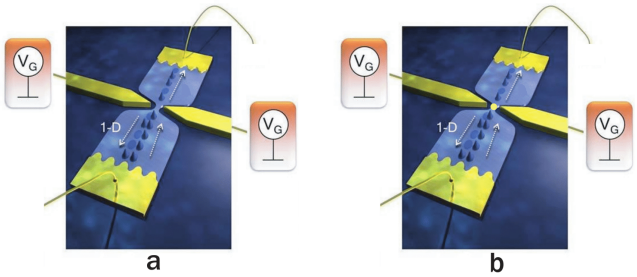

Figure 1.1: a) Quantum point contact[16]. b) Quantum dot.

Mesoscopic physics, roughly speaking, governs structures from nano- to micrometer scales. At low temperature, quantum effects of individual electrons and their correlations become important in mesoscopic systems. Decades of studies have revealed novel physical phenomena and important applications, examples include Coulomb blockade[11, 12], electron teleportation[13] and the fluxonium qubit[14], *etc.* One major triumph of mesoscopic physics is in studies of low dimensional electron transport. With negative voltage gates deposited on top and bottom of a 2D electron gas forming a constriction with width comparable to electronic wavelength(Fig. 1.1a), a quantum point contact is designed to deplete and confine electron so that only a few transverse electron modes can be transmitted through. Conductance from these modes or "channels" are therefore quantized in units of e^2/h and controlled by gate voltage. Additionally, an island can be put in between gates such that we can define single electron energy levels(Fig. 1.1b). If this

quantum dot is weakly coupled to two single-channel leads with non-interacting electrons, when we tune the chemical potential of the dot to be the same of as one of the electron energy levels, electron tunneling is on-resonance and conductance takes the maximum quantized value of e^2/h. On the other hand, electron tunneling off-resonance leads to suppressed temperature dependent conductance. The full theory of electron transport in mesoscopic devices is Landauer-Büttiker formalism which we refer readers to [15] for comprehensive studies.

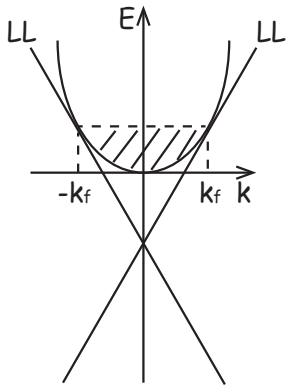

Figure 1.2: Luttinger liquid describes the low energy physics of a 1D electron gas linearized around Fermi points $\pm k_f$.

More interesting scenarios arise with 1D interacting quantum wires modeled by Luttinger liquids[17, 18]. A Luttinger liquid is a low energy model of 1D electron gas linearzied near Fermi energies(Fig. 1.2). Interaction strength between electrons is usually denoted by a parameter g, with $g < 1 (> 1)$ characterizing repulsive(attractive) interactions. Classical works by Kane and Fisher[19, 20] have carefully examed the drastic effect of electron interactions on resonant electron tunnelings. On contrary to non-interacting electrons, with repulsive interactions,

there is no conductance at zero temperature even with only a weak barrier on the quantum dot. With attractive interactions, conductance is ge^2/h and not affected by the barrier no matter how large it is. Spatial dimension being one for Luttinger liquid models also comes handy for solving interaction problems. Two major advantages here is the spin-charge separation and bosonization. Since spin and charge modes in a Luttinger liquid can propagate with different velocities, they are decoupled degrees of freedom each with their own conductance and behave independently under backscattering. As for the method of bosonization, since the low energy excitations of a Luttinger liquid involve particle and hole excitations across the Fermi points $\pm k_f$, they can be mapped exactly to phonon displacement fields in 1D. The bosonized Hamiltonian of the original interacting fermion model will then be quadratic in this displacement boson field and thus exactly solvable.

1.2 Majorana Fermions in Condensed Matter Systems

Soon after Paul Dirac proposed the Dirac equation, Ettore Majorana found his famous solution[21]. Fermions obtained from this solution are real, charge neutral and act as their own anti-particles. Their peculiar physical properties has long puzzled physicists as where to find them. In particle physics, people have tried to associate Majorana fermions with neutrinos since both are quite uninteractive

with the environment. However, recent discovery of neutrino oscillations[22, 23] casts doubts on this view and current efforts of identifying Majorana fermions as fundamental particles remain elusive. However, Majorana fermions turned a corner and emerged in condensed matter systems, and this time as a quasiparticle.

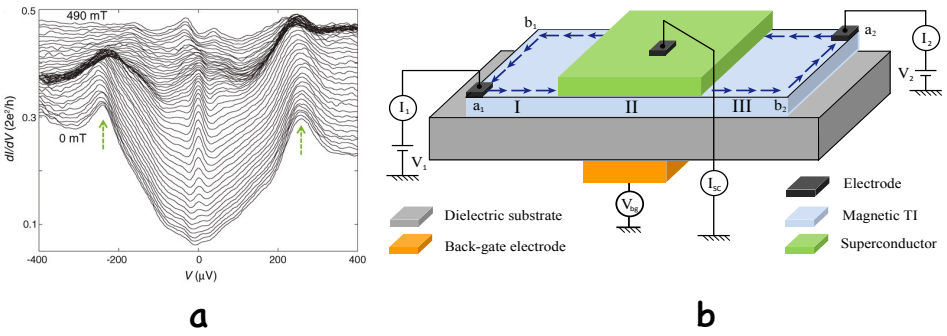

Figure 1.3: a) Magnetic field-dependent spectroscopy(dI/dV vs. V). Data are for different B field from 0 to 490mT in 10mT steps. Arrows indicate the induced gap peaks. b) Quantum anomalous hall insulator - superconductor heterostructure for chiral Majorana modes.

In a superconductor, a single-particle excitation is a coherent superposition of an electron and a hole - a Bogoliubov quasiparticle. The particle-hole symmetry relates a Bogoliubov quasiparticle γ at energy E to its anti-particle $\gamma^\dagger$ at energy $-E$. Therefore, the Majorana condition is automatically satisfied at $E = 0$ and gives rise to Majorana zero modes. There are an abundance of condensed matter systems that are theoretically proposed to host these Majorana bound states. Just to name a few, the surface excitations of B phase of Helium-3[24, 25], quasiparticles in a $\nu = 5/2$ fractional quantum hall state[26, 27], vortex excitations of a p-wave superconductor[27, 29, 30] and defects in a proximity effect induced topological superconductor[28]. Recent experimental progresses in the Majorana fermion hunt,

especially those based on topological material and superconductor heterostructures, have shown great promises. In one dimension, Yazdani's group have found evidences of the existence of Majorana zero modes based on zero-bias conductance peak signals from a ferromagnetic chain proximatized to superconductivity[31, 32](Fig. 1.3a). In two dimension, an experimental setup shown in Fig. 1.3b based on a quantum anomalous Hall insulator and superconductor heterostructure claim to have realized chiral Majorana fermion modes[33]. A more direct probe of Majorana zero modes, especially for chiral Majorana edge modes, is to measure their thermal Hall conductance. This is recently achieved by a beautiful experiment by Heiblum[34] and revives debates surrounding an old mystery of particle-hole symmetry in half-filled Landau levels which is out of the scope of this thesis.

1.3 Quantum Hall Effects in Crystal - Chern Insulator

The discovery of quantum Hall effects[2, 5] fundamentally changed the paradigm of phases of matter. The old symmetry breaking picture fails because there is no local order parameter distinguishing different quantum Hall phases. Instead, robust topological invariants characterizing physical quantities unchanged under smooth deformation can be found and serve as labels for different topological phases. Moreover, the topology is really a ground state feature. As long as the bulk gap is kept

open, matter remains in the same phase. Experimental realizations of quantum Hall effects using 2D electron gas and a perpendicular magnetic field typically require rather large fields and low temperature and are thus hard to construct in ordinary materials. Nevertheless, as first shown by Haldane[35], the same quantum Hall effects with quantized Hall conductance σ_{xy} can be implemented in lattice models and even in a way that has net zero magnetic field. Along this direction, as long as the band gap is large, quantum Hall effects are easier to be observed in realistic materials adequately described by such lattice models. This is indeed the case where we see Chern insulators successfully realized using magnetic topological insulators[36] and in engineered cold-atom systems[37–39]. In the following, we review the Haldane model for Chern insulator.

A generic non-interacting lattice system assume the following form:

$$H = \sum_{ij,\mathbf{GG'}} t^{ij}_{\mathbf{GG'}} \psi^{\dagger i}_{\mathbf{G}} \psi^{j}_{\mathbf{G'}}, \tag{1.3.1}$$

where **G** and **G'** are lattice vectors and $\psi^{\dagger i}_{\mathbf{G}}$ creates an electron with index i at site specified by lattice vector **G**. $t^{ij}_{\mathbf{GG'}}$, records the hopping amplitude and on-site energy. With translational symmetry and periodic boundary conditions, we can Fourier transform each electron operator to k-space.

$$\psi^{\dagger}_{\mathbf{k}} = \frac{1}{\sqrt{N}} \sum_{\mathbf{G}} \psi^{\dagger i}_{\mathbf{G}} e^{-i\mathbf{k}\cdot\mathbf{G}} \tag{1.3.2}$$

where N is the number of lattice sites and k is momentum in the Brillouin zone.

This transforms the Hamiltonian into

$$H = \sum_{ij,\mathbf{k}} h^{ij}(\mathbf{k}) \psi^{\dagger i}_{\mathbf{k}} \psi^{j}_{\mathbf{k}} \tag{1.3.3}$$

and diagonliazation of the Hamiltonian gives

$$H = \sum_{ij,\mathbf{k}} E^{\alpha}(\mathbf{k}) \psi^{\dagger \alpha}_{\mathbf{k}} \psi^{\alpha}_{\mathbf{k}} \tag{1.3.4}$$

where $\psi^{\dagger\alpha}_{\mathbf{k}} = \sum_i U^{\alpha}_{\mathbf{k}i} c^{\dagger i}_{\mathbf{k}}$ and U denotes a unitary transformation. The electron wavefunctions are then given by $\psi^{\dagger\alpha}_{\mathbf{k}}(\mathbf{r}) = \langle \mathbf{r} | \, \psi^{\dagger\alpha}_{\mathbf{k}} \, |0\rangle$. Using Bloch's theorem, these wavefunctions can be written as $\psi^{\alpha}_{\mathbf{k}}(\mathbf{r}) = e^{i\mathbf{k}\cdot\mathbf{r}} u^{\alpha}_{\mathbf{k}}(\mathbf{r})$.

As for each state or band indexed by α on a lattice site we are associated with a wavefunction $u^{\alpha}_{\mathbf{k}}(\mathbf{r})$(a $U(1)$ bundle), this allows us to calculate its Berry connection $\mathcal{A}^{\alpha} = -i \langle u^{\alpha}_{\mathbf{k}} | \, \nabla_{\mathbf{k}} \, | u^{\alpha}_{\mathbf{k}} \rangle$. This is a gauge field in the momentum space, and thus we can further define the Berry curvature $\mathcal{F}^{\alpha} = \nabla_{\mathbf{k}} \times \mathcal{A}^{\alpha}$. Integrating the Berry curvature over the whole Brillouin zone $\frac{1}{2\pi} \int_{BZ} d^2\mathbf{k} \mathcal{F}^{\alpha}$ gives the total flux in momentum space which also equals the Chern number of the α band. Physically, the Chern number C is the amount of quantized conductance e^2/h such that $\sigma_{xy} = C\frac{e^2}{h}$. It is this insight that both non-trivial bands with Chern number and Landau levels can produce the characteristic quantized Hall conductance leads Haldane to his famous model.

Starting with a 2D honeycomb lattice model with two sites per unit cell, ignoring electron spin, we have a two band tight-binding model. The near-neighbor hopping Hamiltonian reads:

$$H(\mathbf{k}) = \vec{h}(\mathbf{k}) \cdot \vec{\sigma}, \tag{1.3.5}$$

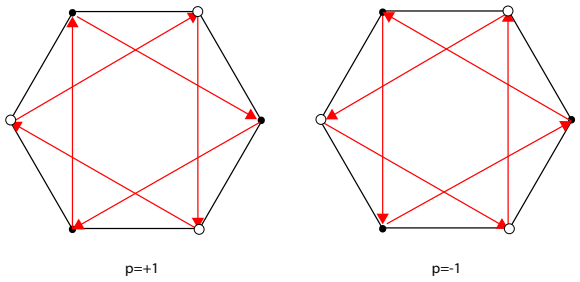

Figure 1.4: Second neighbor hopping terms have complex hopping matrix elements and break time-reversal symmetry. The sign p depend on whether the second neighbor hopping is turning to the left or right.

where

$$h(\mathbf{k}) = (-t\sum_{i=1}^{3}\cos\mathbf{k}\cdot\mathbf{a}_i, -t\sum_{i=1}^{3}\sin\mathbf{k}\cdot\mathbf{a}_i, 0)$$

and $a_1 = (0, a), a_2 = (\frac{\sqrt{3}}{2}a, \frac{1}{2}a), a_3 = (-\frac{\sqrt{3}}{2}a, \frac{1}{2}a)$ are three nearest-neighbor hopping vectors and $\vec{\sigma} = (\sigma_x, \sigma_y, \sigma_z)$ is a vector of Pauli matrices. It is known that near $K, K' = \pm(\frac{4\pi}{3\sqrt{3}a}, 0)$ points of the Brillouin zone, $H(\mathbf{k})$ reduces to massless Dirac equations in 2D. The trick of getting into gapped Chern insulator phase is to come up with mass terms that could open up these Dirac cones protected by inversion and time-reversal symmetry. Imaging adding an imaginary second neighbor hopping term with a sign depending on whether electrons hop to the left or right(Fig. 1.4). Explicitly,

$$h_z(\mathbf{k}) = m\sum_{i<j=1}^{3} p_{ij}\sin(\mathbf{a}_i - \mathbf{a}_j)$$

where the sign convention is $p_{ij} = \pm 1$ when $j = i \pm 1 \mod 3$. For $m > 0$, masses at K and K' points have opposite sign which means $\vec{h}(\mathbf{k})$ winds one time when tracing out the whole Brillouin zone. This is the desired Chern number and gives rise to a quantized Hall conductance $\sigma_{xy} = e^2/h$.

Chapter 2

Universal Symmetry-Protected Resonances in a Spinful Luttinger Liquid

3+2=5

2.1 Introduction

Quantum impurity problems are ubiquitous in condensed matter physics. They are among the simplest problems that exhibit interesting many-body effects. The prototypical model of a quantum impurity problem involves critical bulk degrees of freedom interacting with a quantum mechanical degree of freedom localized on

the boundary. The archetypal example is the Kondo problem[49], along with its multichannel variants[50]. The same Kondo physics is also found in many closely related problems, such as resonant tunneling in non-Abelian quantum Hall states coupled to a quantum dot[51–54], fractional quantum Hall/normal-metal junctions in the strongly coupling regime[55] and resonant tunneling through a weak link in an interacting one dimensional electron gas - or a Luttinger liquid [19, 20, 56–58].

In this chapter, we focus on the resonant tunneling problem in a spinful Luttinger liquid. The resonant tunneling problem in a Luttinger liquid was studied extensively in the 1990's[19, 20, 58]. For spinless electrons, it was found that with repulsive interactions (described by a Luttinger parameter g with $g < 1$) an arbitrarily weak barrier leads to an insulating behavior in the limit of zero temperature. However, for $1/4 < g < 1$ it is possible, by tuning two parameters, to achieve a resonance with perfect conductance at zero temperature. At small but finite temperature, the line shape of the resonance is described by a universal crossover scaling function that connects two renormalization group fixed points: the perfectly transmitting (small barrier) fixed point and the perfectly reflecting (large barrier) fixed point. It was further observed that for symmetric barriers, a perfect resonance could be achieved by tuning only a *single* parameter. Here we note that this is an example of a symmetry protected topological critical point separating two topologically distinct symmetry protected insulating states. We know that an inversion symmetric one dimensional insulator is characterized by a quantized polarization, which takes two

values: $P = 0$ mod e or $P = e/2$ mod e[59]. Likewise, for our resonant tunneling problem, we can define a polarization N mod e to distinguish different symmetry protected insulating states. N is the number of charges transferred across the infinite barrier in the large-barrier limit. Without an inversion symmetric barrier, N can take any continous value. With an inversion symmetric barrier, in the large barrier limit, $N = 0$ or $e/2$ mod e. These insulating states are topologically distinct: one can not go smoothly from one phase to the other without going through a topological quantum critical point - the perfectly transmitting fixed point. Note that states emerged in our resonant tunneling problem are not the usual topological phases which possess a bulk gap. For the special value $g = 1/2$, this fixed point can also be identified with the non-Fermi liquid fixed point of the two-channel Kondo problem, described by a $SU(2)_2$ boundary conformal field theory[60, 61].

Armed with this insight we consider resonances in a spinful Luttinger liquid, which will lead us to a class of symmetry protected resonance fixed points that was not studied in detail in the early work. A spinful Luttinger liquid is characterized by two Luttinger parameters g_ρ and g_σ, with $SU(2)$ spin symmetry fixing $g_\sigma = 1$ [1]. As shown in Ref. [19, 20], the system can achieve perfect resonance by tuning a single parameter for $1/2 < g_\rho < 1$. This resonance, which is controlled by the perfectly transmitting fixed point, corresponds to a transition between insulating states characterized by a polarization N_{pair}. This polarization is defined by whether

[1]The value of Luttinger parameters g_ρ and g_σ is set to 2 for noninteracting electrons in spinful Luttinger liquid in Ref. [19, 20]

or not a pair of electrons with opposite spins is transferred across the infinite barrier in the large-barrier limit. With inversion and time-reversal symmetry, the only possible values of N_{pair} are 0 or e mod $2e$. When $g_\rho < 1/2$, the perfectly transmitting fixed point becomes unstable even on resonance. In that case a new kind of insulating state emerges characterized by $N_{pair} = \pm e/2$ mod $2e$. Like the other two insulating states, the new state is charge insulating. However, with time-reversal symmetry, the spin degrees of freedom in this state is not completed locked due to the fact that an unpaired spin can be transferred across. The new state thus has a finite conductance for spin. Transitions between these insulating states are governed by a quantum critical point that can not be described by a free Luttinger liquid fixed point. Rather, it is an *intermediate* fixed point[63, 64], which could only be described in certain perturbative limits. Here we will show that like the spinless case there is a special value of $g_\rho = 1/3$ for which the nontrivial fixed point maps to a two-channel $SU(3)$ Kondo problem, described by a $SU(3)_2$ boundary conformal field theory[65, 66]. This analysis allows us to compute the nontrivial on-resonance conductance, as well as the scaling behavior of the width of the resonance as a function of temperature, which is determined by the scaling dimension of the leading relevant operators at the fixed point.

We also note that the special point $g_\rho = 1/3$ of the 1D spinful Luttinger liquid model is of direct relevance to a corresponding resonant tunneling problem between edge states in the fractional quantum Hall effect, for which the Luttinger parameter

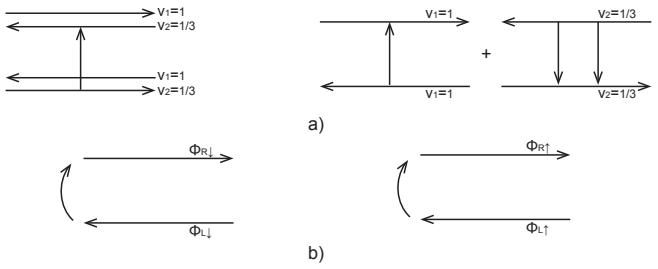

Figure 2.1: a) Two $e = 1/3$ quasiparticle tunneling processes in a $\nu = 2/3$ fractional quantum Hall system. b) Two backscattering processes in a spinful Luttinger liquid.

is not an interaction dependent quantity. Specifically, at filling $\nu = 2/3$, disorder is predicted to lead to an edge state that has an *upstream* neutral mode with an emergent $SU(2)$ symmetry[67]. The effective theory is described by the following K-matrix and charge vector

$$K = \begin{pmatrix} 1 & 2 \\ 2 & 1 \end{pmatrix}, q = \begin{pmatrix} 1 \\ 1 \end{pmatrix}.$$

Further calculations[68] show that the backscattering terms of an electron in a Luttinger liquid can be identified as the tunneling terms of an $e = 1/3$ quasiparticle in the fractional quantum Hall system (Fig. 2.1).

Relationships between the resonant tunneling problem and the Kondo problem is provided by mapping both problems to a quantum Brownian motion model[69–72]. We will argue that both the resonant tunneling problem and the two-channel $SU(3)$ Kondo problem are described by the quantum Brownian motion on a *Kagome* lattice, when they are tuned to an appropriate Toulouse limit[73]. We will show that this, in turn is closely related to the quantum Brownian motion on a *honeycomb* lattice, which was shown earlier to be related to the three-channel $SU(2)$ Kondo

problem. We will argue that this quantum Brownian motion picture provides a new insight into the level-rank duality that relates the $SU(3)_2$ and $SU(2)_3$ conformal field theories.

The chapter is organized as follows. In section 2, we review various symmetry-protected states in both the spinless and spinful Luttinger liquid. In section 3, we analyze our resonant tunneling problem which maps to a quantum Brownian motion model on a Kagome lattice at the Toulouse limit. From the quantum Brownian motion model, an intermediate fixed point is identified. Then we show how our resonant tunneling problem maps to a two-channel $SU(3)$ Kondo problem which comes handy for later analysis of the same fixed point. In section 4, utilizing the boundary conformal field theory, we calculate the on-resonance conductance and by identifying the "knob" controlling resonance we determine the critical exponent determining the scaling of the resonance line-shape with temperature. In section 5, we show that the quantum Brownian motion on both the honeycomb lattice and the Kagome lattice flows to the same fixed point characterized by its mobility which manifests the so called level-rank duality. We also point out some generalizations.

2.2 Symmetry-protected states in resonant tunneling problem

Let us first take a look at the resonant tunneling problem in a spinless Luttinger liquid[20]. Introduced by Haldane[17, 18], for spinless electrons, we can represent electrons in terms of two bosonic fields: the displacement field θ and the phase field φ with the following commutation relation

$$[\partial_x \theta(x), \varphi(x')] = i\pi\delta(x - x'). \tag{2.2.1}$$

Electron operators can then be bosonized as

$$\psi(x) \approx \sum_{m \text{ odd}} e^{im(k_F x + \theta(x))} e^{i\varphi(x)}, \tag{2.2.2}$$

where k_F is the Fermi momentum and the effective Hamiltonian density may be written as

$$\mathcal{H} = \frac{v_F}{2\pi}[g(\partial_x \varphi)^2 + \frac{1}{g}(\partial_x \theta)^2] \tag{2.2.3}$$

where v_F is the Fermi velocity and g is the Luttinger parameter characterizing strength of interaction. Passing from Hamiltonian to Lagrangian, we have two equivalent description of the Luttinger liquid. The actions are

$$S_0 = \int dx d\tau \frac{1}{2\pi g}[v_F(\partial_x \theta)^2 + \frac{1}{v_F}(\partial_\tau \theta)^2] \tag{2.2.4}$$

$$S_0 = \int dx d\tau \frac{g}{2\pi}[v_F(\partial_x \varphi)^2 + \frac{1}{v_F}(\partial_\tau \varphi)^2]. \tag{2.2.5}$$

For the weak barrier limit, Eq. (2.2.4) is a particular convenient representation of the action. The barrier is modeled as a scatter potential $V(x)$ coupling to electrons.

Assuming $\theta(x)$ varies slowly on the scale of the potential and $V(x)$ is nonzero only near $x = 0$, integrating out fluctuations in $\theta(x)$ away from zero, the effective action becomes

$$S_0 = \frac{1}{\pi g} \sum_{i\omega_n} |\theta(\omega_n)|^2, \tag{2.2.6}$$

plus an extra term corresponding to the effect of the potential:

$$- \int d\tau \frac{1}{2} \sum_{n=-\infty}^{\infty} v_n e^{i2n\theta(x=0,\tau)} \tag{2.2.7}$$

where $v_n = v_{-n}^*$ are Fourier components of $V(x)$ at momenta $2nk_F$ and ω_n is the Matsubara frequency. The extra term serves as the effective weak pinning potential for our resonant tunneling problem and we denote it as $V_{\text{eff}}[\theta(x = 0)]$. To leading order in the backscattering, the RG flow equations are

$$\frac{dv_n}{d\ell} = (1 - gn^2)v_n. \tag{2.2.8}$$

Notice that for $1/4 < g < 1$, the only relevant perturbation is the backscattering term at $k = 2k_F$:

$$\text{Re}\,(v_1)\cos(2\theta) - \text{Im}\,(v_1)\sin(2\theta).$$

In general, the system achieves resonance by tuning the two coefficients $\text{Re}(v_1)$ and $\text{Im}(v_1)$. With inversion symmetric barrier ($V(x) = V(-x)$), v_1 is a real number and therefore only one parameter needs to be tuned.

For the opposite limit, the strong barrier at the origin cuts the system into two weakly linked wires. The displacement field $\theta(x)$ is pinned at the origin. Therefore, for each wire, its electron operator at the origin is $\psi_i^\dagger(x = 0) = e^{i\varphi_i(x=0)}$ and Eq.

(2.2.5) becomes the most convenient representation of its action. The appropriate tunneling term of a single electron from one wire to the other is

$$-t(\psi_1^\dagger \psi_2(x=0) + H.c.) = -2t\cos\varphi(x=0) \tag{2.2.9}$$

where $\varphi(x=0) = \varphi_1(x=0) - \varphi_2(x=0)$ and t is the hopping matrix element. Integrating out fields φ_i away from $x \neq 0$, the effective action becomes

$$S_0 = \frac{g}{\pi} \sum_{j=1,2} \sum_{i\omega_n} |\omega_n||\varphi_j(\omega_n)|^2. \tag{2.2.10}$$

In general, n electrons tunneling terms with t_n as the hopping matrix element are also allowed and if we take them into consideration, the RG flow equation is

$$\frac{dt_n}{d\ell} = (1 - n^2/g)t_n. \tag{2.2.11}$$

It is easy to check that when electron-electron interaction is repulsive and within the range $1/4 < g < 1$, from Eq. (2.2.8), the only relevant backscattering perturbation at the small-barrier limit is at $2k_F(n=1)$ which makes the perfectly transmitting fixed point unstable. At the opposite limit, from Eq. (2.2.11), no tunneling perturbations are relevant. Thus, the perfectly reflecting fixed point is stable.

We now turn to the spinless resonant tunneling problem. A concrete model consists of a perfect wire with two δ-function barriers at $x = 0$ and $x = d$. In the weak barrier limit, for $1/4 < g < 1$, the only relevant backscattering perturbation term is at $2k_F$: $\mathrm{Re}\,(v_1)\cos(2\theta) - \mathrm{Im}\,(v_1)\sin(2\theta)$. We need to turn off two parameters($\mathrm{Re}(v_1)$ and $\mathrm{Im}(v_1)$) to tune the system to resonance. However, if the two barriers are symmetric then the inherited inversion symmetry implies that $V(x) = V(-x)$ and only

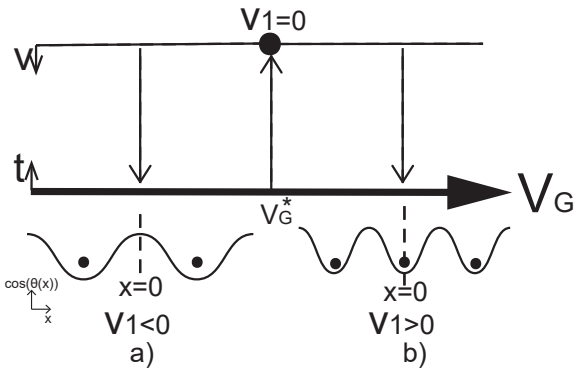

Figure 2.2: Flow diagram for spinless resonant tunneling problem. The top(bottom) line represents small(large) barrier limits. Arrows represent RG flows and the solid dot represents the perfectly transmitting fixed point. At the large-barrier limit, two inversion symmetry protected insulating phases emerge shown in a) and b) represented in their cosine potential configuration. The dashed line indicates the center of inversion. V_G is the gate voltage on the quantum dot one can tune to achieve resonance at V_G^*.

one parameter needs to be tuned(v_1 becomes a real number). Moreover, there is a gate voltage V_G coupling to electrons on the quantum dot between the two barriers. the effective action in the θ representation is

$$\begin{aligned} S =& S_0 + v_1 \int d\tau \cos\theta(x=0) + \cos\theta(x=d) \\ &+ V_G \int d\tau (\theta(x=0) - \theta(x=d)). \end{aligned} \tag{2.2.12}$$

Integrating out the θ field away from the barriers, the effective action becomes

$$S_{\text{eff}} = \frac{1}{\pi g} \sum_{i\omega_n} |\omega_n| (|\theta_\rho(\omega_n)|^2 + |\theta_\sigma(\omega_n)|^2) + \int d\tau V_{\text{eff}}(\theta_\rho, \theta_\sigma) \tag{2.2.13}$$

where $\theta_\rho = (\theta(x=0) + \theta(x=d))/2$, $\theta_\sigma = (\theta(x=0) - \theta(x=d))/2$ represent the number of electrons transferred across or in between the two barriers respectively and

$$V_{\text{eff}}(\theta_\rho, \theta_\sigma) = V_G \frac{\theta_\sigma}{\pi} + v_1 \cos 2\theta_\rho \cos 2\theta_\sigma. \tag{2.2.14}$$

With relevant perturbations, the system flows towards the perfectly reflecting fixed point. $\theta_{\rho,\sigma}$ fields will be locked in minimas of V_{eff} and instanton events connecting degenerate minimas are dominant processes in the large barrier limit($V_G \ll v_1$). Although the system ends up in a insulating state, there is a subtlety that has been overlooked: there are two distinct insulating states respecting inversion symmetry. To demonstrate, let us define a "polarization" for the system. We choose the origin as the center for inversion. If we start with $v_1 > 0$, then we must have V_{eff} pinned in the potential minimum which is at $\theta_\rho = \pi/2$. This corresponds to a polarization $N = e/2 \bmod e$. On the other hand, if we start with $v_1 < 0$, we must have minimum of the potential pinned at $\theta_\rho = 0$ and results in a polarization $N = 0 \bmod e$. The physics of our resonant tunneling problem is then two symmetry-protected insulating states separated by the perfectly transmitting fixed point. Transition between the two states is only possible by tuning the system through resonance(tuning v_1 through 0). This transition in our problem is analogous to the transition from a topological insulator to an ordinary insulator[40]. Both transitions go through a conducting point. For topological/ordinary insulator transition this is the familiar band gap closure.

For electrons with spin, we have two Luttinger parameters, the dimensionless conductance g_ρ and the dimensionless "spin conductance" g_σ for spin-current. For each spin $\mu =\uparrow, \downarrow$, there are two bosonic fields $(\theta_\mu, \varphi_\mu)$. It is convenient to separate

them into charge and spin degrees of freedom:

$$\theta_\rho = \theta_\uparrow + \theta_\downarrow, \theta_\sigma = \theta_\uparrow - \theta_\downarrow. \tag{2.2.15}$$

In the small-barrier limit, there are two competing perturbation terms in the action which are most relevant for $g_\rho < 1$ and $g_\sigma = 1$[20]

$$-\int d\tau v_e \cos(\theta_\rho)\cos(\theta_\sigma) \tag{2.2.16}$$

and

$$-\int d\tau v_1 \cos(2\theta_\rho) + v_2 \sin(2\theta_\rho), \tag{2.2.17}$$

where v_e is the process that backscatters an electron and $v_\rho = v_1 + iv_2$ is the process that backscatters an up spin electron together with a down spin electron. These two perturbation terms combined is the effective weak pinning potential $V_{\text{eff}}(\theta_\rho(x=0), \theta_\sigma(x=0))$ of the spinful resonant tunneling problem and their flow equations are given as

$$\frac{dv_e}{d\ell} = (1 - \frac{g_\rho}{2} - \frac{g_\sigma}{2})v_e \tag{2.2.18}$$

$$\frac{dv_\rho}{d\ell} = (1 - 2g_\rho)v_\rho. \tag{2.2.19}$$

Notice that the v_ρ process is relevant only for $g_\rho < 1/2$. There is another process v_σ which corresponds to backscattering of an up spin electron and a down spin electron incidenting from opposite directions(net charge momentum unchanged). If this process is relevant, it could pin θ_σ to the minimum of pinning potential. However, in the range of Luttinger parameters of our discussion, this process will always be irrelevant.[20]

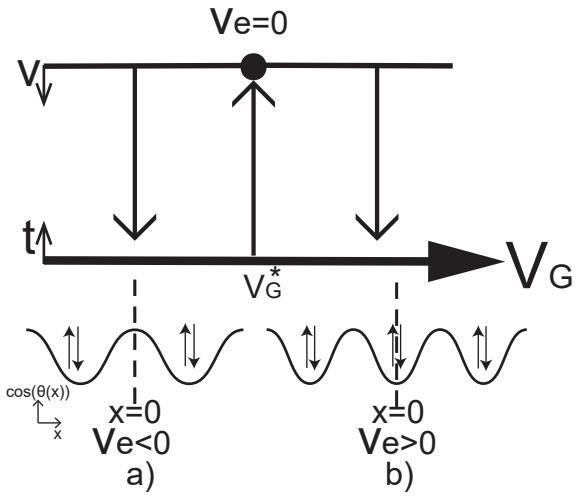

Figure 2.3: Flow diagram for the spinful case with $1/2 < g_\rho < 1$ and $g_\sigma = 1$. The top(bottom) line represents small(large) barrier limits. Arrows represent RG flows and the solid dot represents the perfectly transmitting fixed point. At the large-barrier limit, two inversion and time-reversal symmetry protected insulating phases emerge shown in a) and b) represented in their cosine potential configuration. The dashed line indicates the center of inversion. V_G is the gate voltage on the quantum dot one can tune to achieve resonance at V_G^*.

When $1/2 < g_\rho < 1$ and $g_\sigma = 1$, the v_ρ process will be irrelevant. Two distinct insulating states separated by a perfectly transmitting fixed point again emerge as shown in Fig. 2.3. However, this time, they are protected by both inversion symmetry and time-reversal symmetry with the potential minimum pinned at $(\theta_\rho(x=0) = \pi, \theta_\sigma(x=0) = 0)$ for $v_e > 0$ and $(\theta_\rho(x=0) = 0, \theta_\sigma(x=0) = 0)$ for $v_e < 0$ as the system flows into the large-barrier limit. They are characterized by $N_{pair} = e$ or 0 mod $2e$ respectively. Transition between these two symmetry protected insulting states are achieved by tuning the system to resonance(tuning v_e through 0).

A more interesting intermediate fixed point can be found if we make interactions

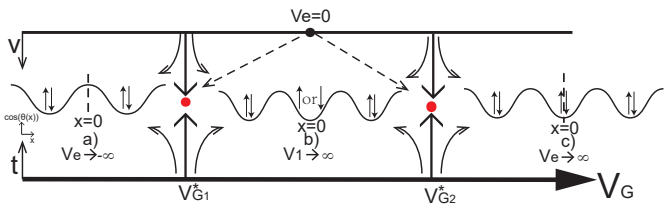

Figure 2.4: For the spinful case with $g_\rho < 1/2$ and $g_\sigma = 1$, the perfectly transmitting fixed point(the black solid dot) becomes unstable and opens up to the intermediate fixed point(the red solid dots) as indicated by the dashed arrows. Under RG flows(indicated by arrows), three inversion and time-reversal symmetry protected phases emerge shown in a), b) and c) represented in their cosine potential configuration. V_G is the gate voltage on the quantum dot one can tune to achieve resonance at $V^*_{G_{1,2}}$.

in charge sector more repulsive ($g_\rho < 1/2$) while keeping spin symmetry ($g_\sigma = 1$). The $v_\rho = v_1$ (due to inversion symmetry, the v_2 term is eliminated) process is now relevant, and we have to take it into account. There are two different situations depending on the sign of v_1. When $v_1 > 0$, the minimum of the potential V_{eff} is pinned to $\theta_\rho(x = 0) = \pi/2$. The v_e process is thus eliminated and the v_1 process dominates under RG flows. The previous perfectly transmitting fixed point becomes unstable and flows into an intermediate fixed point. A new symmetry protected state emerges as shown in Fig. 2.4. Note that at this new state we are free to change θ_σ since the v_σ process is still irrelevant. Thus, it is a charge insulating state characterized by $N_{pair} = \pm e/2 \bmod 2e$ with a finite spin conductance. On the other hand, when $v_1 < 0$, the minimum of the potential is pinned to either $\theta_\rho(x = 0) = 0$ or π. In this case, since the v_e process is also present and its magnitude grows to infinity under RG flows, $(\theta_\rho(x = 0), \theta_\sigma(x = 0))$ will be locked to either $(0, 0)$ or $(\pi, 0)$ depending on the sign of v_e as before. This gives us two charge and spin insulating

states. All three symmetry protected states can be accessed by adjusting a single parameter - the ratio v_e/v_1. A previous study of this intermediate fixed point can be found in Ref. [19, 20]. It was shown that this fixed point becomes perturbatively accessible from the perfectly transmitting fixed point with an ϵ-expansion near critical values of Luttinger parameters $g_\rho^* = 1/2$ and $g_\sigma^* = 3/2$ at the small-barrier limit. Unfortunately, for our $SU(2)$ symmetric case with $g_\sigma = 1$, this intermediate fixed point is not perturbatively accessible using the ϵ-expansion method. However, for $g_\rho = 1/3$, an exact description can be obtained using boundary conformal field theory as shown in section 4.

2.3 Resonant tunneling problem and related quantum impurity problems

In this section, we will further develop our understandings of the resonant tunneling problem in spinful Luttinger liquid and explore the connection between our resonant tunneling problem and other quantum impurity problems. First, the simpler spinless resonant tunneling problem[20] is reviewed. Then, we perform renormalization group calculations for our spinful resonant tunneling problem. At the Toulouse limit, our resonant tunneling problem is nothing but a quantum Brownian motion model on a Kagome lattice. At both small (small v) and large (small t) barrier limits of the quantum Brownian motion model, the system flows to an intermedi-

ate fixed point. To obtain an exact description of this fixed point, we map our resonant tunneling problem to a two-channel Kondo problem with $SU(3)$ impurity spin[65, 66].

2.3.1 Spinless Resonant Tunneling Problem

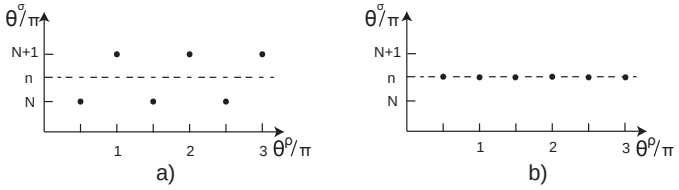

Figure 2.5: Positions of the minima of the action in the θ^ρ-θ^σ plane. a) $K = 1$, b) $K = 0$.

Again we start with the spinless resonant tunneling problem. Taking the large-barrier limit, if the capacity on the quantum dot is small, a large charging energy fixes the number of charge on the dot and transmissions through the dot are suppressed. By tuning the gate voltage, the chemical potential on the dot can be adjusted and resonant tunneling can be achieved. A theoretical model takes a double-barrier structure, it is a wire with two δ-functions on it separated by a quantum dot with size d. On the dot, a gate voltage V_G is assigned. We denote $\theta^{i=1,2}/\pi$ as the number of electrons tunneled through the corresponding barrier. We also define $\theta^\rho/\pi = (\theta^1 + \theta^2)/\pi$ as the number of electrons transferred across two barriers and $\theta^\sigma/\pi = (\theta^2 - \theta^1)/\pi$ as the number of electrons on the dot. Then,the action has deep minima when θ^σ/π is an integer (see Fig. 2.5a). Since for infinite large barriers θ fields are pinned at minima, it is more convenient to use the φ

representation($(\varphi^\rho, \varphi^\sigma)$ are dual bosonic fields of $(\theta^\rho, \theta^\sigma)$). In this case, the partition function describes instantons connecting these degenerate minima representing hopping processes. The partition function can be analyzed in the Coulomb-gas representation in powers of the tunneling amplitude t,

$$Z = \sum_n \sum_{\{q=\pm 1\}} \int \frac{d^{2n}\tau}{\tau_c} \langle (t \left|1\right\rangle \left\langle 0\right| e^{-i(q\frac{1}{\sqrt{g}}\varphi^\rho + \frac{\sqrt{K}}{\sqrt{g}}\varphi^\sigma)} + \text{h.c.})^{2n} \rangle. \tag{2.3.1}$$

where $\left|1\right\rangle, \left|0\right\rangle$ are quantum states on the dot labeling the number of electrons on the dot. K is the renormalization constant and is initially set to be 1. Its value flows under renormalization group.

Integrating out bosonic fields φ mediates a logarithmic interaction between "charges" in the Coulomb-gas representation. The "charges" correspond to physical hopping processes and we have two kind of "charges" in our problem: hopping electrons on and off the dot. After integration, the partition function is in the following form:

$$\begin{aligned} Z &= \sum_n \sum_{\{q_i=\pm 1\}} t^{2n} \int \frac{d^{2n}}{\tau_c} e^{-\sum_{i<j} V_{ij}}, \\ V_{ij} &= \frac{2}{g}(q_i q_j + K r_i r_j) \ln \frac{(\tau_i - \tau_j)}{\tau_c}, \end{aligned} \tag{2.3.2}$$

where $q_i = \theta^\rho/\pi = \pm 1$ denotes the charge transferred to the right in a hopping event and $r_i = \theta^\sigma/\pi = \pm 1$ denotes the change in charge on the dot. Due to the discreteness of charge on the dot which can only change by 1, r_i must alternate whereas q_i can have any ordering.

Tuning into resonance, the system renormalizes according to the RG flow equations[20]

$$\begin{aligned} \frac{dK}{dl} &= -8\tau_c^2 t^2 K, \\ \frac{dt}{dl} &= t[1 - \frac{(1+K)}{4g}]. \end{aligned} \tag{2.3.3}$$

During the process, electrons on the dot can virtually tunnel back to the leads reducing the average charge on the dot θ^σ. On resonance, the hopping directions along θ^σ collapse($K = 0$) which renders θ^σ/π into precisely a half integer(Fig. 2.5b). This reduction of dimensionality of $(\theta_\rho/\pi, \theta_\sigma/\pi)$ plane from two to one at the Toulouse limit greatly simplifies the problem. A similar simplification will arise in the spinful problem discussed below.

It is also worth mentioning that at $g = 1/2$, the spinless resonant tunneling problem can be mapped to a two-channel Kondo problem with $SU(2)$ impurity spin[74, 75].

2.3.2 Spinful Resonant Tunneling Problem

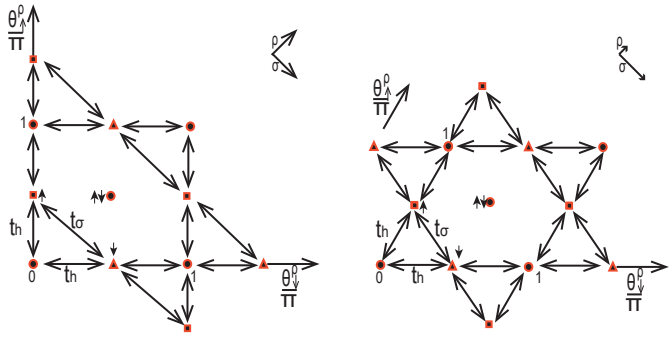

Figure 2.6: Resonant tunneling problem in $\theta^\rho_\uparrow$-$\theta^\rho_\downarrow$ plane at the large-barrier limit. Red spots are minima of the periodic potential. a) $g_\rho = g_\sigma = 1$. b) $g_\rho = 1/3$ and $g_\sigma = 1$. ($\bigcirc = |0\rangle$, $\square = |\uparrow\rangle$, $\triangle = |\downarrow\rangle$)

Examining the spinful case, at the large-barrier limit, for each barrier, there are bosonic fields (θ, φ) as defined in Eq. (2.2.15). We can reorganize (θ, φ) fields into the following

$$\begin{aligned}\theta^{\rho}_{\rho,\sigma} &= \frac{1}{\sqrt{2}}(\theta^{1}_{\rho,\sigma} + \theta^{2}_{\rho,\sigma}), \theta^{\sigma}_{\rho,\sigma} = \frac{1}{\sqrt{2}}(\theta^{1}_{\rho,\sigma} - \theta^{2}_{\rho,\sigma}), \\ \varphi^{\rho}_{\rho,\sigma} &= \frac{1}{\sqrt{2}}(\varphi^{1}_{\rho,\sigma} + \varphi^{2}_{\rho,\sigma}), \varphi^{\sigma}_{\rho,\sigma} = \frac{1}{\sqrt{2}}(\varphi^{1}_{\rho,\sigma} - \varphi^{2}_{\rho,\sigma}).\end{aligned} \tag{2.3.4}$$

The superscript ρ and σ denote physical quantities transferred across two barriers or changed in the dot respectively. The subscript ρ and σ denote charge or spin respectively. Now, the action

$$S = S_0 + \int d\tau V_{\text{eff}}((\theta^{\rho}_{\uparrow}(\tau), \theta^{\rho}_{\downarrow}(\tau), \theta^{\sigma}_{\uparrow}(\tau), \theta^{\sigma}_{\downarrow}(\tau))) \tag{2.3.5}$$

(V_{eff} is a periodic potential possesses lattice symmetry shown in Fig. 2.6) will have deep minima whenever $\theta^{\rho}_{\uparrow}/\pi$(the number of electrons with up spin transferred over two barriers) or $\theta^{\rho}_{\downarrow}/\pi$ (the number of electrons with down spin transferred over two barriers) is an integer(Fig. 2.6). We can adopt the same Coulomb-gas representation of the partition function to describe our resonant tunneling problem. In our case there are three tunneling processes. The processes in which a spin up or down electron hops on or off the quantum dot has a tunneling amplitude $t_{h_\uparrow}$ or $t_{h_\downarrow}$. The process in which both the spin of an electron on the lead and that of an electron on the quantum dot are flipped has a tunneling amplitude t_σ. When $g_\rho = 1/3$ and $g_\sigma = 1$, the three tunneling processes have the same tunneling amplitude $t_\sigma = t_{h_{\uparrow,\downarrow}} = t$(Fig. 2.6).

Expanding the partition function in powers of t_σ and $t_{h_{\uparrow,\downarrow}}$, we arrive at

$$\begin{aligned}
Z = \sum_n \sum_{a=\pm} \int \frac{d^n\tau_j}{\tau_c} \langle (t_\sigma \left|\downarrow\right\rangle \left\langle\uparrow\right| e^{-i[a\frac{1}{\sqrt{g_\sigma}}\varphi_\sigma^\rho + \frac{K_\sigma}{\sqrt{g_\sigma}}\varphi_\sigma^\sigma]} \\
+ t_{h_\uparrow} \left|\uparrow\right\rangle \left\langle 0\right| e^{-i[a(\frac{1}{2\sqrt{g_\rho}}\varphi_\rho^\rho + \frac{1}{2\sqrt{g_\sigma}}\varphi_\sigma^\rho) + (\frac{K_\rho}{2\sqrt{g_\rho}}\varphi_\rho^\sigma + \frac{K_\sigma}{2\sqrt{g_\sigma}}\varphi_\sigma^\sigma)]} \\
+ t_{h_\downarrow} \left|\downarrow\right\rangle \left\langle 0\right| e^{-i[a(\frac{1}{2\sqrt{g_\rho}}\varphi_\rho^\rho - \frac{1}{2\sqrt{g_\sigma}}\varphi_\sigma^\rho) + (\frac{K_\rho}{2\sqrt{g_\rho}}\varphi_\rho^\sigma - \frac{K_\sigma}{2\sqrt{g_\sigma}}\varphi_\sigma^\sigma)]} \\
+ \text{h.c.})^n \rangle \\
= \sum_n \sum_{a=\pm} \int \frac{d^n\tau_j}{\tau_c} \langle (\sum_{k=\sigma,h_\uparrow,h_\downarrow} t_k \delta^{k+} e^{-i(a\vec{H_{k+}}\cdot\vec{\varphi^\rho} + \vec{H_{k+}}\mathbf{K}\vec{\varphi^\sigma})} + \text{h.c.})^n \rangle
\end{aligned} \tag{2.3.6}$$

where $a = \pm 1$, $\left|l\right\rangle \left\langle m\right|_{l\neq m, l,m=\uparrow,\downarrow,0}$ have been relabeled as $\delta^{k\pm}(k = \sigma, h_\uparrow, h_\downarrow)$ and exponents are shortened as dot products of vectors $\vec{H}_{k\pm k=\sigma,h_\uparrow,h_\downarrow}$

$$\vec{H_{\sigma\pm}} = \pm(0, \tfrac{1}{\sqrt{g_\sigma}}) \tag{2.3.7}$$

$$\vec{H_{h\uparrow\pm}} = \pm(\tfrac{1}{2\sqrt{g_\rho}}, \tfrac{1}{2\sqrt{g_\sigma}}) \tag{2.3.8}$$

$$\vec{H_{h\downarrow\pm}} = \pm(\tfrac{1}{2\sqrt{g_\rho}}, -\tfrac{1}{2\sqrt{g_\sigma}}), \tag{2.3.9}$$

$\vec{\varphi^j}_{(j=\rho,\sigma)} = (\varphi_\rho^j, \varphi_\sigma^j)$ and $\mathbf{K} = \begin{pmatrix} K_\rho & 0 \\ 0 & K_\sigma \end{pmatrix}$.

For $g_\rho = 1/3$ and $g_\sigma = 1$, we have $K_{\rho,\sigma} = K$ which is initially set to 1 and $t_{\sigma,h_\uparrow,h_\downarrow} = t$. Integrating out bosonic φ fields mediates logarithmic interactions between "charges" in the following form:

$$\begin{aligned}
Z = \sum_n \frac{1}{n!} t^n \sum_{\{a_i=\pm 1\}} \int \frac{d^n\tau_i}{\tau_c} e^{-\sum_{i<j} V_{ij}}, \\
V_{ij} = (\vec{H}_i \mathbf{K}^2 \vec{H}_j + a_i a_j \vec{H}_i \cdot \vec{H}_j) \ln \frac{\tau_i - \tau_j}{\tau_c}.
\end{aligned} \tag{2.3.10}$$

where $a_i = \pm 1$.

Let us explain this Coulomb-gas model further. Because of the extra spin degrees of freedom, instantons now move in a four-dimensional space coordinated by $(\theta_\rho^\rho, \theta_\sigma^\rho, \theta_\rho^\sigma, \theta_\sigma^\sigma)$ with discrete values. "Charges" here are again different physical hopping processes. Since there are six physical hopping processes: hopping on or off either an up or down electron to the dot and flipping the spin on the dot, relations among all possible processes for a single time step constitute a triangle(see Fig. 2.6). "Charges" are now vectors of the triangle instead of scalars and their physical relevance are encoded in their length which depend on Luttinger parameters. Three "charges" from Eq. (2.3.7)-(2.3.9) characterizing the change of both spin and charge on the quantum dot are analogous to r_i in the spinless case. At each time τ_j, they have to alternate among the three possible occupation states$(|\uparrow\rangle, |\downarrow\rangle, |0\rangle)$. The other three "charges" are $a_i\vec{H}_i$ analogous to q_i, characterizing both spin and charge transferred across two barriers with no restriction of alternation.

To help with visualization, imagine that we have a four-dimensional lattice space representing the minima of pinning potential. There are two kinds of instanton tunneling events, one with tunneling along $\vec{H}_i$s on hyper-surfaces with constant $(\theta_\rho^\rho, \theta_\sigma^\rho)$ and the other with tunneling along $a_i\vec{H}_i$s on hyper-surfaces with constant $(\theta_\rho^\sigma, \theta_\sigma^\sigma)$. Conservation of total spin and charge in our resonant tunneling problem poses two constraints

$$\sum_{i=1}^{2} \theta_\rho^i + \theta_\rho^\sigma = \text{const} \tag{2.3.11}$$

$$\sum_{i=1}^{2} \theta_\sigma^i + \theta_\sigma^\sigma = \text{const}, \tag{2.3.12}$$

and forces spin or charge on the dot to alternate. Following the same reasoning as the spinless case, directions for tunneling between different $(\theta_\rho^\sigma, \theta_\sigma^\sigma)$ hyper-surfaces will get renormalized and eventually leads to the four-dimensional lattice collapsing into the two-dimensional lattice shown in Fig. 2.6(with basis changed to $(\theta_\downarrow^\rho, \theta_\uparrow^\rho)$).

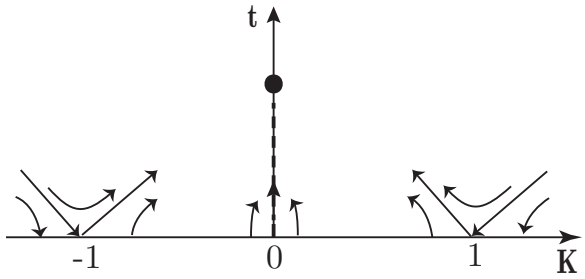

Figure 2.7: Flow diagram for resonant tunneling problem in a spinful Luttinger liquid. The dashed line is the Toulouse limit($K = 0$). The circle denotes the fixed point.

A detailed RG calculation in Appendix 2.A gives the following flow equations with the corresponding flow diagram Fig. 2.7. The Toulouse limit is along the line with $K = 0$.

$$\frac{dt}{d\ell} = (1 - \tfrac{1}{2}(K^2 + 1))t \tag{2.3.13}$$

$$\frac{dK}{d\ell} = -6\tau_c^2 t^2 K \tag{2.3.14}$$

This Toulouse limit($K = 0$) of our resonant tunneling problem, where instantons are confined in a two dimensional sublattice with coordinates $(\theta_\rho^\rho, \theta_\sigma^\rho)$ and directions along the other two bosonic fields decouple, is identical to a quantum Brownian motion model on a *Kagome* lattice. More rigorously, at the Toulouse limit, the

action for our resonant tunneling problem is

$$S_{\mathrm{RT}} = t \int \frac{d\tau}{\tau_c} \sum_{a=\pm 1} \sum_{i=\sigma,h_\uparrow,h_\downarrow} [\delta^{i+} e^{-iaH_{i+}^{\vec{}} \cdot \vec{\varphi^\rho}} + \mathrm{h.c.}]. \tag{2.3.15}$$

If we do the following mapping

$$t \leftrightarrow t_{\vec{\mathcal{R}}} \tag{2.3.16}$$

$$\delta^{i\pm}{}_{i=\sigma,h_\uparrow,h_\downarrow} \leftrightarrow \tau^{i\pm}_{i=\bigcirc,\square,\triangle} \tag{2.3.17}$$

$$\vec{\varphi^\rho} \leftrightarrow 2\pi\vec{k} \tag{2.3.18}$$

$$aH_{i\pm}^{\vec{}} \leftrightarrow a\vec{\mathcal{R}}_{i\pm}, \tag{2.3.19}$$

then this is precisely the action of a quantum Brownian motion model tunneling on a Kagome lattice in the large-barrier limit

$$S = t_{\vec{\mathcal{R}}} \int \frac{d\tau}{\tau_c} \sum_{a=\pm 1} \sum_{i=\bigcirc,\square,\triangle} [\tau^{i+} e^{ia\vec{\mathcal{R}}_{i\pm} \cdot 2\pi\vec{k}(\tau)} + \mathrm{h.c.}]. \tag{2.3.20}$$

where $t_{\vec{\mathcal{R}}}$ is the amplitude of hopping between minima connected by a lattice vector $a\vec{\mathcal{R}_{i\pm}}$, $\vec{k}(\tau)$ is the position of particle in the momentum space and $\bigcirc, \square, \triangle$ describe three distinct minima.

The quantum Brownian motion model was originally proposed as a theoretical model for heavy charged particle in a metal[69]. Although the applicability of this model to its original proposed problem is questioned[76, 77], the model is later shown to be relevant to quantum impurity problems. It describes a Brownian particle moving in a lattice with a periodic potential. The coupling of the potential to the particle generates a frictional force which acts as dissipative bath.

There are two perturbatively accessible limits to analyze the effect of the periodic potential in a quantum Brownian motion model. In the small v limit for which the barrier is small, the action is

$$S = S_0[\vec{l}(\tau)] - \int \frac{d\tau}{\tau_c} \sum_{\vec{G}} v_{\vec{G}} e^{i2\pi \vec{G}\cdot\vec{l}} \tag{2.3.21}$$

where S_0 is the dissipative kinetic energy and the latter integral represents the energy of the periodic potential. In the integrand the periodic potential amplitude at the particle trajectory $\vec{l}(\tau)$ is written in sums of Fourier components $v_{\vec{G}}$($\vec{G}$ is the reciprocal lattice vector).

Under RG calculations in the leading order, the flow equation depends on the length of the reciprocal lattice vector

$$\frac{dv_{\vec{G}}}{d\ell} = (1 - |\vec{G}|)v_{\vec{G}}. \tag{2.3.22}$$

Similarly, for the small t (large barrier) limit, the flow equation depends on the length of the lattice vector

$$\frac{dt_{\vec{\mathcal{R}}}}{d\ell} = (1 - |\vec{\mathcal{R}}|)t_{\vec{\mathcal{R}}} \tag{2.3.23}$$

We know that for a Kagome lattice the product of the shortest reciprocal lattice vector $|\vec{G_0}|$ and the shortest lattice vector $|\vec{R_0}|$ is $|\vec{G_0}||\vec{R_0}| = 1/\sqrt{3}$. Then it follows that for $1/3 < |\vec{G_0}|^2 < 1$, both small and large-barrier limits are *unstable* and there must be a stable intermediate fixed point in between. The intermediate fixed point is characterized by the mobility μ of the Brownian particle under the external frictional force where $\mu = 1$ at $v = 0$ and $\mu = 0$ at $t = 0$. Thus $0 < \mu^* < 1$ for our

intermediate fixed point. In general, μ^* depends on $|\vec{G}_0|^2$ and is hard to calculate.

This reminds us of a previous work by Yi and Kane[63, 64]. In it, they were able to map a quantum Brownian motion model on a $N-1$ dimensional honeycomb lattice to the Toulouse limit of an N-channel Kondo problem with $SU(2)$ impurity spin. We should follow their approach and map our resonant tunneling problem to the corresponding multichannel Kondo problem.

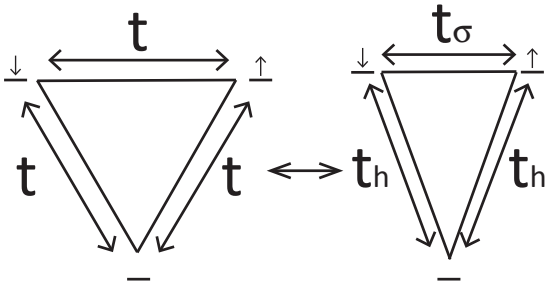

Figure 2.8: Representative triangles of tunneling processes for both the special $g_\rho = 1/3$ and $g_\sigma = 1$ case (left) and the more general case (right).

Before we end this subsection, we note that there is a more general situation for our resonant tunneling problem. With inversion and time-reversal symmetry, it is not guaranteed that the three tunneling processes have the same amplitude, although it does require $t_{h_\uparrow} = t_{h_\downarrow} = t_h$(Fig. 2.8). As a result, $K_\rho \neq K_\sigma$, RG flow

equations are also modified as:

$$\frac{dt_\sigma}{d\ell} = (1 - \tfrac{1}{2}(K_\sigma^2 + 1))t_\sigma, \tag{2.3.24}$$

$$\frac{dt_h}{d\ell} = (1 - \tfrac{1}{2}(\tfrac{3}{4}K_\rho^2 + \tfrac{1}{4}K_\sigma^2 + 1))t_h, \tag{2.3.25}$$

$$\frac{dK_\sigma}{d\ell} = -2((t_h)^2 + 2(t_\sigma)^2)\tau_c^2 K_\sigma, \tag{2.3.26}$$

$$\frac{dK_\rho}{d\ell} = -6(t_h)^2\tau_c^2 K_\rho. \tag{2.3.27}$$

2.3.3 Connection to Multichannel Kondo Problem

In this subsection, we will establish the equivalence between resonant tunneling problems in a Luttinger liquid and the multichannel Kondo problem. This allows us to use the boundary conformal field theory technique developed for the multichannel Kondo problem[78] to obtain an exact description of our newly found intermediate fixed point. The previously mentioned work by Yi and Kane[63, 64] also utilized this method to study the intermediate fixed point of the quantum Brownian motion model on the honeycomb lattice.

Let us recall the Emery-Kivelson solution of the two-channel $SU(2)$ Kondo problem[75]. This Kondo problem can be mapped to our spinless resonant tunneling problem at $g = 1/2$. It was shown that with symmetric channels, at the Toulouse limit, only *half* of the impurity spin degree of freedom is coupled to the conduction electrons resulting in the non-Fermi liquid properties. If we replace the $SU(2)$ impurity spin by the two degenerate charge states of the dot, then the *half* coupling behavior of the Kondo impurity spin at the Toulouse limit is the same as

the *half* occupation of the quantum dot by electrons hopping from leads(i.e. θ^σ/π is a half integer when $K = 0$).

Now, for the spinful case, a suitable Kondo problem would be one with two channels and three spin states for the impurity spin. Naturally, this leads us to the two-channel Kondo problem with $SU(3)$ impurity spin for which the three spin states corresponds to the three possible occupation states on the quantum dot(Fig. 2.9).

The Hamiltonian of a two-channel $SU(3)$ Kondo problem reads

$$H = iv_F \sum_{s=1}^{3}\sum_{a=1}^{2}\int \psi_a^{s\dagger}\partial_x\psi_a^s + 2\pi v_F \sum_{i=1}^{8}\sum_{a=1}^{2} J_i\chi^i S_a^i(x=0), \tag{2.3.28}$$

where a and s are channel and spin indices respectively and $\vec{\chi}$ is the impurity spin. $SU(3)$ has eight generators $\{\lambda_i\}$, $i = 1\ldots 8$ and thus the electron spin operator $\vec{S_a} = \psi_{as}^\dagger(\lambda_{ss'}/2)\psi_{as'}$. We can regroup generators of $SU(3)$ into three pairwise linear combinations of off-diagonal generators in analogy with the $SU(2)$ case as $T_\pm = (\lambda_1 \pm i\lambda_2), U_\pm = (\lambda_4 \pm i\lambda_5)$ and $V_\pm = (\lambda_6 \pm i\lambda_7)$. This allows us to write out the spin operators for electrons.

Following the Emery-Kivelson solution[75], we first bosonize fermions as

$$\psi_a^s = \frac{1}{\sqrt{2\pi v_F \tau_c}} e^{-i\Phi_a^s}, \tag{2.3.29}$$

where Φ_a^s is a bosonic field satisfying

$$[\Phi_a^s(x), \Phi_{a'}^{s'}(x')] = -i\pi\delta_{aa'}\delta^{ss'}\mathrm{sgn}(x-x'). \tag{2.3.30}$$

Then the electron spin operators at each channel are

$$S_a^{T_\pm} = \frac{1}{2\pi v_F \tau_c} e^{\pm i\Phi_a^{\sigma_1}} \tag{2.3.31}$$

$$S_a^{U_\pm} = \frac{1}{2\pi v_F \tau_c} e^{\pm i\frac{(\sqrt{3}\Phi_a^{\sigma_2} + \Phi_a^{\sigma_1})}{2}} \tag{2.3.32}$$

$$S_a^{V_\pm} = \frac{1}{2\pi v_F \tau_c} e^{\pm i\frac{(\sqrt{3}\Phi_a^{\sigma_2} - \Phi_a^{\sigma_1})}{2}} \tag{2.3.33}$$

$$S_a^3 = \frac{1}{4\pi}\partial_x \Phi_a^{\sigma_1} \tag{2.3.34}$$

$$S_a^8 = \frac{1}{4\pi}\partial_x \Phi_a^{\sigma_2}, \tag{2.3.35}$$

where $\Phi_a^{\sigma_1} = \Phi_a^1 - \Phi_a^2$, $\Phi_a^{\sigma_2} = (1/\sqrt{3})(\Phi_a^1 + \Phi_a^2 - 2\Phi_a^3)$ are associated with the two diagonal $U(1)$ subgroups of $SU(3)$. If we further assume that our Kondo problem is anisotropic meaning that the diagonal coupling constants J_3 and J_8 (in analogy with J_z in the $SU(2)$ case) are not equal to the off-diagonal ones for which we call $J_\perp$ (in analogy with $J_\pm$ in the $SU(2)$ case) in general, then the Hamiltonian becomes

$$H = H_K + H_J \tag{2.3.36}$$

with

$$H_K = \sum_{a=1}^{2} \frac{v_F}{8\pi} \int dx [(\partial_x \Phi_a^\rho)^2 + (\partial_x \Phi_a^{\sigma_1})^2 + (\partial_x \Phi_a^{\sigma_2})^2] \tag{2.3.37}$$

$$\begin{aligned} H_J = &\frac{1}{2}\sum_{a=1}^{2} \left\{ v_F \left[J_3 \tau^3 \partial_x \Phi_a^{\sigma_1}(0) + J_8 \tau^8 \partial_x \Phi_a^{\sigma_2}(0) \right] \right\} \\ &+ \frac{J_\perp}{\tau_c} \sum_{i=T,U,V} [\chi^{i_+} S_a^{i_-} + \text{h.c.}] \end{aligned} \tag{2.3.38}$$

where H_K is the kinetic energy of electrons and H_J is the interaction between the impurity and electron spins at origin.

Now we introduce a unitary transformation

$$U_{\epsilon_3,\epsilon_8} = e^{i(\epsilon_3 \sum_a \Phi_a^{\sigma_1}(0) + \epsilon_8 \sum_a \Phi_a^{\sigma_2}(0))}, \tag{2.3.39}$$

to decouple $\partial_x \Phi_a^{\sigma_1}(0)$ and $\partial \Phi_a^{\sigma_2}(0)$ in H_J in Eq. (2.3.38). By setting $\epsilon_{3,8} = J_{3,8}/2$, the system flows along the dash line in Fig. 2.7 which is precisely the Toulouse limit.

Then we perform an orthogonal transformation for variables

$$\begin{bmatrix} \Phi_{sf}^{\sigma_i} \\ \\ \Phi_s^{\sigma_i} \end{bmatrix} = \mathbf{O} \begin{bmatrix} \Phi_1^{\sigma_i} \\ \\ \Phi_2^{\sigma_i} \end{bmatrix}, \tag{2.3.40}$$

with

$$\mathbf{O} = \begin{pmatrix} \frac{1}{\sqrt{2}} & -\frac{1}{\sqrt{2}} \\ \\ \frac{1}{\sqrt{2}} & \frac{1}{\sqrt{2}} \end{pmatrix}. \tag{2.3.41}$$

The partition function of our anisotropic Kondo problem is

$$\begin{aligned} Z = & \sum_n \frac{1}{n!} (\frac{J_\perp}{2})^n \sum_{a=1}^{2} \int \frac{d^n \tau_j}{\tau_c} \langle (\chi^{T_+} e^{-i(\frac{1-J_3}{\sqrt{2}} \Phi_s^{\sigma_1} + O_{a1}^{-1} \Phi_{sf}^{\sigma_1})} \\ & + \chi^{U_+} e^{-\frac{i}{2}((\frac{1-J_3}{\sqrt{2}} \Phi_s^{\sigma_1} + \frac{\sqrt{3}(1-J_8)}{\sqrt{2}} \Phi_s^{\sigma_2}) + (O_{a1}^{-1} \Phi_{sf}^{\sigma_1} + \sqrt{3} O_{a1}^{-1} \Phi_{sf}^{\sigma_2}))} \\ & + \chi^{V_+} e^{-\frac{i}{2}((-\frac{1-J_3}{\sqrt{2}} \Phi_s^{\sigma_1} + \frac{\sqrt{3}(1-J_8)}{\sqrt{2}} \Phi_s^{\sigma_2}) + (-O_{a1}^{-1} \Phi_{sf}^{\sigma_1} + \sqrt{3} O_{a1}^{-1} \Phi_{sf}^{\sigma_2}))} \\ & + \text{h.c.})^n \rangle \\ = & \sum_n \frac{1}{n!} (\frac{J_\perp}{2\tau_c})^n \sum_{a_i = \pm} \int d^n \tau_j e^{\sum_{k<l} V_{kl}} \delta(\sum_p O_{a_p 1} \vec{r_p}), \end{aligned} \tag{2.3.42}$$

the interaction potential is given as

$$V_{kl} = 2(\vec{r_k} \mathbf{R} \vec{r_l} + O_{a_k 1}^{-1} O_{1 a_l} \vec{r_k} \cdot \vec{r_l}) \ln \frac{\tau_k - \tau_l}{\tau_c}, \tag{2.3.43}$$

$$\vec{r_{T_\pm}} = \pm(1,0) \tag{2.3.44}$$

$$\vec{r_{U_\pm}} = \pm(\frac{1}{2}, \frac{\sqrt{3}}{2}) \tag{2.3.45}$$

$$\vec{r_{V_\pm}} = \pm(-\frac{1}{2}, \frac{\sqrt{3}}{2}) \tag{2.3.46}$$

and $\mathbf{R}= \begin{pmatrix} R_3^2 & 0 \\ 0 & R_8^2 \end{pmatrix} = \begin{pmatrix} \frac{(1-J_3)^2}{2} & 0 \\ 0 & \frac{(1-J_8)^2}{2} \end{pmatrix}$.

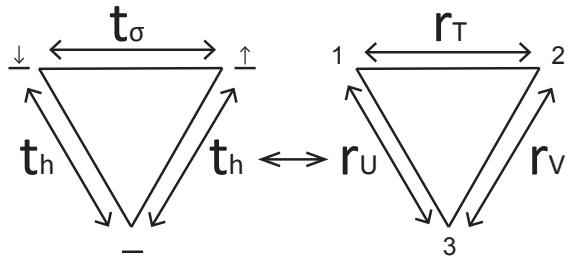

Figure 2.9: Mapping between resonant tunneling problem and Kondo problem. Number 1-3 indicates the three spin states for the impurity spin and **r**s are spin transferring processes of the Kondo problem.

The following mapping turns our resonant tunneling problem to the two-channel $SU(3)$ Kondo problem:

$$\frac{J_\perp}{2} \leftrightarrow t \tag{2.3.47}$$

$$\chi^{i\pm}{}_{i=U,V,T} \leftrightarrow |l\rangle \langle m|_{l\neq m, l,m=\uparrow,\downarrow,0} \tag{2.3.48}$$

$$(\Phi_{sf}^{\sigma_1}, \Phi_{sf}^{\sigma_2}, \Phi_s^{\sigma_1}, \Phi_s^{\sigma_2}) \leftrightarrow (\varphi_\sigma^\rho, \varphi_\rho^\rho, \varphi_\sigma^\sigma, \varphi_\rho^\sigma) \tag{2.3.49}$$

$$\mathbf{R} \leftrightarrow \mathbf{K} \tag{2.3.50}$$

$$\vec{r_i} \leftrightarrow \vec{H_i} \tag{2.3.51}$$

$$O^{-1}_{a_i 1} \leftrightarrow a_i. \tag{2.3.52}$$

The essential idea is to relate the spin and charge transferred in the resonant tunneling problem to spin transferred in the Kondo problem. In this way, when $g_\rho = 1/3$

and $g_\rho = 1$, the spin $SU(2)$ symmetry $\times$ $U(1)$ charge symmetry can be mapped to the $SU(3)$ symmetry of the Kondo problem.

2.4 Universal Resonance

In this section, we utilize the previously established mapping to the multichannel Kondo problem to study our tunneling problem on resonance. As a known result[20], at low but finite temperature, the width of the resonance line-shape vanishes as a power of temperature.

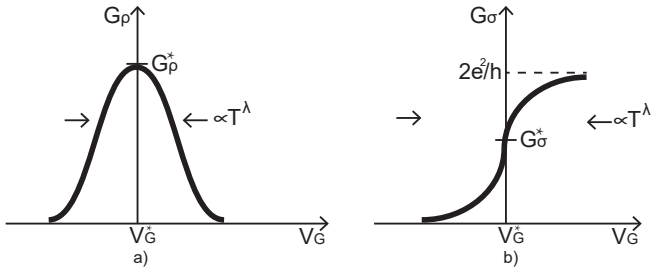

Figure 2.10: Universal scaling function for a) charge conductance and b) spin conductance.

The charge and spin conductance through resonance assume a universal shape following a scaling function[79] (Fig. 2.10)

$$G_\rho(\delta, T) = \mathcal{G}_\rho(c\frac{\delta}{T^\lambda}) \tag{2.4.1}$$

$$G_\sigma(\delta, T) = \mathcal{G}_\sigma(c\frac{\delta}{T^\lambda}) \tag{2.4.2}$$

where c is a non-universal constant and δ is the distance to resonance in gate voltage. Using boundary conformal field theory description of the Kondo problem, we calculate the on-resonance conductance $G^*_{\rho,\sigma}$ at $T = 0$ in section 4.1. Moreover,

in section 4.2, we exam all allowed operators at the fixed point of our resonant tunneling problem and identified the sole relevant operator for which we could tune the system through resonance. The scaling behavior of the resonance line-shape, which depends on the critical exponent $\lambda = 1 - \Delta$, is obtained from calculating the scaling dimension Δ of that relevant operator.

2.4.1 On-Resonance Conductance

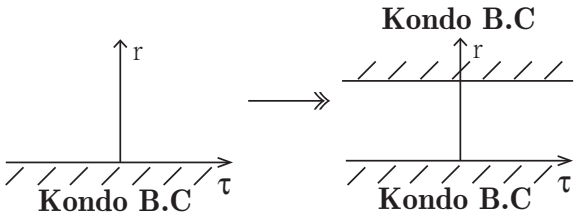

Figure 2.11: Boundary conformal field theory description of Kondo problem

Unlike the spinless case in which the fixed point is perturbatively accessible at the small-barrier limit, here, we can not extract information about conductance without an exact description of the intermediate fixed point. Despite the failure of perturbative methods, since our resonant tunneling problem is equivalent to a two-channel $SU(3)$ Kondo problem, we can study the intermediate fixed point using boundary conformal field theory.

The BCFT description of our Kondo problem resides on the upper half-plane (Fig. 2.11) with Kondo boundary condition encoded on the real axis[78, 80]. It is precisely this non-trivial Kondo boundary condition that gives calculations of correlation functions an extra twist as reflected in Appendix 2.B. Following Eqs.

(2.3.37)-(2.3.42), by identifying electron operators in our tunneling problem with the two-channel $SU(3)$ Kondo problem, we have our current-operator correspondence:

$$J_\sigma^\rho(0^\pm,\tau) \leftrightarrow J_{sf}^{\sigma_1}(0^\pm,\tau) \tag{2.4.3}$$

$$J_\rho^\rho(0^\pm,\tau) \leftrightarrow J_{sf}^{\sigma_2}(0^\pm,\tau). \tag{2.4.4}$$

Using the Kubo formula, the on-resonance Kubo conductance is

$$G_\rho^{K*} = 2g_\rho\mu^*\frac{e^2}{h} \tag{2.4.5}$$

$$G_\sigma^{K*} = 2g_\sigma\mu^*\frac{e^2}{h}. \tag{2.4.6}$$

For $g_\rho = 1/3$ and $g_\sigma = 1$, the mobility μ^* is calculated using the boundary conformal field theory in Appendix 2.B. We have

$$\mu^* = \frac{5-\sqrt{5}}{4} \approx 0.691. \tag{2.4.7}$$

The physical conductance and its relation to the Kubo conductance calculated above is explained in Appendix 2.C. The physical on-resonance conductance is

$$G_{\rho,\sigma}^* = \frac{2g_{\rho,\sigma}\mu^*}{1+(g_{\rho,\sigma}-1)\mu^*}\frac{e^2}{h}. \tag{2.4.8}$$

For $g_\rho = 1/3$ and $g_\sigma = 1$, we have

$$G_\rho^* \approx 0.854\frac{e^2}{h} \tag{2.4.9}$$

$$G_\sigma^* \approx 1.382\frac{e^2}{h}. \tag{2.4.10}$$

2.4.2 Tuning Through Resonance

According to Cardy[81], properties of the boundary operators can be obtained by conformally mapping the upper half-plane to an infinite stripe with Kondo boundary conditions on both ends (Fig. 2.11). Therefore, to obtain the spectrum of Hamiltonian H_{KK} in an infinite stripe with the "Kondo-Kondo" boundary condition, we can use the "double fusion" rule hypothesized by Affleck and Ludwig[78, 80] starting with the free fermion boundary condition "FF" on both ends. Since the conformal embedding of our Kondo problem is $U(1)^{charge} \times SU(2)_3^{flavor} \times SU(3)_2^{spin}$, just like the case for the three-channel $SU(2)$ Kondo problem with spin and flavor interchanged, then any boundary operators can be represented as a triplet (Q, j, λ) where the three quantum numbers are weights in representations of Lie groups $U(1), SU(2)$ and $SU(3)$ respectively[78, 80]. The allowed triplets are of course all possible primary fields at the intermediate fixed point. The calculation from Eq. (2.B.12) shows that both the two-channel $SU(3)$ and the three-channel $SU(2)$ Kondo problems[63, 64] flow to the same intermediate fixed point. Therefore, using the latter Kondo problem, if we start with the free fermion boundary condition $(0, 0, 0)$, and fuse the boundary operators with the impurity spin operator $s = 1/2$ $(0, 1/2, 0)$ twice, the resultant operators are all possible primary fields at the intermediate fixed point. Their scaling dimensions are given as[82]

$$\Delta = \frac{(\lambda, \lambda + 2\rho)}{2(k + g)}, \tag{2.4.11}$$

where $(\cdot)$ is the scalar product induced by Killing forms, λ is the weight of the boundary operator in the corresponding representation of its Lie group, ρ is the Weyl vector, k is the level and g is the Coexter number[82]. The only relevant operators left are $(0,1,0)$ with $\Delta = 1/2$ and $(0,0,[1,1])$ with $\Delta = 3/5$ which transform as elements of the adjoint representation of $SU(2)$ and $SU(3)$, respectively.

Counting the number of available operators is the same as counting the dimension of the two adjoint representations, which gives dim(ad $SU(2)$)+dim(ad $SU(3)$)=11 possible relevant operators. However, channel symmetry and $SU(3)$ spin symmetry in the Kondo problem all impose constraints via conservation laws. Any off-diagonal elements of the adjoint representation will modify either channel number or spin numbers and thus break the conservation laws. We are left with three diagonal relevant operators.

In the familiar two-channel $SU(2)$ Kondo problem, there are two relevant diagonal operators, each from $SU(2)_2^{spin}$ and $SU(2)_2^{flavor}$ sectors, respectively. Inversion symmetry demands there should be no difference between two channels. Therefore, the diagonal operator from $flavor\ SU(2)$ can not be present since it will lead the system flow towards an anisotropic Kondo fixed point with one channel strongly coupled and the other disconnected by breaking the $flavor\ SU(2)$ symmetry[83]. When interpreting this in the spinless resonant tunneling problem, since the fixed point is at the perfect conducting limit, then $\cos(2\theta)$ and $\sin(2\theta)$ are the two aforementioned relevant diagonal operators. Inversion symmetry in this case requires the

two barriers to be the same and eliminates $\sin(2\theta)$. Similarly, in the two-channel $SU(3)$ Kondo problem, inversion symmetry again eliminates any relevant diagonal operator from $flavor\ SU(2)$. Moreover, we know that the relevant diagonal operator in subgroup $spin\ SU(2) \subseteq spin\ SU(3)$ must vanish to make $r_U = r_V$. This is because when translating back to our resonant tunneling problem, time-reversal symmetry requires there be no difference between spin states so that the two t_h processes are equal. Note that t_σ is allowed to have a different amplitude. This extra degree of freedom is precisely controlled by the remaining one relevant diagonal operator from $spin\ U(1) \subseteq spin\ SU(3)$ and can be used to tune the system to resonance.

With this knowledge, at finite temperature, we are able to calculate the critical exponent

$$\lambda = 1 - \Delta = 2/5 \tag{2.4.12}$$

for the resonant line-shape. The exact form of the scaling function $\mathcal{G}$ can be obtained from the Monte-Carol simulation[68].

2.5 Level-Rrank Duality in the Quantum Brownian Motion Model

BCFT has granted us an exact description of our two-channel $SU(3)$ Kondo fixed point. Translating everything into the quantum Brownian motion on a Kagome

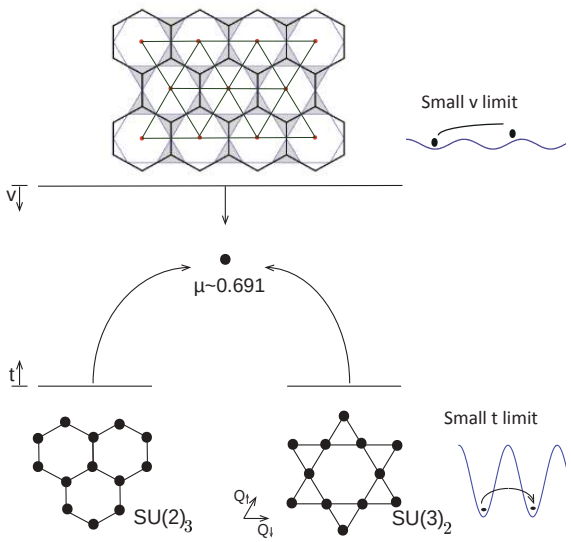

Figure 2.12: Flow diagram for quantum Brownian motion models on a honeycomb and a Kagome lattice. The top(bottom) line represents small(large) barrier limits. Arrows indicate the direction of RG flows and the solid dot represents the intermediate fixed point with its mobility μ labeled. Since the two models flow to the same intermediate fixed point from both limits, this phenomenon manifests the level-rank duality from a quantum Brownian motion model perspective.

lattice using the mapping from section 3, the spin-current conductance in the Kondo problem, becomes the mobility μ of fictitious particles on the lattice of a quantum Brownian motion model(see Appendix 2.B).

The mobility calculated in Eq. (2.B.12) confirms that the quantum Brownian motion on both the honeycomb lattice[63, 64] and the Kagome lattice flows into the same strong coupling fixed point (Fig. 2.12). Mathematically, this can be attributed to the fact that the same conformal embedding is realized at the fixed point, namely $U(1)\times SU(2)_3\times SU(3)_2$. If we dig in a little further, this phenomenon is called level-rank duality relating $SU(3)_2$ conformal field theory to $SU(2)_3$ conformal field theory [82]. However, instead of going through mind-boggling mathematical formalism, here we provide a more physical picture of this equivalency using quantum Brownian motion models.

This equivalency in the large-barrier limit can be assessed by comparing the mobility of the two quantum Brownian motion models since both are related to Kondo problems in the Toulouse limit. From that calculation, a more general pattern emerges. We find that with $n+k$ fixed, any $SU(n)_k$ quantum Brownian motion model flows into an intermediate fixed point with the same mobility $\mu = 2\sin^2[\pi/(n+k)]$. This is checked up to $n+k=10$ using MATHEMATICA.

On the other hand, in the small-barrier limit, to the first order, the quantum Brownian motion model is governed by the renormalization group Eq. (2.3.22) which drives the system towards the intermediate fixed point. The general pattern

stated in the previous paragraph is harder to establish since for general n and k, $v_{\mathbf{G}}$ is a complex number in general ($v_{\vec{G}} = v^*_{-\vec{G}}$). Therefore, it is not clear how the two systems will behave under the first order flow equation. However, for special cases with either n or $k = 2$, there is a simple argument to show their equivalency at the small-barrier limit. First of all, it is not hard to see that the $SU(2)_k$ quantum Brownian motion lives on a generalized honeycomb lattice and the $SU(k)_2$ quantum Brownian motion lives on a generalized Kagome lattice both in $k-1$ dimensional space. In Appendix 2.D, by choosing an appropriate origin, we have shown that all $v_{\vec{G}} \in \mathbb{R}$ and $v^h_{\vec{G}_0}$ of the generalized honeycomb lattice have the same sign as $v^k_{\vec{G}_0}$ of the generalized Kagome lattice. Therefore, the two quantum Brownian motion models flow to the same intermediate fixed point. We leave detailed calculations in Appendix 2.D.

Appendix

2.A Renormalization group for resonant tunneling problem in a spinful luttinger liquid

Here we set $g_\rho = 1/3$ and $g_\sigma = 1$ and adopt the renormalization group calculation developed by Anderson, Yuval, and Hanmann[84].

First, we decimate all possible closely placed pairs of charges with a range between τ_c and $\tau_c + d\tau_c$. Inserting them in between charge i and $i+1$, the partition function becomes

$$\begin{aligned} Z = &\sum_n \frac{1}{n!} t^n \int d^n\tau_i \sum_{a_i} e^{-\sum_{i<j} V_{ij}} \\ &\times [1 - t^2 d\tau_c \sum_i \int_{\tau_i+\tau_c}^{\tau_{i+1}+\tau_c} d\tau \sum_a e^{V_{ia}(\tau)} + \cdots] \end{aligned} \tag{2.A.1}$$

where the interaction of the dipoles with all other charges is

$$V_{ia}(\tau) = -\sum_j \sum_{\vec{r}} [\vec{H}\mathbf{K}^2\vec{H}_j + aa_j\vec{H}\cdot\vec{H}_j]\tau_c\partial_\tau \ln\frac{\tau-\tau_j}{\tau_c}. \tag{2.A.2}$$

Expand the exponent

$$
\begin{aligned}
Z = & \sum_n \frac{1}{n!} t^n \int d^n \tau_i \sum_{a_i} e^{\sum_{i<j} V_{ij}} \\
& \times [1 - t^2 d\tau_c \sum_i \int_{\tau_i}^{\tau_{i+1}} d\tau \sum_a (1 + V_{ia}(\tau) + \cdots) + \cdots].
\end{aligned}
\tag{2.A.3}
$$

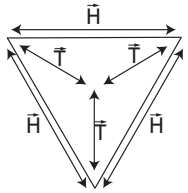

Figure 2.A.1: Hopping vectors $\vec{H}$ and auxiliary vectors $\vec{T}$

Now, define $\vec{H}_i = \vec{T}_{i+1/2} - \vec{T}_{i-1/2}$ (Their relation is depicted in Fig. 2.A.1),

$$
\begin{aligned}
& \sum_{i,a} \int_{\tau_i}^{\tau_{i+1}} V_{ia}(\tau) \\
& = - \sum_{ij} \sum_{\vec{H}} 2\vec{H} \mathbf{K} \vec{H}_j \tau_c (\ln \frac{\tau_{i+1} - \tau_j}{\tau_c} - \ln \frac{\tau_i - \tau_j}{\tau_c}) \\
& = - \sum_{i<j} \sum_{\vec{T} \neq \vec{T}_{i+\frac{1}{2}}} 4(\vec{T} - \vec{T}_{i+\frac{1}{2}}) \mathbf{K} \vec{H}_j \tau_c (\ln \frac{\tau_{i+1} - \tau_j}{\tau_c} \\
& - \ln \frac{\tau_i - \tau_j}{\tau_c}) \\
& = - \sum_{i<j} \sum_{\vec{T}} 4(\vec{T} - \vec{T}_{i+\frac{1}{2}}) \mathbf{K} \vec{H}_j \tau_c (\ln \frac{\tau_{i+1} - \tau_j}{\tau_c} \\
& - \ln \frac{\tau_i - \tau_j}{\tau_c}) \\
& = - \sum_{i<j} (\sum_{\vec{T}} 4\vec{T} - 3 \cdot 4\vec{T}_{i+\frac{1}{2}}) \mathbf{K} \vec{H}_j \tau_c (\ln \frac{\tau_{i+1} - \tau_j}{\tau_c} \\
& - \ln \frac{\tau_i - \tau_j}{\tau_c}) \\
& = - \sum_{i<j} 12 \vec{H}_i \mathbf{K} \vec{H}_j \tau_c \ln \frac{\tau_i - \tau_j}{\tau_c}
\end{aligned}
\tag{2.A.4}
$$

Due to neutrality condition, $\sum_i \vec{H}_i = 0$ gives $\sum_{i<j} \vec{H}_i \cdot \vec{H}_j = -1/2n$. Rescaling τ_c to $\tau_c + d\tau_c$, the partition function becomes

$$\begin{aligned} Z = & \sum_n \sum_{\{a_i\}} t^n (\frac{\tau_c + d\tau_c}{\tau_c})^{-\frac{1}{2}n(1+K^2)} \\ & \times \int d^n\tau_i \exp(-\sum_{i<j} [K^2 \vec{H}_i \cdot \vec{H}_j (1 - 12t^2\tau_c d\tau_c) \\ & + a_i a_j \vec{H}_i \cdot \vec{H}_j] \ln \frac{\tau_i - \tau_j}{\tau_c}), \end{aligned} \tag{2.A.5}$$

which leads to the flow equations

$$\frac{dt}{d\ell} = (1 - \tfrac{1}{2}(K^2 + 1))t \tag{2.A.6}$$

$$\frac{dK}{d\ell} = -6\tau_c^2 t^2 K \tag{2.A.7}$$

2.B Mobility of Quantum Brownian motion on Kagome Lattice

In this section, we calculate the universal mobility μ^* of quantum Brownian motion model on Kagome lattice at the intermediate fixed point using boundary conformal field theory results on Kondo problem. The analog of R_a^i is the spin in our Kondo problem S_a^i. Therefore spin currents for our Kondo problem are

$$J_a^{\sigma_i} = \frac{v_F}{4\pi} \partial_x \Phi_a^{\sigma_i} = \frac{1}{4\pi} \partial_t \Phi_a^{\sigma_i} \tag{2.B.1}$$

and their linear combinations

$$J_s^{\sigma_i} = \sum_{a=1}^2 \tfrac{1}{\sqrt{2}} J_a^{\sigma_i} = \tfrac{1}{4\pi} \partial_t \Phi_s^{\sigma_i} \tag{2.B.2}$$

$$J_{sf}^{\sigma_i} = \sum_{a=1}^2 O_{1a} J_a^{\sigma_i} = \tfrac{1}{4\pi} \partial_t \Phi_{sf}^{\sigma_i} \tag{2.B.3}$$

can be translated into velocity of Brownian particles[63, 64].

For example, the velocity $\partial_t R_{\sigma_i}$ is mapped to the rate of spin σ_i injected into spin-flavor channel

$$J_{sf}^{\sigma_i}(x=0^+) - J_{sf}^{\sigma_i}(x=0^-) \leftrightarrow \partial_t R_{\sigma_i} \tag{2.B.4}$$

where

$$R_{\sigma_i} = \int dx \psi_{as}^{\dagger} \frac{\lambda_{ss'}^{\sigma_i}}{2} \frac{\sigma_{aa'}^{z}}{2} \psi_{a's'} \tag{2.B.5}$$

The mobility μ now becomes the response of spin currents to applied potentials.

$$\begin{aligned} \mu^* = \lim_{\omega \to 0} \frac{1}{2\pi|\omega|} \int d\tau (1 - e^{i\omega\tau}) \langle T_\tau [J_{sf}^{\sigma_i}(0^+, \tau) \\ - J_{sf}^{\sigma_i}(0^-, \tau)][J_{sf}^{\sigma_i}(0^+, 0) - J_{sf}^{\sigma_i}(0^-, 0)] \rangle_0 \end{aligned} \tag{2.B.6}$$

where $\langle \cdots \rangle_0$ is the average with respect to the free non-interacting Hamiltonian.

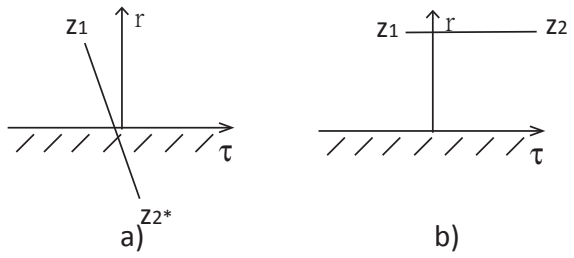

Figure 2.B.1: a) Correlators like $\langle T_\tau J_{sf}^{\sigma_i}(0^+, \tau) J_{sf}^{\sigma_i}(0^-, 0) \rangle_0$ that across the non-trivial boundary can not be translated asymptotically away from the boundary. While in b), correlators like $\langle T_\tau J_{sf}^{\sigma_i}(0^+, \tau) J_{sf}^{\sigma_i}(0^+, 0) \rangle_0$ can and thus produce trivial value which is not affected by the boundary.

Using boundary conformal field theory[78, 80], the correlation functions are calculated

$$\begin{aligned} \langle T_\tau J_{sf}^{\sigma_i}(0^+, \tau) J_{sf}^{\sigma_i}(0^+, 0) \rangle_0 = \langle T_\tau J_{sf}^{\sigma_i}(0^-, \tau) J_{sf}^{\sigma_i}(0^-, 0) \rangle_0 \\ = \frac{1}{2\tau^2}, \end{aligned} \tag{2.B.7}$$

$$\begin{aligned}\langle T_\tau J^{\sigma_i}_{sf}(0^+,\tau)J^{\sigma_i}_{sf}(0^-,0)\rangle_0 &= \langle T_\tau J^{\sigma_i}_{sf}(0^-,\tau)J^{\sigma_i}_{sf}(0^+,0)\rangle_0 \\ &= \frac{a}{2\tau^2},\end{aligned} \tag{2.B.8}$$

where a is a universal complex number depending on Kondo boundary condition and can be calculated using modular S-matrix[78, 80]

$$a = \frac{S^\lambda_s/S^\lambda_0}{S^0_s/S^0_0}. \tag{2.B.9}$$

(λ is the highest weight representation of $J^{\sigma_i}_{sf}$ and s is the highest weight of representation of impurity spin in the corresponding Lie algebra).

The general formula for calculating modular S-matrix is given as[82]

$$\begin{aligned}S^\lambda_s = i^{|\triangle_+|}|P/Q^\vee|^{-\frac{1}{2}}(k+g)^{-r/2} \\ \times \sum_{w\in W}\epsilon(w)e^{-2\pi i(w(\lambda+\rho),s+\rho)/(k+g)}\end{aligned} \tag{2.B.10}$$

where $|\triangle_+|$ is the number of positive roots, $|P/Q^\vee| = detA_{ij}$(A is the Cartan matrix) for simply-laced algebras, k is the level, g is the dual Coexter number, W is the Weyl group, $\epsilon(w)$ is the signature function and ρ is the Weyl vector which is half of the sum of all positive roots.

For our $SU(3)$ case, we have $J^{\sigma_i}_{sf}$ is in the adjoint representation of $SU(3)$ and the impurity spin is in the fundamental representation. Thus, $\lambda = [1,1]$ and $s = [1,0]$ or $[0,1]$. Then

$$a = \frac{(-4\sin\frac{2\pi}{5} + 2\sin\frac{4\pi}{5})/(2\sin\frac{2\pi}{5} + 4\sin\frac{4\pi}{5})}{(4\sin\frac{4\pi}{5} + 2\sin\frac{2\pi}{5})/(4\sin\frac{2\pi}{5} - 2\sin\frac{4\pi}{5})} = \frac{\sqrt{5}-3}{2} \tag{2.B.11}$$

which agrees with a calculated in three-channel $SU(2)$ Kondo problem[63, 64].

The mobility is

$$\begin{aligned} \mu^* &= \frac{1-a}{2} = \frac{5-\sqrt{5}}{4} \\ &\approx 0.691 \end{aligned} \tag{2.B.12}$$

2.C Physical conductance

It is known that the Kubo conductance computed from linear response theory does not match the physical DC conductance measured in a system with Fermi liquid lead[85–91]. The Kubo conductance describes the response of an infinite Luttinger liquid, where the limit $L \to \infty$ is taken *before* $\omega \to 0$, and relates the current to the potential difference between the incident chiral modes of the Luttinger liquid. However, the potential of the chiral modes is not the same as the potential of the Fermi liquid leads. There is a contact resistance between the Luttinger liquid and the electron reservoir where the voltage is defined. An appropriate model to account for this is to consider a 1D model for the leads in which the Luttinger parameter $g_\rho = g_\sigma = 1$ in the leads[91]. Here we review that argument for the simple case of spinless electrons characterized by a single Luttinger parameter g. The generalization to include spin is straightforward.

The relationship between the Kubo conductance and the physical conductance can be determined by specifying the appropriate boundary condition at the interface between the Luttinger liquid and Fermi liquid, where $g = g(x)$ in Eq. (2.2.3) changes. Charge conservation requires $\dot{\theta}$ is continuous, while the condition of zero

backscattering at the interface requires $\dot{\varphi}$ is continuous. Using the equations of motion determined by Eqs. (2.2.1) and (2.2.3), we thus conclude that $gv\partial_x\varphi$ and $v\partial_x\theta/g$ are continuous. Since the Kubo conductance relates the current to the potential difference between the incoming *chiral* modes, it is useful to rewrite this boundary condition in terms of the chiral potentials $V_{R/L} = v(\partial_x\varphi \pm \partial_x\theta/g)$. We thus require the continuity of $g(x)(V_R - V_L)$ (charge conservation) and $V_R + V_L$ (no backscattering).

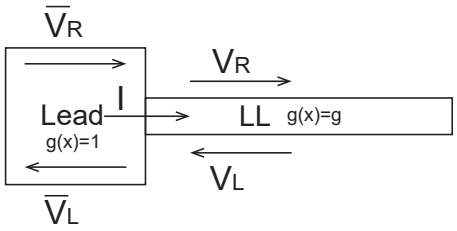

Figure 2.C.1: Chiral currents in the Fermi-liquid lead and the Luttinger liquid.

Applied to a single interface between $g(x) = 1$ and $g(x) = g$ (Fig. 2.C.1), we thus conclude

$$\bar{V}_R - \bar{V}_L = g(V_R - V_L) = (h/e^2)I \tag{2.C.1}$$

$$\bar{V}_R + \bar{V}_L = V_R + V_L. \tag{2.C.2}$$

Elinminating $\bar{V}_L$ and V_L leads to

$$\bar{V}_R - V_R = \frac{h}{e^2}\frac{g-1}{2g}I \tag{2.C.3}$$

Thus, the potential of the incoming chiral mode in the Fermi liquid lead is higher than potential of the chiral mode in the Luttinger liquid. The contact between

$g(x) = 1$ and $g(x) = g$ effectively contributes a *series resistance*

$$R_c = \frac{g-1}{2g}\frac{h}{e^2}. \tag{2.C.4}$$

In a two terminal setup with two Fermi liquid leads the series contact resistance is doubled. Writing the Kubo conductance as $g\mu e^2/h$, where $0 < \mu < 1$ is the mobility, we then conclude the physical conductance is

$$G = \frac{e^2}{h}\frac{g\mu}{1+(g-1)\mu}. \tag{2.C.5}$$

This reproduces the fact that for perfect transmission $\mu = 1$ the physical conductance is e^2/h, while the Kubo conductance is ge^2/h.

For the spinful case, in both the charge and the spin sectors, the contact resistance gets a factor of $1/2$ and the Kubo conductance gets a factor of 2. Therefore, the physical conductance gets an overall factor of 2.

2.D Generalized honeycomb and Kagome lattices in small-barrier limit

In this section we will discuss how our quantum Brownian motion picture of level-rank duality fits to general values of n and k and apply the knowledge to establish proof of equivalence between quantum Brownian motion models on generalized honeycom and Kagome lattice.

First, notice that we can represent primitive vectors of Bravais lattice of the

$SU(n)_k$ quantum Brownian motion model as $n \times k$ matrices N with the only non-zero terms at $N_{11} = N_{ij} = 1$ and $N_{1j} = N_{i1} = -1$ for $i, j > 1$

$$\frac{1}{2}\begin{pmatrix} 1 & \dots & -1 & \dots \\ \vdots & \ddots & \vdots & \ddots \\ -1 & \dots & 1 & \dots \\ \vdots & \ddots & \vdots & \ddots \end{pmatrix} \tag{2.D.1}$$

Basically, a primitive vector hops particle between adjacent lattice site with the same basis label. In Kondo language, it refers to processes which leave intact the impurity spin. Since we can choose arbitrary spin state for our impurity spin from $1 \cdots n$, let it be 1, then each N matrix represents the process which transfers an i spin from channel 1 to channel j via impurity spin.

Clearly we can not put $N_{ij} = 1$ in either the first row or the first column, it leaves only $(n-1)(k-1)$ independent spots. Therefore, the matrices are actually describing a $(n-1)(k-1)$ dimensional lattice. For the corresponding reciprocal lattice, we find primitive vectors are $n \times k$ matrix G:

$$\pm\frac{2}{nk}\begin{pmatrix} 1 & \dots & 1 & -(k-1) \\ \vdots & \ddots & & \vdots \\ 1 & & \ddots & -(k-1) \\ -(n-1) & \dots & -(n-1) & (n-1)(k-1) \end{pmatrix}.$$

Different primitive vectors can be obtained by shifting both the row and column containing entry $(n-1)(k-1)$ around at all nk positions in the matrix.

With the foundation laid, now let us proceed to the special cases with either n or $k = 2$. We will show in the following that all $v_{\vec{G}} \in \mathbb{R}$ and $v^h_{\vec{G}_0} = cv^k_{\vec{G}_0}$ for some positive constant c.

The first trick is to choose the right origin. In general, $v_{\mathbf{G}}$ will be a complex number, however, if we choose the origin of our coordinate system to be at one of the center of inversion, then we are putting $\vec{G}$ and $-\vec{G}$ at the same footing. Therefore, $v_{\vec{G}} = v_{-\vec{G}}$ which makes it a real number. For later calculation convenience, we will choose one of the center of the bond of our generalized honeycomb lattice to be the origin for both lattices (Fig. 2.D.1).

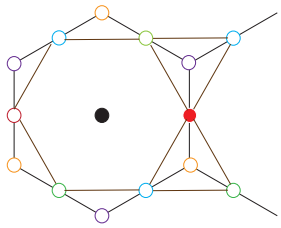

Figure 2.D.1: Two choices of center of inversion for both lattices: 1. the center of hexagon(black), 2. the center of a bond of the honeycomb lattice(red). However, it is hard to define an analogous position of the first one for generalized honeycomb lattice in odd dimensional space.

Next, let us again embed our $k-1$ dimensional lattices into a higher dimensional space, this time a k dimensional space. For generalized k-honeycomb and k-Kagome lattice, we found basis vectors are:

$$\vec{l}^h_1 = \frac{1}{2}(1, \overbrace{\cdots}^{0\text{s}}), \quad \vec{l}^h_2 = \frac{1}{2}(-1, \overbrace{\cdots}^{0\text{s}}) \tag{2.D.2}$$

and

$$\vec{l}^k_{i=1,\ldots,k-1} = \frac{1}{2}(1, \overbrace{\cdots}^{0\text{s}}, \underset{i+1}{-1}, \overbrace{\cdots}^{0\text{s}}), \quad \vec{l}^k_k = 0, \tag{2.D.3}$$

and the shortest vectors for their reciprocal lattice are:

$$\vec{G}_0^{j=1,\ldots,k} = \frac{2\pi}{k}(\overbrace{\cdots}^{1\text{s}}, \underset{j}{-k+1}, \overbrace{\cdots}^{1\text{s}}). \tag{2.D.4}$$

What's left is just plug and chug. Substitute our vectors into

$$v_{\vec{G}} = \sum_{\vec{G}} e^{i\vec{G}\cdot\vec{l}} \tag{2.D.5}$$

we find

$$v^h_{\vec{G}_0^j} = \begin{cases} 2\cos\frac{\pi}{k}, & \text{if } j \neq 1 \\ -2\cos\frac{\pi}{k}, & \text{otherwise} \end{cases} \tag{2.D.6}$$

and

$$v^k_{\vec{G}_0^j} = \begin{cases} k-2, & \text{if } j \neq 1 \\ 2-k, & \text{otherwise} \end{cases}. \tag{2.D.7}$$

Since $k \in \mathbb{Z}$ and $k \geq 2$, we conclude that $v^h_{\vec{G}_0}$ has the same sign as $v^k_{\vec{G}_0}$.

Chapter 3

Fibonacci Topological Superconductor

γ

3.1 Introduction

Current interest in topological quantum phases is heightened by the proposal to use them for quantum information processing[92, 93] and by prospects for realizing them in experimentally viable electronic systems. There is growing evidence that the fractional quantum Hall (QH) state at filling $\nu = 5/2$ is a non-Abelian state[26, 34, 94–96] with Ising topological order. A simpler form of Ising order is predicted in topological superconductors (T-SC)[27, 29] and in SC proximity effect devices[28,

97–100]. In these systems the Ising σ particle is not dynamical, but is associated with domain walls or vortices that host gapless Majorana fermion modes. Recent experiments have found promising evidence for Majorana fermions in 1D and 2D SC systems[32, 101, 102].

Ising topological order is insufficient for universal quantum computation, but the richer Fibonacci topological order is sufficient[103]. Fibonacci order arises in the Z_3 parafermion state introduced by Read and Rezayi[104], which is a candidate for the fractional QH state at $\nu = 12/5$. Parafermions can also be realized by combining SC with the fractional QH effect[106, 108, 109]. This line of inquiry culminated in the tour de force works[110, 111] that showed a $\nu = 2/3$ QH state, appropriately proximitized, could exhibit a Fibonacci phase.

In this chapter we introduce a different formulation of the Fibonacci phase based on a model of interacting Majorana fermions. Our starting point is a system of chiral Majorana edge states, which can in principle be realized in SC proximity effect structures. We show that a particular four fermion interaction leads to an essentially exactly solvable model that realizes the Fibonacci phase. In addition to providing a direct route to the Fibonacci phase *without parafermions*, our theory reveals a distinct but closely related "anti-Fibonacci" state that is a kind of particle-hole conjugate to the Fibonacci state with a topological order that combines Ising and Fibonacci. Our formulation also suggests a method for experimentally probing the Fibonacci state. We introduce a generalization of the interferometer introduced

earlier for Majorana states[112, 113], and argue that it provides a method for unambiguously detecting Fibonacci order.

The fact that interacting Majorana fermions can exhibit a Fibonacci phase is foreshadowed by Rahmani, et al. [114](RZFA), who showed that a 1D Majorana chain with strong interactions can be tuned to the tricritical Ising (TCI) critical point. The same critical point arises in the 1D "golden chain" model of coupled Fibonacci anyons[115], as well as at interfaces connecting Ising and Fibonacci order in the QH effect[116]. There is a sense in which the TCI point of the RZFA model is like a Fibonacci chain, but it is not clear how to extend it to 2D. Our theory provides a method for accomplishing that.

3.2 $SO(7)_1/(G_2)_1$ Coset

Mong et al. [110] formulated the Fibonacci phase using a "trench" construction that began with 1D strips of $\nu = 2/3$ QH states coupled along trenches in the presence of a SC. A single trench mapped to the 3 state clock model, with a critical point described by the Z_3 parafermion conformal field theory (CFT). The resulting 1D states were coupled to create a gapped 2D phase.

This is similar to the coupled wire construction[117] for the Read Rezayi state introduced in Ref. [118], but differs in an important way. That model was based on the coset construction[119–121], which allows a simple CFT ($[SU(2)_1]^3$ with central charge $c = 3$) to be factored into less trivial CFTs ($SU(2)_3 + SU(2)_1^3/SU(2)_3$ with

$c = 9/5 + 6/5$). This exact factorization identifies a solvable coupled wire Hamiltonian, where counter-propagating modes of the two factors pair up differently, resulting in a non-trivial unpaired chiral edge mode.

Different from previous proposals, our construction of the Fibonacci phase is based on the coset $SO(7)_1/(G_2)_1$[123] without Z_3 parafermions. $SO(7)_1$ describes 7 free chiral Majorana modes with $c = 7/2$. G_2 is a Lie group that sits inside $SO(7)$. $(G_2)_1$, with $c = 14/5$, is the Fibonacci CFT[110, 124]. The quotient is a CFT with

$$c = 7/2 - 14/5 = 7/10, \tag{3.2.1}$$

which can be identified with the TCI model. Thus, the edge states of a non-interacting T-SC with Chern number $n = 7$ factor into a $(G_2)_1$ Fibonacci (FIB) sector and a $SO(7)_1/(G_2)_1$ TCI sector. In the following we will design an interaction that separates the factors and leads to $2D$ topological phases with either $c = 14/5$ (Fibonacci) or $c = 7/10$ (anti-Fibonacci) edge states.

We begin with some facts about G_2, which is well known in mathematical physics[123, 125]. G_2 is the simplest exceptional Lie group. Its relation to $SO(7)$ involves the mathematics of the octonion division algebra[126]. An octonion is specified by 8 real numbers: $q = q_0 + \sum_{a=1}^{7} q_a e_a$, where e_a are 7 square roots of -1 that satisfy the non-associative multiplication rule

$$e_a e_b = -\delta_{ab} + C_{abc} e_c. \tag{3.2.2}$$

C_{abc} is a totally antisymmetric tensor. It is not unique, but can be chosen to

satisfy[126]

$$C_{a+1b+1c+1} = C_{abc}, \quad C_{124} = 1, \tag{3.2.3}$$

where the indices are defined mod 7. Eq. 3.2.3 along with antisymmetry specifies all the non-zero elements of C_{abc}. e_a define a set of 7 unit vectors that transform under $SO(7)$. However, not all $SO(7)$ rotations preserve (3.2.2). G_2 is the automorphism group of the octonions: the subgroup of $SO(7)$ that preserves C_{abc}.

The 21 generators of $SO(7)$ can be represented by 7×7 skew symmetric matrices $T^{m,n}$ of the form $T^{m,n}_{ab} = i(\delta_{ma}\delta_{nb} - \delta_{mb}\delta_{na})$. There are 14 combinations that preserve C_{abc}, which can be written[125]

$$M^A = \begin{cases} \frac{T^{A,A+2} - T^{A+1,A+5}}{\sqrt{2}} & 1 \leq A \leq 7 \\ \frac{T^{A,A+2} + T^{A+1,A+5} - 2T^{A+3,A+4}}{\sqrt{6}} & 8 \leq A \leq 14. \end{cases} \tag{3.2.4}$$

These matrices are normalized by $\mathrm{Tr}[M^A M^B] = 2\delta_{AB}$ and represent the generators of G_2 in the 7D fundamental representation, analogous to the Pauli matrices of $SU(2)$. In what follows, it will be useful to express the quadratic Casimir operator as

$$\sum_A M^A_{ab} M^A_{cd} = \frac{2}{3}(\delta_{ad}\delta_{bc} - \delta_{ac}\delta_{bd}) - \frac{1}{3} * C_{abcd} \tag{3.2.5}$$

where $*C_{abcd} = \epsilon_{abcdefg} C_{efg}/6$ is the dual of C_{abc} whose non-zero elements follow from $*C_{3567} = -1$, as in (3.2.3).

We now consider the coset factorization of a 1D system of 7 free chiral Majorana fermions described by

$$H_0 = -\frac{iv}{2} \sum_{a=1}^{7} \gamma_a \partial_x \gamma_a. \tag{3.2.6}$$

We adopt a Hamiltonian formalism[1] with Majorana operators satisfying $\{\gamma_a(x), \gamma_b(x')\} = \delta(x-x')\delta_{ab}$. H_0 describes a $SO(7)_1$ Wess Zumino Witten (WZW) model with $c = 7/2$. The coset construction allows this to be written $H_0 = H_{\rm FIB} + H_{\rm TCI}$. The FIB sector is expressed in terms of $(G_2)_1$ currents in Sugawara form [121][2],

$$H_{\rm FIB} = \sum_A \frac{\pi v J^A J^A}{k+g}, \quad J^A = \sum_{ab} \frac{1}{2} M^A_{ab} \gamma_a \gamma_b, \tag{3.2.7}$$

with $k = 1$, $g = 4$. Using (3.2.5), the operator product gives

$$\begin{aligned} H_{\rm FIB} &= -\frac{2iv}{5} \sum_a \gamma_a \partial_x \gamma_a - \frac{\pi v}{60} \sum_{abcd} *C_{abcd} \gamma_a \gamma_b \gamma_c \gamma_d, \\ H_{\rm TCI} &= -\frac{iv}{10} \sum_a \gamma_a \partial_x \gamma_a + \frac{\pi v}{60} \sum_{abcd} *C_{abcd} \gamma_a \gamma_b \gamma_c \gamma_d. \end{aligned} \tag{3.2.8}$$

The correlator of $H_{\alpha={\rm FIB,TCI}}$ is $\langle H_\alpha(x) H_\beta(x')\rangle = v^2 \delta_{\alpha\beta} c_\alpha / 8\pi^2 (x-x')^4$, with $c_{\rm FIB} = 14/5$ and $c_{\rm TCI} = 7/10$ [3]. This shows that H_0 decouples into two independent sectors, as depicted in Fig. 3.2.1a.

$H_{\rm FIB}$ describes a $(G_2)_1$ WZW model, with two primary fields 1, τ of dimension $h = 0, 2/5$. τ transforms under the 7D representation of G_2 and obeys the Fibonacci fusion algebra $\tau \times \tau = 1 + \tau$. $H_{\rm TCI}$ describes the $M(5,4)$ minimal CFT with 6 primary fields 1, ϵ, ϵ', ϵ'', σ, σ', with $h = 0$, 1/10, 3/5, 3/2, 3/80, 7/16[121]. The

[1]The Hamiltonian density is equivalent to the CFT energy momentum tensor on a cylinder: $H_0 = vT_{\rm cyl}/2\pi$.

[2]In addition to [127], J^A differs in normalization from the WZW current defined in Ref. [121], which is $2\pi J^A$

[3]Note that $\langle \gamma_a(x)\gamma_b(0)\rangle = \delta_{ab}/2\pi i x$ and $\sum *C^2_{abcd} = 168$.

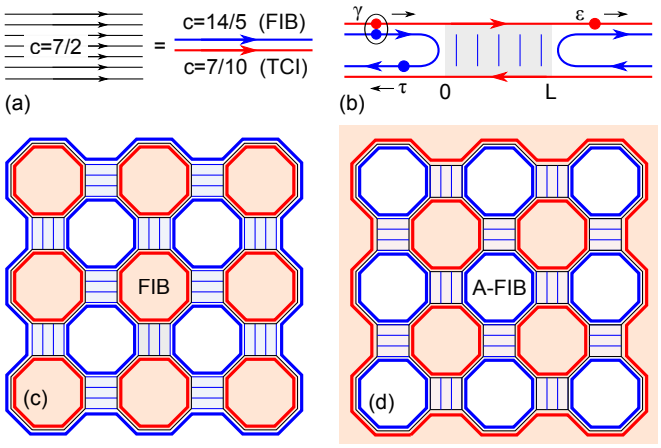

Figure 3.2.1: (a) 7 chiral Majorana edge modes factor into FIB and TCI sectors with $c = 14/5 + 7/10 = 7/2$. (b) A 1D non-chiral system with interaction $\lambda \sum_A J_R^A J_L^A$ transmits the TCI sector, but reflects the FIB sector. The bottom panels show network constructions for the Fibonacci phase (c) and the anti-Fibonacci phase (d).

Majorana fermion operator γ_a factors into the product

$$\gamma_a = \tau_a \times \epsilon \tag{3.2.9}$$

with $h = 2/5 + 1/10 = 1/2$. The 21 bilinears $i\gamma_a\gamma_b$ decompose into 14 J^A's, along with 7 operators $\tau_a \times \epsilon'$ with $h = 2/5 + 3/5 = 1$. J^A act only in the FIB sector: $[J^A, H_{\rm TCI}] = 0$. The trilinear combination $C_{abc}\gamma_a\gamma_b\gamma_c$ is ϵ'' with $h = 3/2$ and acts only in the TCI sector.

3.3 G_2 Interactions and Network Construction

We now introduce a 1D model of 7 non-chiral Majorana fermions $\gamma_{aR/L}$with an interaction that gaps the FIB sector, leaving the TCI sector gapless. Consider

$$H = -\frac{iv}{2}\sum_a (\gamma_{aR}\partial_x\gamma_{aR} - \gamma_{aL}\partial_x\gamma_{aL}) + \lambda \sum_A J_R^A J_L^A, \tag{3.3.1}$$

where $J^A_{R/L}$ are given in (3.2.7). The λ term commutes with $H_{\rm TCI}$, so it operates only in the FIB sector. A perturbative renormalization group analysis gives $d\lambda/d\ell = -2\lambda^2/\pi v$, so $\lambda < 0$ is marginally relevant. When λ flows to strong coupling it is natural to expect that it leads to a gap $\Delta \propto e^{-\pi v/2|\lambda|}$ in the FIB sector and a gapless TCI critical point. This is similar to the RZFA model, except the G_2 symmetry locates the critical point exactly.

The exact factorization allows the two sectors to be separated. Consider the 1D system in Fig. 3.2.1b, with $\lambda(x) \neq 0$ for $0 < x < L$. Provided $L \gg \xi = v/\Delta$, the gap in the FIB sector leads to an exponential suppression of transmission. The FIB sector will be perfectly reflected, while the TCI sector will be perfectly transmitted. Interestingly, this means an incident Majorana fermion γ_a *splits*, with τ_a reflected and ϵ transmitted. This forms the basis for the interferometer to be discussed below.

We wish to use (3.3.1) to construct a 2D gapped topological phase. One approach is to adapt the coupled wire model[117]. This requires coupling right movers of the TCI sector on wire i to left movers of the TCI sector on wire $i+1$. If this gaps the TCI sector, then we will have a 2D gapped phase with TCI edge states. This is problematic, however, because the simplest tunneling term that can be built from local operators and does not couple to the gapped FIB sector is the trilinear $C_{abc}\gamma_a\gamma_b\gamma_c$. The resulting tunneling term $u\epsilon''_{iR}\epsilon''_{i+1L}$, with dimension 3, is perturbatively irrelevant. This does not preclude the possibility of a gapped phase for large u, but a non-perturbative analysis would be necessary to establish it. Fortunately,

however, the exact factorization of the coset model allows for an alternative *network construction*, inspired by the Chalker Coddington model[130].

Fig. 3.2.1c shows a network of $n = 7$ T-SC islands in which each island has 7 chiral Majorana modes. In the absence of coupling the Majorana modes are localized on each island, so the system is a trivial SC. If the islands are strongly coupled by single particle tunneling they will merge, and the system is a $n = 7$ T-SC. In the absence of interactions, the transition between these phases will have 7 gapless $2 + 1D$ Majorana modes. For strong interactions intermediate topological phases can arise. We turn off the single particle tunneling and couple the neighboring islands with the interaction term in (3.3.1). Provided the contact length $L \gg \xi$, the excitations in the FIB sector will be reflected from the contact, which means they are transmitted to the next island. Excitations in the TCI sector, however, are transmitted by the contact, so they remain localized on the same island. From Fig. 3.2.1c, it can be seen that both the TCI and the FIB sectors are localized in the interior of the network. The TCI states are localized on the islands, while the FIB states are localized on the dual lattice of voids between the islands. Since all bulk states are localized in finite, lattice scale regions, there will be a bulk excitation gap. The perimeter of the network, however has a gapless FIB edge state with $c = 14/5$. We emphasize that though fine tuning is required to achieve the exactly solvable Hamiltonian (3.3.1), the tuning does *not* need to be perfect. This gapped Fibonacci *phase* will be robust to finite single particle tunneling and other interactions.

	1	ψ	σ_i
1	1	ϵ''	σ'
τ	ϵ'	ϵ	σ

Table 3.3.1: The 6 quasiparticles of the TCI model can be identified with combinations of Ising and Fibonacci quasiparticles.

Fig. 3.2.1d shows a similar network that is surrounded by a $n = 7$ chiral Majorana edge state. This leads to a distinct phase that also has a bulk gap, but has TCI edge states with $c = 7/10$. This state can be viewed as a Fibonacci phase sitting inside a $n = 7$ T-SC, with $c = 7/2 - 14/5$. We call this the "anti-Fibonacci" in analogy with the "anti-pfaffian" [131, 132], which is the pfaffian sitting inside a $\nu = 1$ QH state. The anti-Fibonacci has a topological order associated with the TCI CFT. However, the 6 TCI quasiparticles can also be understood as a combination of 1, τ Fibonacci quasiparticles with the 1, ψ, σ_i Ising quasiparticles. The TCI fusion rules[121] of the quasiparticles identified in Table 1 are reproduced by the simpler Fibonacci and Ising fusion rules (e.g. $\sigma_i \times \sigma_i = 1 + \psi$). Similar fusion rule decompositions have been identified for other theories[116, 124]. As in the T-SC σ and σ' are not dynamical quasiparticles, but they will be associated with $h/2e$ vortices in the SC. Depending on the energetics, a SC vortex in the anti-Fibonacci phase will bind either a σ or σ'. If it is σ, then the vortex binds a Fibonacci anyon. Likewise in the Fibonacci phase, a vortex could bind 1 or τ[110].

The above considerations suggest a possible route towards realizing the Fi-

bonacci phase is to start with a system close to a multi-component T-SC - trivial SC transition. This could be achieved by introducing SC via the proximity effect into a 2D electron gas in the vicinity of a quantum Hall plateau transition with degenerate Landau levels. Progress in this direction has recently been reported in a quantum anomalous Hall insulator coupled to a SC, where a plateau observed in the two terminal conductance was attributed to T-SC[102]. Another promising venue is graphene, which has a four-fold degenerate zeroth Landau level. Coexistence of SC with the quantum Hall effect in these systems appears feasible[133, 134].

3.4 Fibonacci Interferometer

If the Fibonacci and/or the anti-Fibonacci T-SC can be realized, then it will be important to develop experimental protocols for probing them. One approach is to measure the thermal Hall conductance, which directly probes the central charge c of the edge states: $\kappa_{xy} = c\pi^2 T k_B^2/3h$. This has proven to be a powerful method for identifying the topological order of QH states[34, 135, 136], but it does not directly probe the non-Abelian quasiparticle statistics. In the QH effect, Fabry Perot[137–139] and Mach Zehnder[140, 141] interferometers have been proposed for this purpose. Here we introduce a distinct interferometer that generalizes the Majorana fermion interferometer[112, 113].

Fig. 3.4.1 shows a Hall bar with 4 Ohmic contacts (C1-4) where the electron density is adjusted so that adjacent regions have QH filling factors $\nu = 1$ and $\nu = 4$.

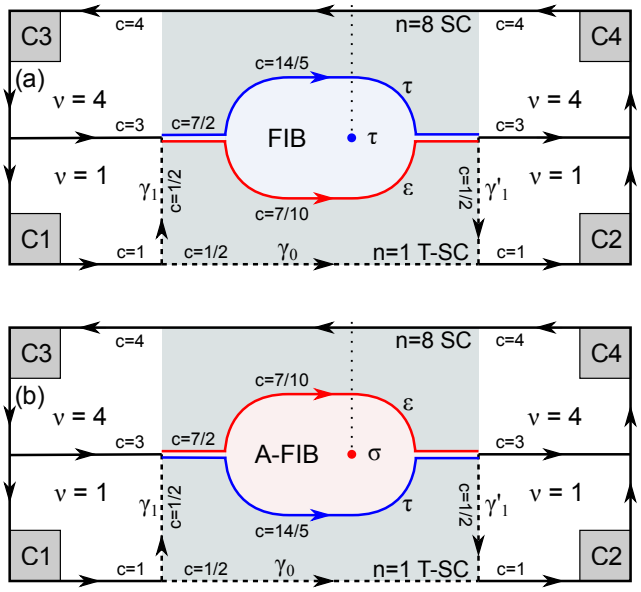

Figure 3.4.1: A Fibonacci interferometer in a Hall bar with Ohmic contacts C1-4 and SC in the shaded region. Dirac (Majorana) edge states are indicated by solid (dashed) lines. The $c = 7/2$ edge splits into FIB and TCI edges around the Fibonacci (a) or anti-Fibonacci (b) island. A quasiparticle adds a branch cut (dotted line) that modifies transmission from C1 to C2.

The middle is coupled to a SC that leads to a $n = 1$ T-SC region and a trivial $n = 8$ SC region. We assume that at the boundary between the $n = 1$ and $n = 8$ SCs there is an island of either Fibonacci (Fig. 3.4.1a) or anti-Fibonacci (Fig. 3.4.1b). This leads to the pattern of edge states shown.

Suppose contact $C1$ is at voltage V_1, and that the SC and the other 3 contacts are grounded. We compute the current I_2 in C2 using a Landauer-Büttiker formalism. The current operator for the $\nu = 1$ edge entering C2 is proportional to $i\gamma_0\gamma_1'$. γ_0 comes directly from C1, but γ_1' comes from the region where τ and ϵ split and then recombine. First suppose there are no quasiparticles on the island. γ_1' will be a linear combination $\sum_{j=1}^{7} t_{1j}\gamma_j$ of the incident Majorana modes, where t_{ij} is a real

orthogonal scattering matrix and γ_{2-7} are associated with the $c = 3$ edge. Ignoring the contributions from the grounded contact C3, $i\gamma_0\gamma_1' = t_{11} i\gamma_0\gamma_1$. This relates I_2 to the current coming out of C1, $I_2 = t_{11}(e^2/h)V_1$.

Quasiparticles localized on the island will modify this result. The transmitted particles will encounter a branch cut due to non-Abelian statistics that can modify the state of the localized quasiparticle. Provided the local Hamiltonian near the edge is not modified by the presence of the extra quasiparticle, this will be purely of topological origin. The expectation value of the current will only be non-zero if the localized quasiparticle returns to its original state. The probability amplitude that anyon a returns to its original state when circled by anyon b is given by the *monodromy matrix*[139] $M_{ab} = S_{ab}S_{11}/S_{a1}S_{b1}$, which depends the topological data in the modular S-matrix S_{ab}. We therefore predict

$$I_2 = \frac{e^2}{h} t_{11} M_{ab} V_1, \tag{3.4.1}$$

where a and b are labels for the transmitted and localized quasiparticles. Provided quasiparticles can be introduced to the island without modifying t_{11}, (which depends on the local Hamiltonian near the edges) the ratios of the conductances for different localized quasiparticles will be *universal* (note $M_{a1} = 1$). Other proposed interferometric measurements of Fibonacci statistics have challenges similar to controlling t_{11}[124, 139]. A possible (albeit more complicated) way to overcome that is to include a contact inside the island that allows quasiparticles to come and go, leading to telegraph noise[143].

For the FIB phase, where the transmitted quasiparticle is τ the universal ratio is determined by

$$M_{\tau\tau}^{\mathrm{FIB}} = -1/\varphi^2, \tag{3.4.2}$$

where $\varphi = (1+\sqrt{5})/2$ is the golden mean. In the A-FIB phase, the ratios are determined by $M_{\epsilon b}^{\mathrm{TCI}}$ for $b = 1, \epsilon, \epsilon', \epsilon'', \sigma, \sigma'$. These can be evaluated from the 6×6 TCI S-matrix[114]. However, the same results are obtained by treating the A-FIB as the FIB sitting inside Ising. Then, $M_{\epsilon b}^{\mathrm{TCI}} = M_{\psi b_i}^{\mathrm{I}} M_{\tau b_f}^{\mathrm{FIB}}$, where $b_{i(f)}$ are the Ising (Fibonacci) decomposition of particle b from Table 1. The non-trivial Ising term is $M_{\psi\sigma_i}^{\mathrm{I}} = -1$ (which is probed in the Majorana interferometer). In the A-FIB state, if a vortex binds σ, the extra quasiparticle can be controlled with a magnetic flux, and $M_{\epsilon\sigma}^{\mathrm{TCI}} = +1/\varphi^2$.

Chapter 4

Fractional Excitonic Insulator

$$3 \; or \; \frac{1}{3}$$

4.1 Introduction

The quantum Hall effect was originally understood as a consequence of the emergence of Landau levels for two dimensional electrons in a magnetic field [2], but was reformulated in the framework of topological band theory [144]. This introduced the notion of "Chern bands", which have a rich structure due to the interplay between lattice translations and magnetic translations [145], and allow for the existence of a Chern insulator in the absence of a uniform magnetic field [35]. There is a sense in which all quantum Hall states are the same and can be adiabatically connected to a flat band limit that resembles a Landau level. However, the *opposite* to the

flat band limit occurs near a quantum Hall transition, which occurs when the conduction band and valence band invert at a Dirac point [146]. A weakly inverted quantum Hall state differs from a trivial insulator only near the Dirac point, and can be viewed as a quantum fluid formed by the low energy electrons and holes of the original trivial insulator. The band inversion paradigm has proven to be a powerful tool for engineering topological phases of non-interacting fermions [3, 27, 147, 148].

In recent years there has been effort to study analogs of the Chern insulator for the fractional quantum Hall (FQH) effect. Theoretical work has focused on the proposal for creating nearly flat Chern bands [149–151] that can be fractionally filled and can host states—called fractional Chern insulators [152]—that resemble the Laughlin state of a fractionally filled Landau level (see the reviews [153–155] and references therein). Experimental progress has been reported in twisted bilayer graphene [156], where the commensuration with the moiré pattern leads to interesting structure in the observed FQH states at finite magnetic field. The zero field fractional Chern insulator is more challenging because it requires a non-stoichiometric band filling. Here we consider the opposite limit and propose a wavefunction describing a *fractional excitonic insulator*: a gapped FQH state built from a strongly correlated fluid of electrons and holes. We argue that this provides an alternative route to realizing a FQH state at zero field in a stoichiometric system that is close to a special kind of band inversion.

We consider a wavefunction inspired by the celebrated Laughlin wavefunction [157]

of the form

$$|\Psi_m\rangle = \sum_N \frac{f^N}{N!}|\psi_m^N\rangle, \tag{4.1.1}$$

where $|\psi_m^N\rangle$ describes a state with N electrons and holes described by a Jastrow wavefunction

$$\psi_m^N(\{z_i, w_j\}) = \frac{\prod_{i<i'}(z_i - z_{i'})^m \prod_{j<j'}(w_j - w_{j'})^m}{\prod_{i,j}(z_i - w_j)^m}. \tag{4.1.2}$$

Here $z_{1,\ldots,N}$ ($w_{1,\ldots,N}$) are complex coordinates for electrons (holes) and m is an odd integer. ψ_m^N is similar to a Halperin bilayer wavefunction [158], except that the Gaussian associated with the lowest Landau level is absent, and it has a singular denominator. The denominator can be fixed without changing the long distance behavior by introducing a cutoff ξ in a prefactor $\prod_{ij} h(|z_i - w_j|/\xi)$, where $h(x \to 0) \sim x^{2m}$ and $h(x \to \infty) = 1$ [159]. A similar wavefunction was mentioned by Dubail and Read [204] in connection with tensor network trial states. Like them, we will argue that $|\Psi_m\rangle$ is topologically equivalent to a single component $\nu = 1/m$ Laughlin state.

4.2 Chern Insulator from p-wave Excitonic Pairing

We will begin by showing that for $m = 1$, $|\Psi_1\rangle$ (despite the denominator) is the *exact* ground state of a simple non-interacting model of a Chern insulator, and can be viewed as a condensate of $p+ip$ excitons. We then present several pieces of evidence

that $|\Psi_{m>1}\rangle$ describes a FQH state. This includes an analysis of the Laughlin plasma analogy, as well as the ground state degeneracy on a torus. We introduce a composite fermion mean field theory as well as a coupled wire model that reproduce the phenomenology of the FQH state. We also identify an interacting Hamiltonian whose exact ground state is (4.1.2). Finally, we propose that a feasible route towards realizing this state is to find a material whose band structure features the touching of two bands that differ in angular momentum by 3. We argue that coupling the bands favors excitonic pairing in a $(p_x + ip_y)^3$ channel, and that interactions could stabilize the $m = 3$ state.

To describe the $m = 1$ state, consider the non-interacting spinless fermion Hamiltonian,

$$\mathcal{H}_1 = \sum_{\mathbf{k}} \epsilon_{\mathbf{k}} (c^\dagger_{e\mathbf{k}} c_{e\mathbf{k}} + c^\dagger_{h\mathbf{k}} c_{h\mathbf{k}}) + \Delta_{\mathbf{k}} c^\dagger_{e\mathbf{k}} c^\dagger_{h-\mathbf{k}} + h.c., \tag{4.2.1}$$

with

$$\epsilon_{\mathbf{k}} = (k^2 - v^2)/2; \quad \Delta_{\mathbf{k}} = iv(k_x - ik_y). \tag{4.2.2}$$

This is a two band model in which $c^\dagger_{e(h)\mathbf{k}}$ create conduction band electrons (valence band holes). We particle-hole transformed the valence band, so that the vacuum $|0\rangle$ (annihilated by $c_{e,h\mathbf{k}}$) is the topologically trivial filled valence band. This model is properly regularized for $k \to \infty$, and describes a Chern insulator in which the conduction and valence bands are inverted at $\mathbf{k} = 0$. Note that (4.2.2) has a single parameter v [1]. The coefficient of k^2 can be fixed by a choice of units, but a more

[1]The phase of $\Delta_{\mathbf{k}}$ can be chosen by defining the phase of $c_{h\mathbf{k}}$. The choice in (4.2.2) makes f

generic model [161, 162] has independent coefficients for the other terms. For this particular choice the energy eigenvalues are $\pm E_{\mathbf{k}} = \pm(k^2 + v^2)/2$. The analysis of this model is similar to the BCS theory of superconductivity. The ground state is

$$|\Phi_{m=1}\rangle = \prod_{\mathbf{k}} (u_{\mathbf{k}} + v_{\mathbf{k}} c^\dagger_{e\mathbf{k}} c^\dagger_{h-\mathbf{k}})|0\rangle, \tag{4.2.3}$$

where $u_{\mathbf{k}} = i(k_x + ik_y)/\sqrt{2E_{\mathbf{k}}}$ and $v_{\mathbf{k}} = v/\sqrt{2E_{\mathbf{k}}}$. Following the Read Green analysis of a $p + ip$ superconductor [27], this can be written in the real space form

$$|\Phi_{m=1}\rangle \propto e^{\int d^2\mathbf{z} d^2\mathbf{w} g(\mathbf{z}-\mathbf{w}) \psi^\dagger_e(\mathbf{z}) \psi^\dagger_h(\mathbf{w})}|0\rangle, \tag{4.2.4}$$

where $c^\dagger_{e,h\mathbf{k}}$ and $g_{\mathbf{k}} \equiv v_{\mathbf{k}}/u_{\mathbf{k}} = -iv/(k_x + ik_y)$ have Fourier transforms $\psi^\dagger_{e,h}(z = x + iy)$ and $g(z) = v/(2\pi z)$. $|\Phi_{m=1}\rangle$ then has the form (4.1.1) with $f = v/(2\pi)$ and

$$\phi^N_{m=1}(\{z_i, w_j\}) = \det\left[\frac{1}{z_i - w_j}\right]. \tag{4.2.5}$$

The equivalence of $\phi^N_{m=1}$ and $\psi^N_{m=1}$ follows from the Cauchy determinant identity [163], which can be checked by writing the determinant over a common denominator, noting its units and antisymmetry.

Though the precise form of $g(\mathbf{z})$ that makes the Jastrow form exact is particular to our choice of parameters, the topological structure of the Chern insulator dictates that the $1/z$ behavior for $z \to \infty$ remains in a more generic theory. The short distance behavior, however, depends on the details as well as the lattice cutoff. A related model was studied in Ref. [162], where the connection was made to a Halperin $(1, 1, -1)$ bilayer state. Viewed as a bilayer system, this is related to

in (4.1.1) real.

a $(1,1,1)$ state by a particle-hole transformation in one layer [164]. The $(1,1,1)$ state describes a single component "spin polarized" quantum Hall fluid with broken spin symmetry. In our problem the spin symmetry corresponds to the independent conservation of electrons and holes, which is violated by the "p+ip pairing term" $\Delta_{\mathbf{k}}$. Thus, we can view the Chern insulator as an *excitonic insulator* that is distinguished from the trivial insulator by a condensation of $p+ip$ excitons. Unlike the original excitonic insulator [166, 195], this condensation does not involve a spontaneously broken symmetry, since electrons and holes are not independently conserved. It is analogous to a *proximitized* $p+ip$ superconductor.

4.3 Fractional Excitonic Insulator From Wavefunction Analysis

Encouraged by the success of $|\Psi_{m=1}\rangle$, we now consider the generalization to a fractional excitonic insulator. To motivate that this should be possible, we first introduce a composite fermion mean field theory. Consider a $2D$ two band system and perform a statistical gauge transformation that attaches $\pm(m-1)$ flux quanta to the electrons (holes) [167]. This is accomplished in Eqs. (4.2.1) and (4.2.2) by replacing $\mathbf{k}c_{e(h)\mathbf{k}} \to (-i\nabla \pm \mathbf{a})\psi_{e(h)}$, where the statistical vector potential satisfies

$$\nabla \times \mathbf{a} = 2\pi(m-1)(\psi_e^\dagger \psi_e - \psi_h^\dagger \psi_h). \tag{4.3.1}$$

Equivalently, in a Lagrangian formulation, flux attachment is implemented by adding a Chern-Simons term $\mathcal{L}_{CS} = \epsilon_{\mu\nu\lambda} a_\mu \partial_\nu a_\lambda / (4\pi(m-1)) \equiv a\partial a / 4\pi(m-1)$ [168]. This is different from the conventional composite fermion model, because in the valence band flux is attached to the *holes* rather than the electrons. This transformation has no effect on electrons deep in the valence band and is compatible with exact particle-hole symmetry [169].

When the electron and hole densities are equal, the average statistical flux seen by each particle is zero. Thus, in mean field theory we can consider a system of composite fermions with Hamiltonian given by (4.2.1) and (4.2.2). Assuming the composite fermions are in a Chern insulator phase, we integrate them out in the presence of $\mathbf{a}$ and the external vector potential $\mathbf{A}$. This leads to $\mathcal{L}_{\text{eff}} = \mathcal{L}_{CS} + (a + A)\partial(a + A)/4\pi$. Integrating out $\mathbf{a}$ then gives $\mathcal{L}_{\text{eff}} = A\partial A / 4\pi m$. This shows the resulting phase is a FQH state with $\sigma_{xy} = (1/m)e^2/h$. A second indication this phase is possible is provided by the coupled wire construction [117]. In Appendix 4.A, we show that an array of alternating n-type and p-type wires can support this phase at zero magnetic field.

We now analyze the wavefunction of Eq. (4.1.1) and (4.1.2). To determine whether it describes a FQH fluid, we follow Laughlin [157] and view $\langle \Psi_m | \Psi_m \rangle$ as the partition function of a classical plasma. Like Laughlin's plasma, our charges interact by a 2D Coulomb interaction $-\beta V = \sum_{i<j} 2m q_i q_j \log |z_i - z_j| / \xi$, where m plays the role of inverse temperature. Unlike Laughlin's plasma, our plasma

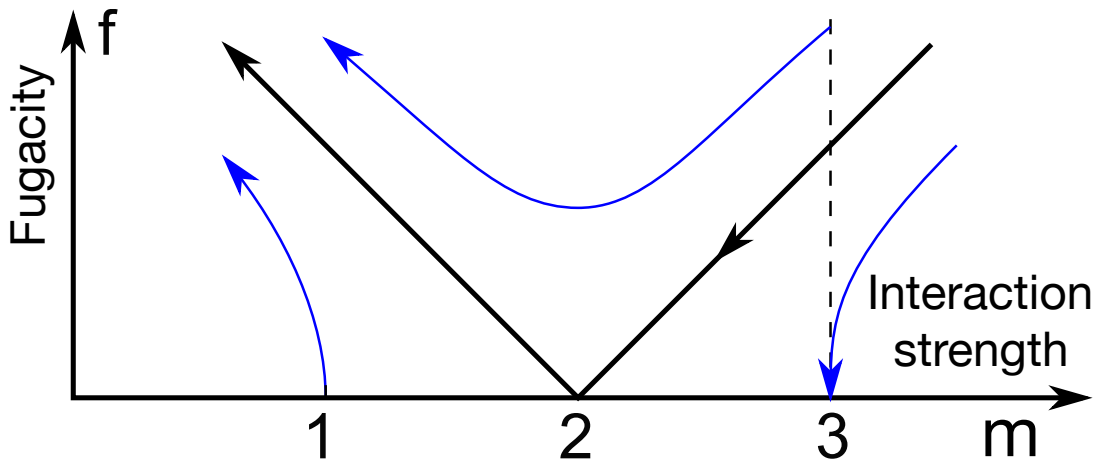

Figure 4.3.1: Kosterlitz Thouless renormalization group flow diagram [170] for the plasma analogy of (4.1.1) and (4.1.2) as a function of fugacity f and the coefficient of the Coulomb interaction, the bare value of which is controlled by m.

has charges $q_i = \pm 1$, and the neutralizing background (due to the Gaussian) is absent. It is in the grand canonical ensemble with a fugacity f. This plasma maps precisely to the Kosterlitz Thouless problem [170, 204], and exhibits two phases: a high temperature phase characterized by perfect screening, and a low temperature phase with bound charges. For small f the transition is determined by balancing the energy $m \log L$ of an unbound charge with the entropy $\log L^2$ giving a critical point at $m = 2$. For $m = 1$ the plasma is in the screening phase, which is consistent with our understanding of $|\Psi_1\rangle$ as a quantum Hall state. For $m = 3$ the plasma is in a bound phase for small f. This is similar to the Laughlin wavefunction for large m, which describes a crystal. However, for larger f screening renormalizes the Coulomb interaction, and a screening phase is expected above a critical value of f, as indicated in Fig. 4.3.1. Since the only length in the problem is the cutoff scale

ξ, the screening phase will occur at high density, when electrons and holes have a typical separation of order ξ.

The structure of the plasma analogy is reminiscent of the wire construction for the $\nu = 1/m$ state [117], which involves coupling edge states with an irrelevant sine-Gordon type coupling that leads to exactly the same plasma. The correspondence of the plasmas is not an accident, given the expectation that the ground state wavefunction can be interpreted as a correlator of the same conformal field theory that describes the edge states [26]. The only difference with the conventional Laughlin state is the absence of the background charge. Following this logic, we construct a wavefunction for a quasi-hole at position Z as

$$\psi_N^{e^*}(Z, \{z_i, w_j\}) = \prod_i \frac{Z - z_i}{Z - w_i} \psi_N(\{z_i, w_j\}). \tag{4.3.2}$$

In the plasma analogy, this state has an external charge at Z. Assuming the plasma perfectly screens, this leads to a charge $e^* = e/m$ quasi-hole. Quasi-electron states are constructed similarly by exchanging z_i and w_j.

Another probe of topological order is the ground state on a torus, which may also be useful for numerical studies. Following Haldane and Rezayi [171], we consider a torus with $z = z + L$ and $z = z + L\tau$ identified (τ is a complex number describing the shape of the torus). The periodic generalization of (4.1.2) then involves two modifications. First, the terms in the denominator become

$$(z_i - w_j)^m \to \vartheta_1(\pi(z_i - w_j)/L|\tau)^m, \tag{4.3.3}$$

where $\vartheta_1(u|\tau)$ is the odd elliptic theta function [172]. The terms in the numerator

are modified similarly. Second, ψ_m^N is multiplied by a function of the center of mass coordinates $Z = \sum_i z_i$, $W = \sum_j w_j$, given by

$$F_{CM}(Z, W) = e^{iK(Z-W)}\vartheta_1(\pi(Z - W - z_0)/L|\tau)^m. \tag{4.3.4}$$

From the periodicity properties of $\vartheta_1(u|\tau)$, it can be checked that this modified wavefunction is properly periodic, with K and z_0 depending on the phase twisted boundary conditions. For fixed boundary conditions there are m independent choices for K and z_0, establishing the m-fold ground state degeneracy. We have also checked that for $m = 1$ the non-interacting ground state of (4.2.2) on a torus has the form $\det[g(z_i - w_j)]$, with $g(z) \propto e^{iKz}\vartheta_1(\pi(z - z_0)/L|\tau)/\vartheta_1(\pi z/L|\tau)$. ($K, z_0$ again depend on boundary conditions). A generalization of the Cauchy identity [173] shows that this is precisely equivalent to the wavefunction described above.

4.4 Designer Hamiltonian and Higher Angular Momentum Pairing

Having established that (4.1.1) and (4.1.2) describe an excitonic fractional quantum Hall state, we now seek a Hamiltonian that can realize it. One approach is to find an "exact question to the answer": a Hamiltonian designed to have $|\Psi_m\rangle$ as its exact ground state [174]. While we do not have an analog of the two body δ-function type interaction [175] that stabilizes the Laughlin state, we adopt the construction in Ref. [176], which provides a natural generalization of (4.2.2) to $m > 1$ at the

price of introducing several-body interactions. By applying $\partial_{z_j^*} \equiv \frac{1}{2}(\partial_{x_j} + i\partial_{y_j})$ (or $\partial/\partial_{w_j^*}$) to (4.1.2) and noting that due to analyticity only the poles contribute, we show in Appendix 4.B.1 that the operators

$$Q_e(z) = 2\partial_{z^*}\psi_e - v_m\psi_h^\dagger(\partial_z - ia)^{m-1}$$
$$Q_h(z) = 2\partial_{z^*}\psi_h - v_m\psi_e^\dagger(\partial_z + ia)^{m-1} \tag{4.4.1}$$

satisfy $Q_{e,h}(z)|\Psi_m\rangle = 0$. Here $v_m = 2\pi f/(m-1)!$, and ∂_z acts to the left on $\psi_{h,e}^\dagger(z)$ and

$$a(z) = m\int d^2u \frac{\rho(u)}{i(z-u)}; \quad \rho = \psi_e^\dagger\psi_e - \psi_h^\dagger\psi_h. \tag{4.4.2}$$

This can be interpreted as $a(z) = a_x - ia_y$, where $\mathbf{a}$ is a statistical vector potential similar to (4.3.1), except with m fluxes per particle, rather than $m-1$. We then define

$$\mathcal{H}_m = \frac{1}{2}\int d^2\mathbf{z}\left[Q_e^\dagger(z)Q_e(z) + Q_h^\dagger(z)Q_h(z)\right]. \tag{4.4.3}$$

Since $\mathcal{H}_m$ is the sum of positive operators, $|\Psi_m\rangle$ is guaranteed to be a ground state.

For $m = 1$, $Q_{e,h}(z)$ is the Fourier transform of $\sqrt{2E_\mathbf{k}}\gamma_{e,h\mathbf{k}}$, where $\gamma_{e(h)\mathbf{k}} = u_{\pm\mathbf{k}}c_{e(h)\mathbf{k}} \pm v_{\pm\mathbf{k}}c_{h(e)-\mathbf{k}}^\dagger$ are Bogoliubov quasiparticle annihilation operators. It follows that (4.4.3) reduces to (4.2.1) and (4.2.2) up to an additive constant. For $m > 1$, (4.4.3) involves up to $(2m-1)$ body interactions. While we have not proven that $\mathcal{H}_m$ has a gap, it is plausible that it does, provided $|\Psi_m\rangle$ is in the screening phase and has short ranged correlations [2]. If so, then turning down the several-body in-

[2] In Appendix 4.B.1 we also introduce a second set of operators $P_{e,h}(z)$ that annihilate $|\Psi_m\rangle$ and define a second term in $\mathcal{H}_m$ that can also contribute to the energy gap.

teractions will not immediately destroy the state. This motivates a more practical strategy for realizing this state.

Imagine turning off the interaction terms in (4.4.3), so that $Q_e = 2\partial_z^* \psi_e - v_m \partial_z^{m-1} \psi_h^\dagger$. This leads to a non-interacting Hamiltonian of the form (4.2.1), where for $\mathbf{k} \to 0$

$$\epsilon_{\mathbf{k}} = k^2/2; \quad \Delta_{\mathbf{k}} = v_m (ik_x + k_y)^m / 2^{m-1}. \tag{4.4.4}$$

This describes a system with quadratically dispersing bands that touch at $\mathbf{k} = 0$ and are coupled by angular momentum m excitonic pairing. We now argue that this gapless "$(p+ip)^m$ pairing" state is a candidate for supporting a fractional excitonic insulator in the presence of strong repulsive interactions.

The ground state $|\Phi_m\rangle$ of Eq. (4.2.1) with $\epsilon_{\mathbf{k}}$ and $\Delta_{\mathbf{k}}$ as defined in Eq. (4.4.4) can be written in the form (4.2.4). Using $g_{\mathbf{k}} \propto (ik_x + k_y)^m / k^2$ for $k \ll \xi^{-1}$ the component with N particles and holes has the form

$$\phi_m^N(\{z_i, w_j\}) = \det\left[g(z_i - w_j)\right]; \quad g(|z| \gg \xi) \propto z^{-m}. \tag{4.4.5}$$

If we multiply out the determinant and put it over a common denominator, then ϕ_m^N gets the denominator in (4.1.2) right—at least in the universal $z_i - w_j \gg \xi$ limit. The numerator of ϕ_m^N is not the same as ψ_m^N, but if we use the large z limit of $g(z)$ then it will be a degree $mN(N-1)$ polynomial. As a function of one of its variables (say z_1) the numerator has $m(N-1)$ zeros - the same as the numerator of ψ_m^N. $N-1$ of the zeros are guaranteed by Fermi statistics to sit on $z_{2,\ldots,N}$, but the remaining $(m-1)(N-1)$ zeros are "wasted" and sit between the particles. This is similar to

a $1/m$ filled Landau level, where the magnetic field guarantees there are m times as many zeros as there are particles. In that case, repulsive interactions stabilize the Laughlin state, which puts the required zeros on top of the particles. The above argument strictly applies to the dilute limit, where electrons and holes are separated by more than ξ, so $|\Psi_m\rangle$ is in a bound phase. In the dense limit, however, $|\Psi_m\rangle$ is still more effective than $|\Phi_m\rangle$ at keeping the electrons (holes) apart, and it also builds in the $(p+ip)^m$ pairing of electrons and holes favored by (4.4.4). It will be interesting to test our conjecture that (4.4.4), along with strong repulsive interactions can stabilize the fractional excitonic insulator state by the numerical analysis of model systems.

Eq. (4.4.4) presents an appealing target for band structure engineering. It requires the crossing of two bands that differ in angular momentum by m. For $m = 3$ this can occur at the Γ point in a crystal with C_6 rotational symmetry but broken time reversal and in-plane mirrors. For example, this could arise if two bands with $m_j = \pm 3/2$ touch at the Fermi energy. Here we introduce a simple two band model for spinless electrons that provides a starting point for numerical studies.

Consider a triangular lattice with an s state and a single f state with $m = 3$ on each site. A Hamiltonian with first and second neighbor hopping can be written as Eq. (4.2.1) with

$$\epsilon_{\mathbf{k}} = \epsilon_0 - t_0\gamma_0(\mathbf{k}); \quad \Delta_{\mathbf{k}} = t_1\gamma_1(\mathbf{k}) + it_2\gamma_2(\mathbf{k}) \tag{4.4.6}$$

where $\gamma_0(\mathbf{k}) = \sum_n \cos \mathbf{k}\cdot\mathbf{a}_{1n}$, $\gamma_1(\mathbf{k}) = \sum_n (-1)^n \sin \mathbf{k}\cdot\mathbf{a}_{1n}$ and $\gamma_2(\mathbf{k}) = \sum_n (-1)^n \sin \mathbf{k}\cdot\mathbf{a}_{2n}$. Here $\mathbf{a}_{1(2)n}$ are the 6 first (second) neighbor lattice vectors at angles $\theta = n\pi/3$ $(+\pi/6)$. t_0 connects nearest neighbors of the same orbitals, while t_1 and t_2 connect first and second neighbor s and f orbitals with an angle dependent phase $e^{3i\theta}$.

For $-6 < \epsilon_0/t_0 < 2$ (4.4.6) is a Chern number 3 insulator. Outside that range it is a trivial insulator. For $\epsilon_0 = 2t_0$ the gap closes at the 3 M points, while for $\epsilon_0 = -6t_0$ the critical point is at Γ. While it is not our primary focus, the Chern number 3 transition is of interest on its own. For $\epsilon_0 = -6t_0 + \delta$ the small $\mathbf{k}$ behavior is

$$\epsilon_{\mathbf{k}} = \delta + 3t_0 k^2/2; \quad \Delta_{\mathbf{k}} = t_+ k_+^3 + t_- k_-^3, \tag{4.4.7}$$

with $t_\pm = (t_1 \pm 3\sqrt{3}t_2)/8$ and $k_\pm = k_x \pm ik_y$. For $\delta > 0$ the gap $E_g \propto \delta$ is at $\mathbf{k} = 0$, but for $\delta < 0$ $E_g \propto |\delta|^{3/2}$, and is located on a "Fermi surface" of radius $\propto |\delta|^{1/2}$. The critical point $\delta = 0$ has precisely the structure of (4.4.4) when $t_- = 0$ [160]. For non-zero t_-, the vorticity 3 winding of $\Delta_{\mathbf{k}}$ around $\mathbf{k} = 0$ remains, so the long distance phase winding of $g(z)$ is not altered. It will be interesting to study this model near the transition to determine whether electron interactions stabilize the fractional excitonic insulator by addressing signatures such as ground state degeneracy, spectral flow under flux insertion and entanglement spectrum. Importantly, in contrast to the case of fractional Chern insulators, this model should be studied at *integer* filling per unit cell.

Appendix

4.A Coupled wire construction

In this section we introduce a simple modification of the coupled wire construction [117] that allows us to describe a fractional excitonic insulator at zero magnetic field. We consider an array of alternating n type and p type wires, as indicated in Fig. 4.A.1. On the n-type wires the right (left) moving states are at momentum $+k_F$ ($-k_F$), but on the p-type wires they are at $-k_F$ ($+k_F$). This allows momentum conserving processes that lead to the quantum Hall effect in zero magnetic field.

Specifically, we consider the Hamiltonian $\mathcal{H} = \mathcal{H}_0 + V$, where

$$\mathcal{H} = -i \sum_i \int dx \psi^\dagger_{i,R} \partial_x \psi_{i,R} - \psi^\dagger_{i,L} \partial_x \psi_{i,L} \tag{4.A.1}$$

describes the low energy excitations on each wire. The electron annihilation operator is given by

$$c_i(x) = e^{\pm i k_F x} \psi_{i,R} + e^{\mp i k_F x} \psi_{i,L} \tag{4.A.2}$$

where the upper (lower) sign corresponds to the n type (p type) wires for i odd (even).

The $\nu = 1/m$ Laughlin state (for m an odd integer) is generated by introducing the m body coupling term $V^m = \sum_i \int dx (V_i^m(x) + h.c.)$, where

$$V_i^m(x) = v_m \psi_{i,R}^{\dagger (m+1)/2} \psi_{i,L}^{(m-1)/2} \psi_{i+1,R}^{\dagger (m-1)/2} \psi_{i+1,L}^{(m+1)/2} \tag{4.A.3}$$

Here, powers of $\psi_{i,R}$ are understood as an operator product expansion and include appropriate derivatives. Note that V^m conserves momentum in zero magnetic field for all m. No tuning of the electron or hole densities is required, provided they are equal, so that the Fermi energy is at the band crossing point.

In the absence of other interactions, v_m has scaling dimension $(1 + m^2)/2$, and will be irrelevant for $m > 1$. Nonetheless, as argued in Ref. [117], it is possible to choose forward scattering interactions that can make any particular v_m relevant. In the presence of such interactions, v_m will flow to strong coupling, which leads to an energy gap and the $\nu = 1/m$ fractional excitonic insulator phase.

The connection with Laughlin's plasma analogy can be understood by considering a particular limit where the problem decouples into independent 1D problems. When forward scattering interactions on each wire make them Luttinger liquids with $K = 1/m$, the v_m term couples only to a purely chiral operator on each wire. In this case, v_m is identical to electron tunneling between the edge states of strips of $\nu = 1/m$ fractional quantum Hall states, which upon bosonization lead to a $1 + 1$D sine-Gordon type model. In this case, v_m has scaling dimension m. Expanding the partition function in powers of v_m leads to exactly the same Coulomb plasma as the analysis of the Laughlin type wavefunction.

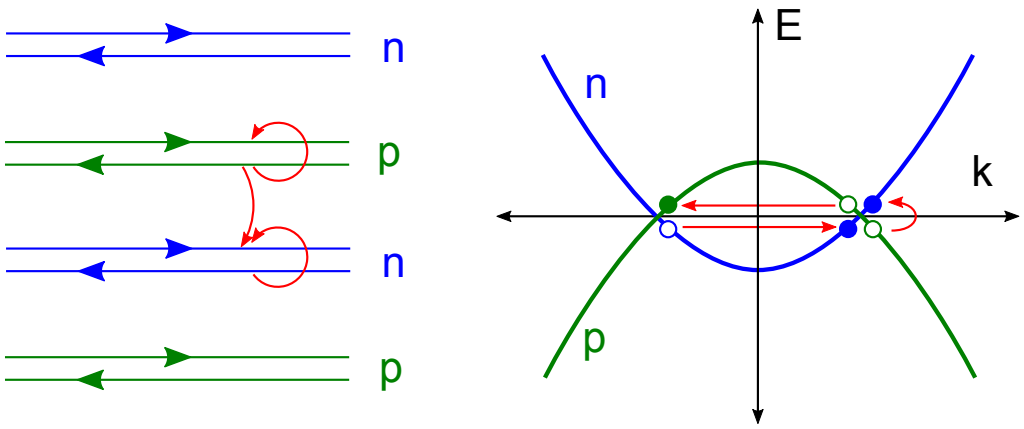

Figure 4.A.1: (a) An array of alternating n-type and p-type wires. (b) Energy bands as a function of momentum, showing the electron like (hole like bands), that live on the odd (even) wires. The red arrows indicate the correlated tunneling processes that lead to the $\nu = 1/m$ fractional excitonic insulator for the case $m = 3$.

4.B Exact Hamiltonian

In this section we demonstrate that the state $|\Psi_m\rangle$ as defined in the main text is the exact ground state wavefunction of Hamiltonian (14) of the main text. Our strategy is to seek operators X which annihilate the ground state, i.e., $X|\Psi_m\rangle = 0$. With the help of such operators one may then construct positive (and manifestly Hermitian) operators $\sim X^\dagger X$, which can be used to define a Hamiltonian with $|\Psi_m\rangle$ as its ground state. Any operator X satisfying $X|\Psi_m\rangle = 0$ can be used to define a term which may enter in the exact Hamiltonian. In fact, by explicitly constructing two sets of such operators, we will demonstrate that the space of exact Hamiltonians is larger than $\mathcal{H}_m$ given in the text. The full exact Hamiltonian, which is a sum of all allowed terms, can be used to study more physical few-body pseudopotential Hamiltonians, for which the wavefunction $|\Psi_m\rangle$ may still describe

the ground state properties. With this goal in mind, we will conclude this section with a brief comparison to a class exact Hamiltonians for the Laughlin wavefunction introduced in Ref. [176]. In these case of the latter two sets of operators are needed to construct an exact Hamiltonian with the Laughlin state as its ground state and a gap to excited states.

4.B.1 Construction of Hamiltonian

To begin, first recall that $|\Psi_m\rangle$ is defined as

$$|\Psi_m\rangle = \sum_N \frac{f^N}{N!} |\Psi_m^N\rangle , \tag{4.B.1}$$

where $|\Psi_m^N\rangle$ is a state with N particle-hole pairs defined as

$$|\Psi_m^N\rangle = \int \left(\prod_{i=1}^{N} dz_i dw_i \right) \Psi_m^N(\{z_i, w_i\}) \, |N, \{z_i, w_i\}\rangle , \tag{4.B.2}$$

with $|N, \{z_i, w_i\}\rangle$ given by $(1/N!) \prod_{i=1}^N \psi_e^\dagger(z_i)\psi_h^\dagger(w_i) \, |0\rangle$. Note that the factor $1/N!$ ensures proper normalization.

A natural choice for the annihilation operators involves the derivative operators $\partial_z = \frac{1}{2}(\partial_z - i\partial_y)$ and $\partial_{z^*} = \frac{1}{2}(\partial_z + i\partial_y)$. Consider first the derivative operator ∂_z. It is a simple matter to verify that the (second quantized) operators

$$P_e(z) = (\partial_z - ia)\psi_e(z), \tag{4.B.3}$$

$$P_h(z) = (\partial_z + ia)\psi_h(z), \tag{4.B.4}$$

annihilate the states $|\Psi_m^N\rangle$ with N particle-hole pairs, i.e., $P_{e,h}(z) \, |\Psi_m^N\rangle = 0$, where

$a = a(z) = a_x - ia_y$ is the statistical gauge field defined as

$$ia(z) = m \int d^2u \frac{\rho(u)}{z-u}, \quad \rho = \psi_e^\dagger \psi_e - \psi_h^\dagger \psi_h. \tag{4.B.5}$$

The statistical gauge field attaches $\pm m$ flux quanta to the particles (holes). Note that within the sector of Fock space defined by $N-1$ electrons and N holes $a(z)$ takes the form

$$ia(z) = \sum_{i=1}^{N-1} \frac{m}{z-z_i} - \sum_{i=1}^{N} \frac{m}{z-w_i}, \tag{4.B.6}$$

from which it directly follows that $P_{e,h}(z)$ annihilate each $|\Psi_m^N\rangle$, and thus annihilate $|\Psi_m\rangle$. It is worth pointing out that the first quantized operators

$$\Pi_\pm \equiv \partial_z \pm ia \tag{4.B.7}$$

have the commutators $[\Pi_\pm, \Pi_\pm^\dagger] = \pm 2\pi\rho = \pm \boldsymbol{\nabla} \times \mathbf{a}$. We then use the operators $P_{e,h}(z)$ to define the Hamiltonian $\mathcal{H}_m^{(1)}$ given by

$$\mathcal{H}_m^{(1)} = \frac{1}{2} \int d^2\mathbf{z} \left[P_e^\dagger(z) P_e(z) + P_h^\dagger(z) P_h(z) \right]. \tag{4.B.8}$$

By construction this Hamiltonian annihilates the wavefunction, which implies that $|\Psi_m\rangle$ is eigenstate with eigenvalue 0. Since $\mathcal{H}_m^{(1)}$ is positive $|\Psi_m\rangle$ must be a ground state.

Next, consider the derivative operator ∂_{z^*}. Since only the holomorphic coordinates z_i enter the wavefunction, the action of ∂_{z^*} requires a more careful treatment. We first define and evaluate

$$\Phi(z) = \partial_{z^*} \psi_e(z) \, |\Psi_m^N\rangle \, . \tag{4.B.9}$$

Note that $\psi_e(z)$ picks one of the N electron coordinates z_i and sets it to z. Furthermore, $\Phi(z)$ describes a state with one electron removed from $|\Psi_N\rangle$, which we may alternatively view as a state with one hole added to $|\Psi_m^{N-1}\rangle$. We will therefore seek to relate $\Phi(z)$ to $|\Psi_m^{N-1}\rangle$.

Note that ∂_{z^*} gives zero when acting on an analytic function except at the poles. Since there are N such poles, located at w_i, we can rename each pole w and then relabel the remaining $N-1$ w_i's. We separate out the dependence on z and w and obtain

$$\psi_e(z)\,|\Psi_m^N\rangle = N\int dw \frac{1}{(z-w)^m}\psi_h^\dagger(w)\,|\widetilde{\Psi}_m^{N-1}(z,w)\rangle\,, \tag{4.B.10}$$

where the state $|\widetilde{\Psi}_m^{N-1}(z,w)\rangle$ is defined as

$$|\widetilde{\Psi}_m^{N-1}(z,w)\rangle = \int\left(\prod_{i=1}^{N-1} dz_i dw_i\right)\widetilde{\Psi}_m^{N-1}(z,w,\{z_i,w_i\}) \times |N-1,\{z_i,w_i\}\rangle \tag{4.B.11}$$

with a wavefunction given by

$$\widetilde{\Psi}_m^{N-1}(z,w,\{z_i,w_i\}) = F(z,w,\{z_i,w_i\})\Psi_m^{N-1}(\{z_i,w_i\}). \tag{4.B.12}$$

Here $\Psi_m^{N-1}(\{z_i,w_i\})$ is the wave function of $|\Psi_m^{N-1}\rangle$ and F defined as

$$F(z,w,\{z_i,w_i\}) = \prod_i^{N-1}\frac{(z-z_i)^m(w-w_i)^m}{(w-z_i)^m(z-w_i)^m}. \tag{4.B.13}$$

We observe that F can be rewritten as

$$\begin{aligned} F &= e^{m\sum \log\frac{z-z_i}{w-z_i}-\log\frac{z-w_i}{w-w_i}} \\ &= e^{\int_w^z du\sum_i(\frac{m}{u-z_i}-\frac{m}{u-w_i})} = e^{i\int_w^z du a(u)}, \end{aligned} \tag{4.B.14}$$

where $a(u)$ is the gauge field introduced in (4.B.5) and is given by

$$ia(u) = \sum_{i=1}^{N-1} \left(\frac{m}{u - z_i} - \frac{m}{u - w_i} \right). \tag{4.B.15}$$

We thus find that the Eq. (4.B.11) can be expressed in the concise form

$$|\widetilde{\Psi}_m^{N-1}(z, w)\rangle = e^{\int_w^z du a(u)} |\Psi_m^{N-1}\rangle . \tag{4.B.16}$$

The next step is to consider the action of ∂_{z^*} on the pole at w. One finds that

$$\begin{aligned} \partial_{z^*} \frac{1}{(z-w)^m} &= \frac{\partial_w^{m-1}}{(m-1)!} \partial_{z^*} \frac{1}{z-w} \\ &= \frac{\pi}{(m-1)!} \partial_w^{m-1} \delta^{(2)}(z-w) \end{aligned} \tag{4.B.17}$$

where we used Cauchy's integral formula and

$$\partial_{z^*} \frac{1}{z-w} = \pi \delta^{(2)}(z-w) \tag{4.B.18}$$

As a result, $\Phi(z)$ defined in Eq. (4.B.9) becomes

$$\Phi(z) \quad = \quad \frac{\pi N}{(m-1)!} \int dw [\partial_w^{m-1} \delta(z \ - \ w)] \psi_h^\dagger(w) e^{i \int_w^z du a(u)} |\Psi_{N-1}\rangle \tag{4.B.19}$$

The right hand side can be integrated by parts to obtain

$$\partial_{z^*} \psi_e(z) |\Psi_N\rangle = \frac{\pi N}{(m-1)!} \psi_h^\dagger (\overleftarrow{\partial_z} - ia)^{m-1} |\Psi_{N-1}\rangle . \tag{4.B.20}$$

Equation (4.B.20) gives the desired relation between $\Phi(z)$ and $|\Psi_{N-1}\rangle$, and we use it to define the operator

$$Q_e(z) = \partial_{z^*} \psi_e(z) - \frac{\pi f}{(m-1)!} \psi_h^\dagger (\overleftarrow{\partial_z} - ia)^{m-1}, \tag{4.B.21}$$

which, by construction $Q_e(z)$, annihilates the state $|\Psi_m\rangle$. A very similar analysis can be applied to $\partial_{z^*}\psi_h(z)$ and leads to the definition of $Q_h(z)$, which is given by (4.B.21) after exchanging $\psi_e, \psi_e^\dagger \leftrightarrow \psi_h, \psi_h^\dagger$ and substituting $a \to -a$.

We use the operators $Q_{e,h}(z)$ to construct another positive Hermitian $\mathcal{H}_m^{(2)}$ given by

$$\mathcal{H}_m^{(2)} = \frac{1}{2}\int d^2\mathbf{z}\left[Q_e^\dagger(z)Q_e(z) + Q_h^\dagger(z)Q_h(z)\right], \tag{4.B.22}$$

which has $|\Psi_m\rangle$ as a zero energy ground state. Combining Eqs. (4.B.8) and (4.B.22), one may form the exact Hamiltonian

$$\mathcal{H}_m = \lambda_1\mathcal{H}_m^{(1)} + \lambda_2\mathcal{H}_m^{(2)}. \tag{4.B.23}$$

Note that in the case $m = 1$ the $\mathcal{H}_{m=1}^{(2)}$ simply reduces to the non-interacting for $p_x + ip_x$ excitonic pairing, see Eqs. (3) and (4) of the main text. This implies that for $m = 1$ the exact Hamiltonian $\mathcal{H}_m$ is specified by $(\lambda_1, \lambda_2) = (0, 1)$.

4.B.2 Comparison to lowest Landau level

Let us now compare the operators $Q_{e,h}$ and $P_{e,h}$ to operators which annihilate the Laughlin wavefunction Ψ_m^{Laughlin} describing a fractional quantum Hall liquid in the lowest Landau level at filling factor $\nu = 1/m$. In the symmetric gauge the single-particle states in the lowest Landau level are eigenstates of angular momentum. The Laughlin wave function takes the form

$$\Psi_m^{\text{Laughlin}} \propto \prod_{i<j}(z_i - z_j)^m e^{-\sum_i z_i z_i^*}. \tag{4.B.24}$$

It is worth pointing out that the Gaussian piece originates from the magnetic field (and we have taken twice the magnetic length as the unit of length).

Now consider the following two (first-quantized) operators involving the derivatives ∂_z and ∂_{z^*}:

$$\Pi = \partial_{z^*} + z, \tag{4.B.25}$$

$$\Lambda = \partial_z + z^* - ia. \tag{4.B.26}$$

The operator Π annihilates all single-particle states of the lowest Landau level and therefore annihilates Ψ_m^{Laughlin}. This can be understood by recognizing that Π and $\Pi^\dagger$ are the ladder operators of the Landau levels, i.e., Π ($\Pi^\dagger$) lowers (raises) the Landau level index. The Hamiltonian constructed from Π, given by $\Pi^\dagger\Pi$, simply corresponds to the kinetic energy of a particle in a magnetic field (up to an additive constant). Therefore, $\Pi^\dagger\Pi$ does not by itself lead to energy gap at filling $\nu = 1/m$. One may also note that since $\Pi^\dagger\Pi$ annihilates all wavefunctions constructed from states in the lowest Landau level, it is certainly not sufficient to single out the Laughlin wavefunction as the ground state wavefunction.

Instead, the Laughlin wavefunction is selected by interactions, and an exact interacting Hamiltonian can be constructed by including $\Lambda^\dagger\Lambda$. Note that $\partial_z + z^*$ lowers the angular momentum of the single-particle states, i.e., Λ is defined as the angular momentum lowering operator minus a statistical gauge field a given by

$$ia(z_i) = m\sum_{j\neq i}\frac{1}{z_i - z_j}. \tag{4.B.27}$$

It is then straightforward to verify that Λ indeed annihilates the Laughlin state. As a result, in the fractional quantum Hall problem both operators Π and Λ are needed to construct an exact interacting Hamilonian with (4.B.24) as its ground state wave function. Such Hamiltonian can be related to an interacting Hamiltonian with short-ranged two-body interactions [175], of which the ground state properties are described by (4.B.24).

This leads to the expectation that in the case of the fractional excitonic insulator a general Hamiltonian of the form (4.B.23), involving both the $Q_{e,h}$ and $P_{e,h}$ operators, should be considered for $m \neq 1$.

Chapter 5

Higher Angular Momentum Band Inversions in Two Dimensions

5.1 Introduction

The notion of a band inversion provides a central paradigm for the understanding of free fermion topological phases[3, 147, 177]. A band inversion marks the transition between two gapped electronic phases in the same symmetry class but with distinct topology, and must necessarily lead to a closing of the energy gap[40, 41]. At the gapless band touching point, where the order of bands is reversed, the topological index associated with the symmetry class changes [178, 179]. As a result, knowledge of the type of band inversion gives access to information on the topological distinction between the two phases separated by a topological phase transition. This is

most clearly exemplified by those band inversions which can be described by a single Dirac fermion theory. In such theories a sign change of the Dirac fermion mass indicates a change of bulk topology. In two dimensions this defines the low-energy theory for the quantum Hall transition [146] and in three dimensions this describes the transition between a trivial and a topological insulator [4].

In general, when band inversions occur at high-symmetry momenta, the type of such band inversion can be indicated by the eigenvalues of spatial symmetry operators of the bands which invert [147, 180–183]. For instance, the Fu-Kane formula can be viewed as a symmetry indicator for a band inversion transition occurring at a time-reversal invariant momentum which changes the $\mathbb{Z}_2$ topological index [147]. Another example of established symmetry indicators are crystal rotation symmetries [180, 184, 185]. Two bands characterized by different crystal rotation eigenvalues have different angular momentum, which implies that, in two dimensions, an inversion of such bands leads to a change of the Chern number (assuming the existence of an energy gap on both sides of the transition). In this chapter we study this type of band inversion, with a particular focus on higher angular momentum band inversions. Such band inversions mark the transition to a Chern insulator with higher Chern number and generalize the transition described by a Dirac fermion.

Our understanding of Chern insulators and Chern bands fundamentally relies on their connection to (flat) Landau levels in a magnetic field [35]; as far as their topological classification is concerned, Chern bands and Landau levels are equiva-

lent [144]. To a large extent, it is this equivalence, and its implications for properties such as edge state spectrum and Hall conductance quantization [2], which has motivated and driven much of the research on Chern insulating phases. Furthermore, the connection to Landau levels has been successfully exploited to, for instance, address the effect of electronic interactions in partially filled Chern bands, and thereby explore the possibility of realizing correlated liquid states akin to fractional quantum Hall states without magnetic field [152–155]. Here we take a rather different, and in some sense contrary, perspective on Chern insulators, by focusing not on isolated Chern bands but instead on the band inversion transition to the Chern insulating state. Notably, the low-energy description of such transition, which can be viewed as a higher angular momentum generalization of a Dirac fermion transition, exposes a connection to the BCS theory of paired states of fermions in two dimensions [177]. In particular, this connection, which was previously recognized in the context $p+ip$ pairing phases [162], suggests that the transition to a Chern insulator phase can be phrased in terms of pairing of electrons and holes—rather than pairs of electrons. One of our aims is to examine this connection in more detail.

We are further motivated by the broader aim to find many-body generalizations of band inversion transitions. In the search for such many-body generalizations higher angular momentum band inversions are of particular interest since the bands disperse quadratically at the critical point of the transition (i.e., when the gap closes and the bands touch, see Fig. 5.2.1). This property, which is protected by rotation

symmetry, leads to a non-vanishing density of states and implies that—in contrast to band inversion transitions described by a Dirac fermion—interactions are likely to affect the nature of the band inversion [186–194].

In previous chapter we have argued that, given the importance of interactions, higher angular momentum band inversions provide a promising route towards correlated fluids of electrons and holes. This argument is based on the pairing formulation of the Chern band inversion and was encouraged by the well-established connections between pairing states and fractional quantum Hall wave functions [177]. In this chapter we focus attention on a second possibility for a correlation-driven phase in the vicinity of the band inversion: the excitonic insulator [195]. The excitonic insulator is defined by the condensation of electrons and holes into exciton bound states, which can be called excitonic pairing, and is associated with rotation symmetry breaking [193].

5.2 Band inversions and Chern insulators

We begin by introducing a low-energy theory for band inversion transitions which signal a change of the Chern number index. To describe a band inversion of this type it is sufficient to consider two bands, and we thus consider a system with a filled valence band and an empty conduction band, which we study in the vicinity of a band inversion at $\mathbf{k} = 0$. We define the annihilation operators of the conductions band and valance band states as $c_{\mathbf{k}e}$ and $c_{\mathbf{k}h}$, respectively, and collect them in the

spinor

$$\psi_{\mathbf{k}} = \begin{pmatrix} c_{\mathbf{k}e} \\ \\ c_{\mathbf{k}h} \end{pmatrix}. \tag{5.2.1}$$

Note that the choice of vacuum (i.e., a filled valence band) implies that $c_{\mathbf{k}h}$ creates holes in the valence band and can be viewed as a creation operator with respect to the vacuum. In this sense, $\psi_{\mathbf{k}}$ may be compared to a Nambu spinor of electrons and holes. In terms of $\psi_{\mathbf{k}}$ and $\psi_{\mathbf{k}}^{\dagger}$ the Hamiltonian can be expressed as

$$H = \sum_{\mathbf{k}} \psi_{\mathbf{k}}^{\dagger} h_{\mathbf{k}} \psi_{\mathbf{k}}, \quad h_{\mathbf{k}} = \begin{pmatrix} \varepsilon_{\mathbf{k}} & \Delta_{\mathbf{k}} \\ \\ \Delta_{\mathbf{k}}^{*} & -\varepsilon_{\mathbf{k}} \end{pmatrix}. \tag{5.2.2}$$

Here $\varepsilon_{\mathbf{k}}$ describes the dispersion of the conduction and valence band close to the band inversion at $\mathbf{k} = 0$. To lowest order in momentum the dispersion takes the form $\varepsilon_{\mathbf{k}} = \mathbf{k}^2/2m^* - \delta$, where m^* is an effective mass and δ is the energy difference between the two bands. The parameter δ determines whether the bands are inverted ($\delta > 0$) or have normal band ordering ($\delta < 0$). This is schematically shown in Fig. 5.2.1, where (**A**) corresponds to the uninverted regime and (**C**) corresponds to the inverted regime.

It is important to note that δ is not determined or constrained by symmetry. This should be contrasted with systems exhibiting a symmetry-protected degeneracy of two bands at $\mathbf{k} = 0$, in which case δ represents a gap opening associated with the breaking of a symmetry [186]. Here, on the other hand, we consider a transition between two phases with the same symmetry but different topology. Note further that the inverted regime $\delta > 0$ leads to the notion of an electron-hole Fermi surface

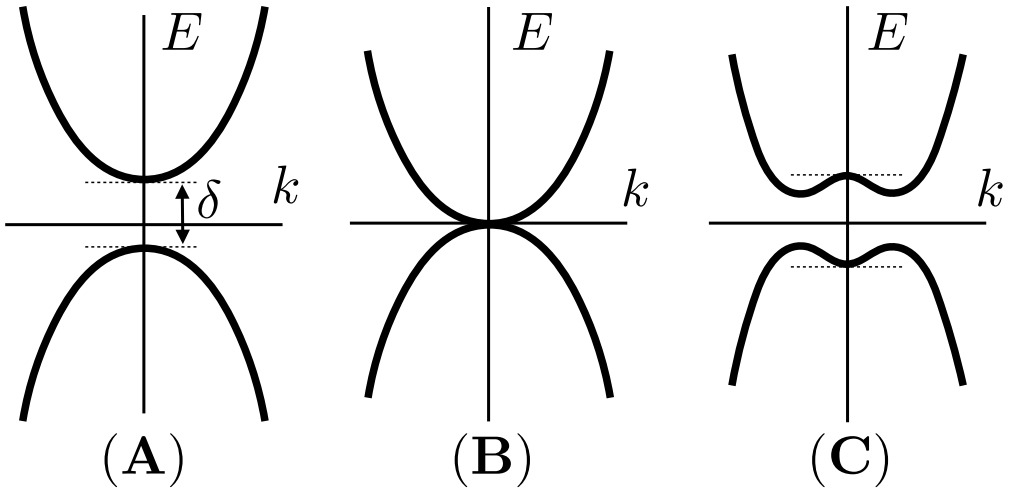

Figure 5.2.1: Band inversion transition with higher angular momentum. A band inversion transition with higher angular momentum in two dimensions separates a trivial insulating phase (**A**) from a topological Chern insulating phase (**C**) with higher Chern number. At the critical point, shown in (**C**), the band dispersion is quadratic, in sharp contrast to band inversion transitions described by a Dirac fermion, for which it is linear. The non-vanishing density of states of the former makes interaction effects relevant, making higher angular momentum band inversions promising venues for many-body generalizations of topological band inversion transitions.

defined by the condition $\varepsilon_{\mathbf{k}} = 0$ and the wave vector $k_F = \sqrt{2m^*\delta}$.

The coupling of the electron and hole bands is given by $\Delta_{\mathbf{k}}$ and is constrained by the symmetry properties of the electron and hole bands. In this work we focus on a class of band inversion Hamiltonians $h_{\mathbf{k}}$ for which the function $\Delta_{\mathbf{k}}$ describing the coupling is chiral and characterized by a definite nonzero angular momentum l. Couplings with angular momentum l can expressed in the general form

$$\Delta_{\mathbf{k}} = \Delta(k_x + \kappa i k_y)^{|l|}, \tag{5.2.3}$$

where Δ is the strength of the coupling (which may be complex) and $\kappa = \mathrm{sgn}(l)$. With $\Delta_{\mathbf{k}}$ given by Eq. (5.2.3) it is straightforward to see that the energy spectrum of $h_{\mathbf{k}}$, which consists of two branches $\pm E_{\mathbf{k}}$ with $E_{\mathbf{k}} = (\varepsilon_{\mathbf{k}}^2 + |\Delta_{\mathbf{k}}|^2)^{1/2}$, has a full energy

gap except for the special case $\delta = 0$. This shows that δ controls the transition between two gapped phases with different topological character, as we now explain.

The form of (5.2.3) combined with the form of Eq. (5.2.2) suggests a formal connection to the BCS theory of chiral superconductors in two dimensions [177, 201]. In the latter case, $\Delta_{\mathbf{k}}$ corresponds to the pairing potential and is associated with the breaking of $U(1)$ charge conservation. In this sense, the class of systems we consider here is very different, since all terms present in the Hamiltonian of Eq. (5.2.2), including $\Delta_{\mathbf{k}}$, represent symmetry-allowed couplings between single-particle states. In particular, the number of conduction band electrons and valence band holes is not separately conserved. Given the absence of a broken symmetry one might compare the "pairing" of particles and holes described by Eq. (5.2.2) to proximitized superconductors [194].

The formal connection of Eq. (5.2.2) to chiral superconductors can nevertheless be fruitfully exploited for the purpose of analyzing the ground state wavefunction and its properties. A gapped chiral superconductor in two dimensions with angular momentum l is known to have a topological ground state characterized by a nonzero Chern number $C = l$ [177]. This leads to the conclusion that $h_{\mathbf{k}}$ with $\Delta_{\mathbf{k}}$ given by (5.2.3) describes a band inversion transition from a trivial insulator to a Chern insulator with Chern number $C = l$. These two insulating phases are separated by a gap closing at $\delta = 0$ (depicted in Fig. 5.2.1 **B**), with $\delta > 0$ corresponding to the Chern insulator, as shown in Fig. 5.2.1 (**C**). Following the work of Read and

Green [177] the ground state of Eq. (5.2.2) can be expressed in the form

$$|\Phi\rangle = \prod_{\mathbf{k}} (u_{\mathbf{k}} + v_{\mathbf{k}} c^{\dagger}_{\mathbf{k}e} c_{\mathbf{k}h}) \, |\Omega\rangle \propto e^{\sum_{\mathbf{k}} g_{\mathbf{k}} c^{\dagger}_{\mathbf{k}e} c_{\mathbf{k}h}} \, |\Omega\rangle \, , \tag{5.2.4}$$

where $u_{\mathbf{k}}$ and $v_{\mathbf{k}}$ are solutions to the equations $(\varepsilon_{\mathbf{k}} + E_{\mathbf{k}})v_{\mathbf{k}} + \Delta_{\mathbf{k}} u_{\mathbf{k}} = 0$ and $\Delta^{*}_{\mathbf{k}} v_{\mathbf{k}} + (E_{\mathbf{k}} - \varepsilon_{\mathbf{k}})u_{\mathbf{k}} = 0$ with constraint $|u_{\mathbf{k}}|^2 + |v_{\mathbf{k}}|^2 = 1$, and $|\Omega\rangle$ is the vacuum defined by a filled valence band and empty conduction band (see Appendix 5.A). The ground state $|\Phi\rangle$ describes a Chern insulating phase defined by a "condensate" of electrons and holes with nonzero angular momentum l. The topology of the many-body wavefunction is encoded in pair correlation function $g(\mathbf{r}) = \int d^2\mathbf{k} \; g_{\mathbf{k}} e^{-i\mathbf{k}\cdot\mathbf{r}}/(2\pi)^2$ with $g_{\mathbf{k}} = v_{\mathbf{k}}/u_{\mathbf{k}}$. In Sec. 5.4 we study the pair correlation function in more detail and discuss its connection to the lattice models introduced in Sec. 5.3.

To address the question how a band inversion of the type defined by Eqs. (5.2.2) and (5.2.3) can arise, and in particular which model systems can describe higher Chern number transitions, it is helpful consider the symmetry properties of $\Delta_{\mathbf{k}}$. Since $\Delta_{\mathbf{k}}$ is chiral and carries nonzero angular momentum, it can only arise when time-reversal and vertical reflection symmetry are both broken. Furthermore, definite angular momentum implies that the form of $\Delta_{\mathbf{k}}$ is constrained by rotational symmetry. To see this, consider the case $l = -m$, where m is a positive integer. The Hamiltonian $h_{\mathbf{k}}$ can be expressed as

$$h_{\mathbf{k}} = \varepsilon_{\mathbf{k}} \tau_z + \Delta(k_+^m \tau_- + k_-^m \tau_+), \tag{5.2.5}$$

where $\tau_{x,y,z}$ are Pauli matrices and we have defined $\tau_{\pm} = (\tau_x \pm i\tau_y)/2$ as well as $k_{\pm} = k_x \pm i k_y$. Under rotations by an angle θ one has $k_{\pm}^m \to e^{im\theta} k_{\pm}^m$ and, as a

result, one must have $\tau_\pm \to e^{im\theta}\tau_\pm$ for $h_\mathbf{k}$ to be invariant under rotations. We may formulate this in real space by noting that the Hamiltonian takes the form

$$h = \tau_z(-\partial^2 - \delta) + \Delta\left[\tau_-(\partial_{z^*}/i)^m + \tau_+(\partial_z/i)^m\right], \tag{5.2.6}$$

where $\partial_{z,z^*} = \partial_x \mp i\partial_y$. Invariance under rotations implies that the Hamiltonian commutes with the angular momentum operator L_z (i.e., the generator of rotations). To satisfy $[h, L_z] = 0$ L_z must have the form

$$L_z = z\partial_z - z^*\partial_{z^*} + \frac{m}{2}\tau_z, \tag{5.2.7}$$

where $z = x + iy$. This leads to the conclusion that the electron and hole bands must have relative angular momentum m, i.e., their rotation symmetry quantum numbers must differ by m. It is this conclusion which provides the basis for the construction of the lattice models in the next section.

Before we come to a discussion of such models, however, two remarks are in order. First, since the dispersion of the electron and hole band is chosen as $\pm\varepsilon_\mathbf{k}$, Eq. (5.2.2) has a particle-hole symmetry given by $e \leftrightarrow h$ and $l \to -l$. This is a convenient starting point for analysis but it is not an essential assumption, and in general one expects this symmetry to be broken by the different band curvature of electron and hole bands. Second, to ensure that the topology of $h_\mathbf{k}$ is well-defined for $|l| > 1$, i.e., that $h_\mathbf{k}$ is un-inverted at $\mathbf{k} \to \infty$, higher order terms in $\mathbf{k}^2$ should be added to $\varepsilon_\mathbf{k}$.

5.3 Lattice Models for Chern Band Inversions

In this section we present a construction of simple lattice models which realize band inversion transitions to Chern insulators with Chern number $C = l$. Here l corresponds to the angular momentum of the band coupling $\Delta_{\mathbf{k}}$ defined in Eq. (5.2.3). As demonstrated in the previous section, the constituent degrees of freedom of such models are required to have nonzero relative angular momentum and thus transform nontrivially under the symmetry group of the lattice. Since symmetry plays a central role, we begin by reviewing the generic symmetry properties of Chern insulators and Chern bands and then survey the point symmetry groups compatible with the symmetry requirements of higher angular momentum band inversions.

Note first that the existence of a Chern insulating state requires broken time-reversal (T) and mirror (M) symmetry, which follows directly from the transformation property of the Berry curvature under T and M symmetry [202]. Here M is a reflection with respect to a vertical mirror plane which inverts one of the coordinates, e.g., $(x, y) \to (x, -y)$. Broken T and M is consistent with the chiral nature of nonzero angular momentum excitonic pairing described by Eq. (5.2.3). When the system has multiple inequivalent vertical mirror planes all these reflection symmetries must be broken. As a result, in what follows broken M symmetry should be understood as the absence of all vertical mirror symmetry. A similar result holds for twofold rotations about an axis in the plane, as the Berry curvature is odd under such rotations.

Chern insulators are compatible with rotation symmetry and our aim is to construct Chern insulator models which preserve the rotation symmetry of the lattice. More precisely, our aim is to construct models which exhibit maximal rotation symmetry. The discrete symmetry of the crystal lattice sets limits for rotation invariance: in lattice systems with an n-fold rotation symmetry $C_{n=2,3,4,6}$ angular momentum l is only defined $\mathrm{mod}\, n$. As a result, the largest possible angular momentum that can be distinguished is $l = \pm 3$, which implies that the construction of lattice models for excitonic Chern insulators is limited to $C = \pm 3$.

In the context of rotationally invariant Chern insulating phases it is worth noting that the relation between the Chern number and angular momentum is also reflected in the fact that the Chern number can be obtained from energy band rotation eigenvalues at rotation invariant momenta (up to multiples of n) [185].

Next, we examine the crystallographic point groups which may in principle support Chern insulating states with rotation symmetry. Since we consider layer systems with a two-dimensional lattice the appropriate symmetry groups are axial point groups. Admissible symmetry groups are those which leave an angular momentum l along the z axis invariant and allow to distinguish different values of l. Consider first the hexagonal groups. There are three groups which satisfy the first condition: C_6, C_{6h}, and C_{3h}. The latter, however, only allows to distinguish $l = \pm 1$ and is not of interest. Of the trigonal point groups only C_3 and $C_{3i} = S_6$ are compatible with chiral pairing along the z axis. Since S_6 includes an inversion s-wave

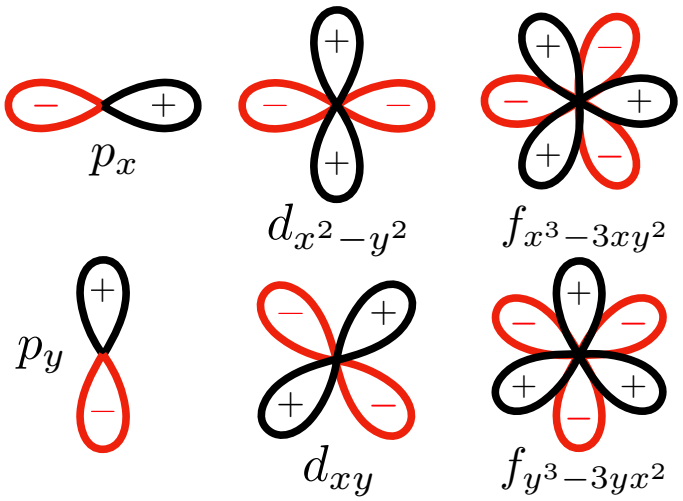

Figure 5.3.1: Symmetry of orbital states. Graphical representation of the symmetry of the orbital degrees of freedom with integral angular momentum $l = 1, 2, 3$. The p-, d-, and f-wave states form the basis of the Chern insulator models of Sec. 5.3.1.

and f-wave angular momenta have distinct symmetry. In systems with tetragonal symmetry we can only hope to distinguish angular momenta up to $l = \pm 2$. Of the groups which preserve angular momentum along z, given by C_4, C_{4h}, and S_4, all are sufficient to protect $l = \pm 2$ pairing.

To summarize, the symmetry groups of interest are: C_6 and C_{6h} (hexagonal); S_6 (trigonal); C_4, C_{4h}, and S_4 (tetragonal). With this knowledge we now introduce models for systems in these symmetry classes.

5.3.1 Orbital Angular Momentum Models

The Square Lattice

We first focus on the square lattice. Since the square lattice has C_4 rotation symmetry angular momentum can be distinguished up to $l = \pm 2$. As a result, the square lattice can support models for band inversion transitions up to Chern number $C = \pm 2$. To obtain such models it is natural to choose on-site orbital degrees of freedom with relative angular momentum ± 2. We thus consider s-wave and d_{xy}-wave orbitals and define $s_{\mathbf{k}}$ and $d_{\mathbf{k}}$ as the electron annihilation operators corresponding to the s- and d-wave states. (The symmetry of the higher angular momentum orbitals is shown in Fig. 5.3.1.) We write the Hamiltonian H for this two-band system as

$$H = \sum_{\mathbf{k}} \varphi_{\mathbf{k}}^{\dagger} h_{\mathbf{k}} \varphi_{\mathbf{k}}, \quad \varphi_{\mathbf{k}} = \begin{pmatrix} s_{\mathbf{k}} \\ \\ d_{\mathbf{k}} \end{pmatrix}, \tag{5.3.1}$$

where the Hamiltonian matrix $h_{\mathbf{k}}$ may be expanded in Pauli matrices $\tau_{x,y,z}$.

As outlined in the beginning of this section, the form of $h_{\mathbf{k}}$ is determined by the symmetry requirements of a C_4 symmetric Chern insulator and symmetry of the s- and d-wave states. An elegant and simple way to derive the form of $h_{\mathbf{k}}$ is to formulate the allowed couplings in terms of lattice harmonic functions, which may be viewed as lattice analogs of spherical harmonics and describe hoppings with distinct symmetry. As an example, the (lowest order) s-wave harmonic $\lambda_{\mathbf{k}}^{s}$ given by

$$\lambda_{\mathbf{k}}^{s} = \cos k_x + \cos k_y, \tag{5.3.2}$$

corresponds to the standard nearest neighbor hopping. Note that due to the discrete symmetry of a lattice the lattice harmonics are labeled by the finite set of point group representations (see Table 5.3.1). The two d-wave harmonics with $d_{x^2-y^2}$ and d_{xy} symmetry are given by

$$\lambda_{\mathbf{k}}^{d_1} = \cos k_x - \cos k_y, \quad \lambda_{\mathbf{k}}^{d_2} = \sin k_x \sin k_y, \tag{5.3.3}$$

and the p-wave harmonics are given by $(\lambda_{\mathbf{k}}^{p_1}, \lambda_{\mathbf{k}}^{p_2}) = (\sin k_x, \sin k_y)$. The symmetry properties and the point group labels of the lattice harmonics are summarized in Table 5.3.1 and are shown schematically in Fig. 5.3.1.

Using the symmetry of both the orbital basis states and the lattice harmonics, it is straightforward to construct a Hamiltonian H which satisfies all symmetry requirements and has a gapped ground state. We write H as a sum of two parts: H_δ and H_Δ. Here H_δ describes both nearest neighbor intra-orbital hopping and an energy splitting $\varepsilon_s - \varepsilon_d$ of the s and d states, and H_Δ describes the (inter-orbital) couplings between the s and d states. The splitting between the s and d states is conveniently parametrized as $\varepsilon_s - \varepsilon_d = 2t - \delta$, where t is the nearest neighbor hopping parameter; H_δ then takes the form

$$H_\delta = \sum_{\mathbf{k}} (2t - \delta - t\lambda_{\mathbf{k}}^s)(s_{\mathbf{k}}^\dagger s_{\mathbf{k}} - d_{\mathbf{k}}^\dagger d_{\mathbf{k}}). \tag{5.3.4}$$

The structure of H_Δ follows from the observation that $d_{\mathbf{k}}^\dagger s_{\mathbf{k}}$ transforms as a d_{xy} wave. The simplest rotationally invariant but T- and M-broken coupling then takes the

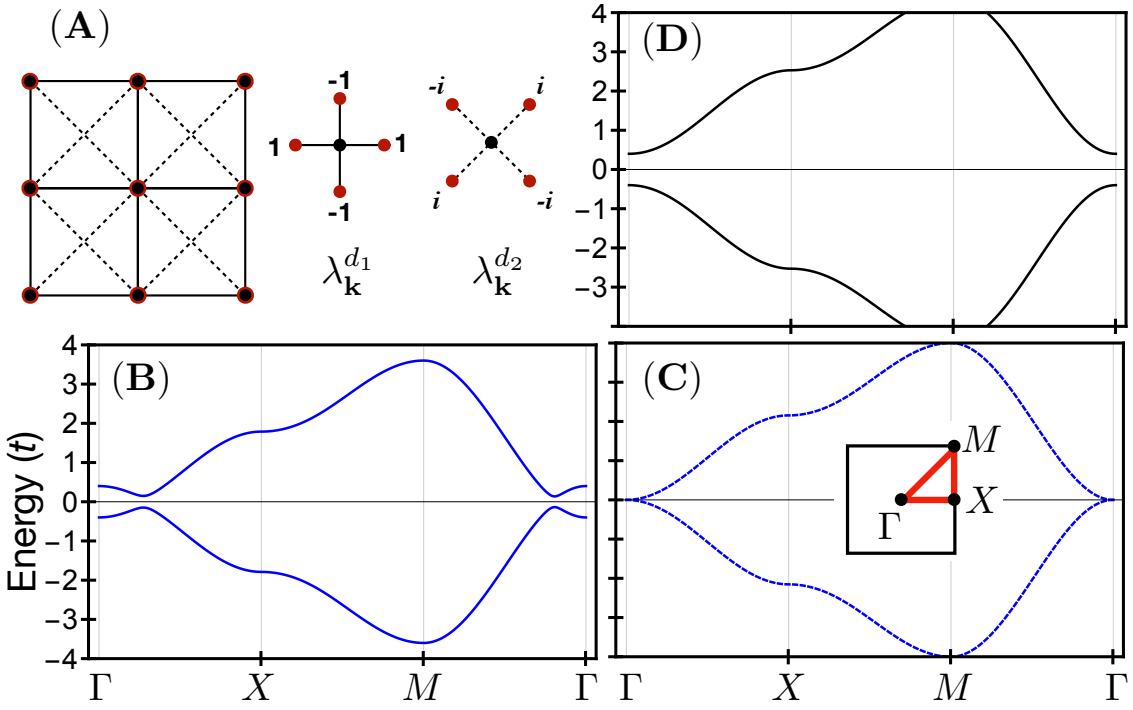

Figure 5.3.2: Square lattice model. Panel (**A**) shows the two-orbital square lattice model introduced in Eq. (5.3.6), with inter-orbital nearest neighbor hopping (Δ_1) and next-nearest neighbor (Δ_2) hopping. The onsite orbitals with s- and d-wave symmetry are represented by (superimposed) black and red dots. Shown is also the real space structure of the inter-orbital hoppings defined in Eq. (5.3.5) and described by the square lattice harmonics $\lambda^{d_1}_{\mathbf{k}}$ and $\lambda^{d_1}_{\mathbf{k}}$ of Eq. (5.3.3). (**B**), (**C**), and (**D**) show the spectrum of the square lattice model in the inverted regime, at the critical point, and in the normal regime, respectively. As parameters we chose $\delta = 0.4t, 0, -0.4t$ and $(\Delta_1, \Delta_2) = (0.4t, 0.4t)$.

form

$$H_\Delta = \sum_{\mathbf{k}} (i\Delta_1 \lambda_{\mathbf{k}}^{d_1} + \Delta_2 \lambda_{\mathbf{k}}^{d_2}) d_{\mathbf{k}}^\dagger s_{\mathbf{k}} + \text{H.c.}, \tag{5.3.5}$$

where $\Delta_{1,2}$ are both real and the relative phase is responsible for broken T. Combining these two terms we arrive at the form of $h_{\mathbf{k}}$ given by

$$h_{\mathbf{k}} = \varepsilon_{\mathbf{k}} \tau_z + \Delta_1 \lambda_{\mathbf{k}}^{d_1} \tau_y + \Delta_2 \lambda_{\mathbf{k}}^{d_2} \tau_x, \tag{5.3.6}$$

where we defined $\varepsilon_{\mathbf{k}} = 2t - \delta - t\lambda_{\mathbf{k}}^s$. The square lattice model defined by (5.3.6) is shown pictorially in Fig. 5.3.2 (**A**).

It is straightforward to verify that $h_{\mathbf{k}}$ has a gapped spectrum for nonzero $(\delta, \Delta_1, \Delta_2)$ and supports Chern bands with $C = \pm 2$ for $4t > \delta > 0$. The parameter δ can be directly identified with the band inversion parameter of Eq. (5.2.2). The spectrum of (5.3.6) is shown in Fig. 5.3.2 (**B**)–(**D**), corresponding to the inverted regime ($\delta > 0$), the critical point ($\delta = 0$), and the normal regime ($\delta < 0$). A more detailed analysis of Eq. (5.3.6) from the perspective of Eq. (5.2.2) will be presented below.

The Triangular Lattice

Next, we turn to the triangular lattice, which has sixfold rotation symmetry and allows to resolve angular momentum up to $l = \pm 3$. We introduce s-wave and f-wave states as on-site orbital degree of freedom and define the corresponding electron (annihilation) operator as

$$\varphi_{\mathbf{k}} = \begin{pmatrix} s_{\mathbf{k}} \\ \\ f_{\mathbf{k}} \end{pmatrix}. \tag{5.3.7}$$

Symmetry	Lattice harmonics	Square (D_{4h})	Hexagonal (D_{6h})
s	$\lambda^s_{\mathbf{k}}$	A_{1g}	A_{1g}
p_x, p_y	$\lambda^{p_1}_{\mathbf{k}}, \lambda^{p_2}_{\mathbf{k}}$	E_u	E_{1u}
$d_{x^2-y^2}$, d_{xy}	$\lambda^{d_1}_{\mathbf{k}}, \lambda^{d_2}_{\mathbf{k}}$	B_{1g}, B_{2g}	E_{2g}
$f_{x^3-3xy^2}$, $f_{y^3-3yx^2}$	$\lambda^{f_1}_{\mathbf{k}}, \lambda^{f_2}_{\mathbf{k}}$	E_u	B_{1u}, B_{2u}

Table 5.3.1: Symmetry of angular momentum states. Table summarizing the point group symmetry properties of angular momentum basis functions on the square and hexagonal lattices with (axial) point groups D_{4h} and D_{6h}, respectively. These groups are the maximal symmetry groups of a two-dimensional layer. Second column lists the lattice harmonics with given symmetry. Final two columns lists the symmetry quantum numbers.

As there are two symmetry-distinct f waves, we fix the symmetry by declaring that $f^\dagger_{\mathbf{k}}$ creates electrons in a $f_{x^3-3xy^2}$ orbital state, see Fig. 5.3.1.

To determine the form of the Hamiltonian $h_{\mathbf{k}}$ on the triangular lattice we must first specify the triangular lattice harmonics. To this end, it is helpful to define the three lattice vectors $\mathbf{a}_{i=1,2,3}$ as

$$\mathbf{a}_i = \begin{pmatrix} \cos\theta_i \\ \\ \sin\theta_i \end{pmatrix}, \quad \theta_i = (i-1)\frac{2\pi}{3}. \tag{5.3.8}$$

The symmetric s-wave harmonic then takes the form $\lambda^s_{\mathbf{k}} = \sum_{i=1}^3 \cos k_i$, where $k_i = \mathbf{k}\cdot\mathbf{a}_i$. The two lowest order symmetry-distinct f-wave harmonics are given by

$$\lambda^{f_1}_{\mathbf{k}} = \sum_{i=1}^3 \sin k_i, \quad \lambda^{f_2}_{\mathbf{k}} = \frac{1}{3\sqrt{3}} \sum_{i=1}^3 \sin(k_i - k_{i+1}), \tag{5.3.9}$$

where the latter corresponds to next-nearest neighbor coupling (the proportionality constant is chosen for convenience). The f waves f_1 and f_2 are identified with $f_{x^3-3xy^2}$ and $f_{y^3-3yx^2}$, respectively. In systems with hexagonal symmetry both the p waves $(\lambda_{\mathbf{k}}^{p_+}, \lambda_{\mathbf{k}}^{p_-})$ and the d waves $(\lambda_{\mathbf{k}}^{d_+}, \lambda_{\mathbf{k}}^{d_-})$ are degenerate, i.e., they form partners of a two-dimensional representation. Expressed in the chiral basis $p_\pm = p_x \pm ip_y$ and $d_\pm = d_{x^2-y^2} \pm id_{xy}$, the triangular lattice p- and d-waves harmonics take the form

$$\lambda_{\mathbf{k}}^{p_+} = \sum_{i=1}^{3} \omega^{i-1} \sin k_i, \quad \lambda_{\mathbf{k}}^{d_+} = \sum_{i=1}^{3} \omega^{1-i} \cos k_i, \tag{5.3.10}$$

with $\omega = e^{2\pi i/3}$ and $\lambda_{\mathbf{k}}^{-} = (\lambda_{\mathbf{k}}^{+})^*$. Note that the $p_{x,y}$ waves $(\lambda_{\mathbf{k}}^{p_1}, \lambda_{\mathbf{k}}^{p_2})$ are simply obtained via the relation $\lambda_{\mathbf{k}}^{p_\pm} = \lambda_{\mathbf{k}}^{p_1} \pm i\lambda_{\mathbf{k}}^{p_2}$, and similarly for the d waves.

Given the triangular lattice harmonics and their symmetry properties, we directly obtain the triangular lattice analog of Eq. (5.3.6) given by

$$h_{\mathbf{k}} = \varepsilon_{\mathbf{k}} \tau_z + \Delta_1 \lambda_{\mathbf{k}}^{f_1} \tau_y - \Delta_2 \lambda_{\mathbf{k}}^{f_2} \tau_x. \tag{5.3.11}$$

Here we have defined the difference of on-site energies $\varepsilon_s - \varepsilon_f$ as $3t - \delta$ and $\varepsilon_{\mathbf{k}} = 3t - \delta - t\lambda_{\mathbf{k}}^{s}$, where t denotes ordinary nearest neighbor hopping. The invariance of $h_{\mathbf{k}}$ under C_6 rotations of follows directly from the symmetry of the f-waves couplings. This may be seen, for instance, from Fig. 5.3.1. Since the f-wave harmonics are odd functions of $\mathbf{k}$, the second term in Eq. (5.3.11) is invariant under T, whereas the third term breaks both T and M. A schematic representation of the triangular lattice model of (5.3.11), in particular the inter-orbital hoppings described by $\Delta_{1,2}$, is shown in Fig. 5.3.3 (**A**). For nonzero $(\delta, \Delta_1, \Delta_2)$ the spectrum of $h_{\mathbf{k}}$ has a full

energy gap and the two non-degenerate bands are Chern bands with $C = \pm 3$ when $4t > \delta > 0$. A plot of the energy bands in the inverted regime, $\delta = 0.5t$, is shown in Fig. 5.3.3 (**B**). Note that the gap is proportional to $\delta^{3/2}$. Below, in Sec. 5.3.1, we discuss the low-energy limit of the transition as function of δ in more detail.

In addition to the model with $C = \pm 3$ bands, it is straightforward to construct a triangular lattice model with $C = \pm 2$ bands. This is achieved by considering s-orbital and d-orbital states as local degrees of freedom. Since the two d-wave states $(d_{x^2-y^2}, d_{xy})$ are degenerate, both should be included a priori. Consider the following model describing the coupling of s and d states, where $d_{\mathbf{k}1,2}$ annihilate electrons with $d_{x^2-y^2,xy}$-orbital symmetry:

$$H = \sum_{\mathbf{k}} \varepsilon_{\mathbf{k}} (s^\dagger_{\mathbf{k}} s_{\mathbf{k}} - d^\dagger_{\mathbf{k}\alpha} d_{\mathbf{k}\alpha}) + \Omega \sum_{\mathbf{k}} d^\dagger_{\mathbf{k}-} d_{\mathbf{k}-} + \sum_{\mathbf{k}} \Delta(\lambda^{d_+}_{\mathbf{k}} s^\dagger_{\mathbf{k}} d_{\mathbf{k}-} + \lambda^{d_-}_{\mathbf{k}} s^\dagger_{\mathbf{k}} d_{\mathbf{k}+}) + \text{H.c.} \quad (5.3.12)$$

Once more we have defined $\varepsilon_{\mathbf{k}} = 3 - \lambda^s_{\mathbf{k}} + \delta$ and the operators $d_{\mathbf{k}\pm} = d_{\mathbf{k}1} \pm i d_{\mathbf{k}2}$ correspond to the chiral basis of the d-wave states; a sum over $\alpha = 1, 2$ is implied. Observe that the term proportional to Δ, which couples the s- and d-states, is fully invariant under rotations. Furthermore, it is invariant under T and M. The second term, on the other hand, which is proportional to Ω and energetically splits chiral d-waves, breaks T and M symmetry. We may choose this energy scale to be positive and very large, i.e., $\Omega \gg 1$, and project out the $d_{\mathbf{k}-}$ states to obtain an effective model for the s and d_+ states. Note that projecting out the $d_{\mathbf{k}-}$ states is consistent

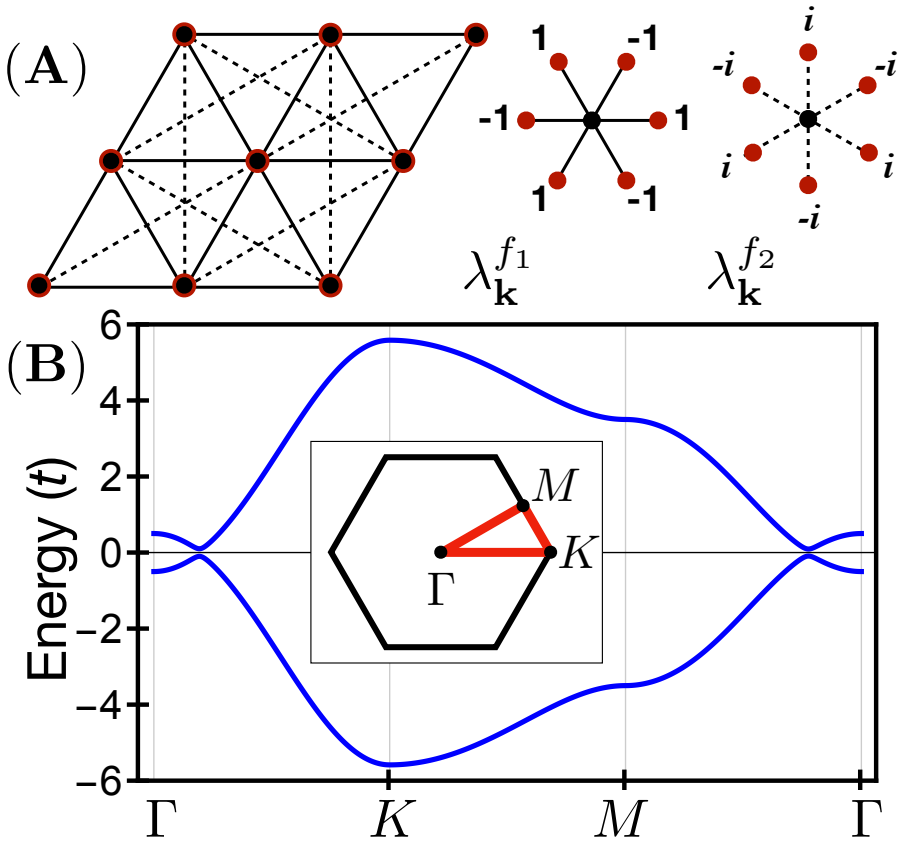

Figure 5.3.3: Triangular lattice model. Panel (**A**) shows two-orbital triangular lattice model introduced in Eq. (5.3.11), with inter-orbital nearest neighbor hopping (Δ_1) and next-nearest neighbor hopping (Δ_2). In case of the triangular lattice, the onsite orbitals have s- and f-wave symmetry, and the real space structure of the inter-orbital hopping, described by the lattice harmonics $\lambda^{f_1}_{\mathbf{k}}$ and $\lambda^{f_1}_{\mathbf{k}}$, is schematically shown on the right. (**B**) Spectrum of the triangular lattice model in the inverted regime, i.e., $\delta = 0.5t > 0$, for the parameters $(\Delta_1, \Delta_2) = (1.5t, 1.5t)$. In inset shows the Brillouin zone path.

with C_6 symmetry and broken T and M symmetry. The reduced two-band model can then be expressed in the form of (5.3.1) with $h_{\mathbf{k}}$ given by

$$h_{\mathbf{k}} = \varepsilon_{\mathbf{k}}\tau_z + \Delta\lambda_{\mathbf{k}}^{d_-}\tau_+ + \Delta^*\lambda_{\mathbf{k}}^{d_+}\tau_-, \tag{5.3.13}$$

where $\tau_\pm \equiv (\tau_x \pm i\tau_y)/2$. This Hamiltonian describes a transition from a trivial insulator to a Chern insulator with $C = \pm 2$ on the triangular lattice. Note that, contrary to Eq. (5.3.11) or (5.3.6), there is only one parameter Δ describing the coupling of s- and d-states, which is due to C_6 symmetry.

Clearly, by simply making the replacement $d \to p$ in Eq. (5.3.12) this construction directly applies to states with p-wave symmetry, in which case one obtains a $C = \pm 1$ Chern insulator model. Furthermore, the p-wave model is easily generalized to the square lattice using the square lattice harmonics [203], leading to the spinless (and lattice-regularized) Bernevig-Hughes-Zhang (BHZ) model [3].

The Honeycomb Lattice

Up to this point, we have considered onsite orbital degrees of freedom with nonzero angular momentum. This might suggest that the models introduced here require higher angular momentum atomic-like states (see Fig. 5.3.1) at sites of the crystal lattice. In fact, our construction is more general, and also applies when effective higher angular momentum states arise as a result of the structure of the unit cell. More specifically, in crystal lattices with a nontrivial unit cell, i.e., a unit cell containing multiple atoms which map to each other under symmetry operations,

one can form symmetrized states within the unit cell. These symmetrized states transform nontrivially under the symmetry group, in a way that is equivalent to nonzero angular momentum states. Therefore, the orbital states shown in Fig. 5.3.1 should be understood in a more general sense as states of a specific symmetry type, rather than atomic orbitals.

To illustrate this with an example, we now consider a simple honeycomb lattice model for spinless electrons. The honeycomb lattice, which has a triangular Bravais lattice, consists of two (triangular) sublattices, the A and B sublattice, and we define the corresponding electron operators as $a_{\mathbf{k}}$ and $b_{\mathbf{k}}$. As before, we collect these in a spinor

$$\varphi_{\mathbf{k}} = \begin{pmatrix} a_{\mathbf{k}} \\ \\ b_{\mathbf{k}} \end{pmatrix}. \tag{5.3.14}$$

The Hamiltonian H is defined as $H = \sum_{\mathbf{k}} \varphi^{\dagger}_{\mathbf{k}} h_{\mathbf{k}} \varphi_{\mathbf{k}}$ with $h_{\mathbf{k}}$ given by

$$h_{\mathbf{k}} = (t\phi_{\mathbf{k}} - t'\phi'_{\mathbf{k}})\tau_+ + (t\phi^*_{\mathbf{k}} - t'\phi'^*_{\mathbf{k}})\tau_- + t_H \lambda^{f_1}_{\mathbf{k}} \tau_z. \tag{5.3.15}$$

Here $\phi_{\mathbf{k}}$ is a honeycomb lattice harmonic describing nearest neighbor hopping and is defined as $\phi_{\mathbf{k}} = \sum_i e^{i\mathbf{k}\cdot\mathbf{d}_i}$, where $\mathbf{d}_{i=1,2,3}$ are the three nearest neighbor bond vectors $\mathbf{d}_{i=1,2,3} = (\sin\theta_i, \cos\theta_i)^T/\sqrt{3}$. [The angles $\theta_{i=1,2,3}$ are the same as in Eq. (5.3.8).] Furthermore, the honeycomb lattice harmonic $\phi'_{\mathbf{k}} = \sum_i e^{-2i\mathbf{k}\cdot\mathbf{d}_i}$ describes third nearest neighbor hopping across a hexagon, and the final term proportional to t_H is the Haldane term [35], with $\lambda^{f_1}_{\mathbf{k}}$ defined in Eq. (5.3.9). The three hoppings are shown in Fig. 5.3.4 (**B**), where arrows indicate T-breaking imaginary hopping.

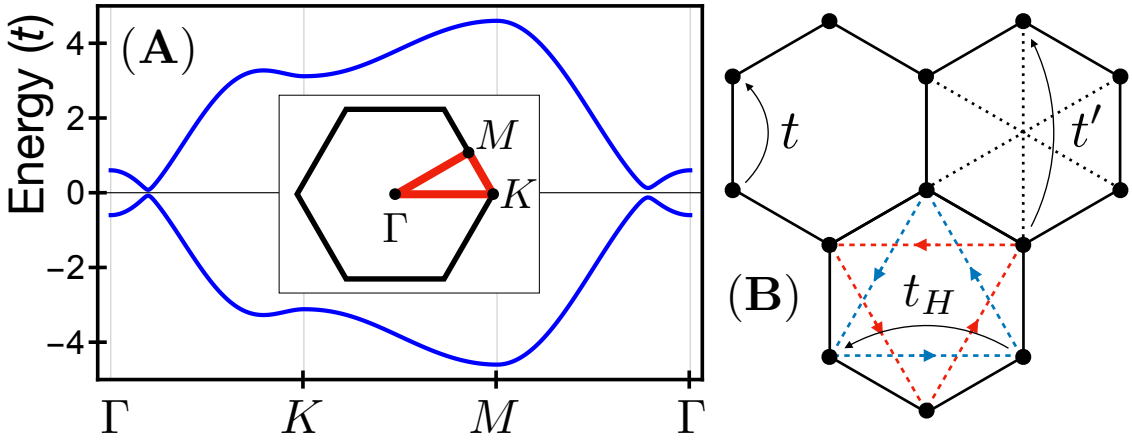

Figure 5.3.4: Honeycomb lattice model. (**A**) Spectrum of the honeycomb lattice model defined in Eq. (5.3.15) for hopping parameters $(t', t_H) = (1.2t, 1.2t)$; the inset shows the Brioullin zone path. (**B**) The honeycomb lattice model is defined by three hopping parameters t, t', and t_H. Here, t' describes hopping across the hexagon, which is taken to have negative sign in (5.3.15), and t_H corresponds to the Haldane term and describes T-breaking next-nearest neighbor hopping.

To see how Eqs. (5.3.14) and (5.3.15) give rise to states which have the symmetry of higher angular momentum orbitals consider the Hamiltonian at $\mathbf{k} = 0$. The Hamiltonian takes the form $h_{\mathbf{k}=0} = (t - t')\tau_x$, which implies that the eigenstates are the even and odd linear combinations $a_{\mathbf{k}=0} \pm b_{\mathbf{k}=0}$. Clearly, the odd linear combination is odd under all symmetries of the honeycomb lattice which exchange the sublattices, and therefore the eigenstates at $\mathbf{k} = 0$ transform as s and f waves. Now, if we redefine $t' = t - \delta$, then δ parametrizes a band inversion transition of two bands with relative angular momentum $l = 3$ at $\mathbf{k} = 0$. As a result, Eq. (5.3.15) falls in the class of models of which the low-energy description is captures by Eq. (5.2.2).

It is easy to recognize that the Hamiltonian of Eq. (5.3.15) can be viewed as a simple generalization of the Haldane model introduced in Ref. [35]. In the context

of the Haldane model, the band inversion transition described by Eq. (5.3.15) can be understood as follows. First, we take $t' = 0$ but choose t_H nonzero; this is the Haldane model and describes a Chern insulator with $C = \pm 1$ bands. Now we turn on and increase t' (which we take positive). As long as the gap stays open the ground state is a Chern insulator with $C = \pm 1$ bands. At $t' = t$ the gap closes and reopens for $t' > t$. Since this transition is an angular momentum $l = \pm 3$ transition, the Chern numbers must have changed by ± 3 and indeed we find the resulting bands to have Chern number $C = \mp 2$. (Note that the sign of C is determined by the sign of t_H.) As a result, neither side of the transition corresponds to the trivial insulator. A plot of the bands for $t' > t$ is shown in Fig. 5.3.4 (**A**). Note that a large t_H leads to a large separation of bands at K, which can be viewed as a large mass for the graphene Dirac points.

Low-energy Limit

In the models presented above, in particular the square and triangular lattice models, we have made use only of the lowest order lattice harmonics, i.e., we included the nearest (or at most next-nearest) neighbor couplings. As our considerations have shown, for the purpose of constructing models with a low-energy description given by Eqs. (5.2.2) and (5.2.3) this is sufficient. In general, one may include higher order lattice harmonics of the same symmetry type, without affecting the essential physics described by the model.

We now turn to a more detailed analysis of Eqs. (5.3.6) and (5.3.11) from the viewpoint of higher angular momentum band inversion transitions. We begin by expanding the coupling terms of the former [which should be identified with $\Delta_{\mathbf{k}}$ of Eq. (5.2.3)] to lowest order in $\mathbf{k}$, and find for $m = 2, 3$

$$\Delta_{\mathbf{k}} \propto (\Delta_1 - \Delta_2)k_+^m + (\Delta_1 + \Delta_2)k_-^m, \tag{5.3.16}$$

where $m = 2$ and $m = 3$ correspond to Eqs. (5.3.6) and (5.3.11), respectively. The fact that both k_+^m and k_-^m appear is due to discrete crystal symmetry; the form of Eq. (5.2.3) is only recovered at a fine-tuned point when $\Delta_1 = \Delta_2$. The dominant term is determined by the relative magnitude of $|\Delta_1 + \Delta_2|$ and $|\Delta_1 - \Delta_2|$, which also determines the Chern number in the inverted regime. By changing one of the two parameters $\Delta_{1,2}$ while keeping the other fixed, the system undergoes a transition from a Chern number $C = \pm m$ phase to a Chern number $C = \mp m$ phase. This transition occurs via a mass inversion at $2m$ Dirac points located on the electron-hole Fermi surface defined by k_F (see Sec. 5.2). Note that this is consistent with the fact that in a C_n-symmetric system the Chern number can only be determined from the rotation eigenvalues mod n [185]; here we have $2m = n$ for $m = 2, 3$ and $n = 4, 6$.

Now, let us address the question whether (5.3.6) and (5.3.11) represent the most general form a Hamiltonian consistent with C_4 or C_6 rotation symmetry. That is to say, we ask whether there might be additional terms which can be added to (5.3.6) and (5.3.11) while preserving its generic structure. In the case of C_4

symmetry, we can reconsider Eq. (5.3.5) and observe that in general Δ_1 and Δ_2 can be complex. This more general Hamiltonian is still symmetric under C_4 rotations and translates into an additional term for the lattice model of Eq. (5.3.6) given by $\Delta_1' \lambda_{\mathbf{k}}^{d_1} \tau_x + \Delta_2' \lambda_{\mathbf{k}}^{d_2} \tau_y$. Expanding this full C_4-symmetric Hamiltonian in small momenta $\mathbf{k}$ one finds

$$\Delta_{\mathbf{k}} \propto \tilde{\Delta}_+ k_+^2 + \tilde{\Delta}_- k_-^2, \tag{5.3.17}$$

with $\tilde{\Delta}_\pm$ given by

$$\tilde{\Delta}_\pm = \Delta_1' \pm \Delta_2' - i(\Delta_1 \mp \Delta_2). \tag{5.3.18}$$

From this we conclude that a full account of the symmetry-allowed couplings leads to a low-energy Hamiltonian of the form Eqs. (5.2.2) and (5.2.3) with $\Delta_{\mathbf{k}}$ given by (5.3.17) in terms of $\tilde{\Delta}_\pm$. Only the magnitudes $|\tilde{\Delta}_\pm|$ are important for the topological classification in the inverted regime ($\delta > 0$). Clearly, this conclusion holds equally for the case $m = 3$ and C_6 symmetry; in particular, Eq. (5.3.18) is still valid.

5.3.2 Spin Angular Momentum Models

The two-band models constructed in the previous subsection all rely on on-site orbital states with integral angular momentum. This property is not strictly required by Eq. (5.2.7), since it only fixes the relative angular momentum. Therefore, a different approach to engineering a band inversion with relative angular momentum l relies on exploiting the spin degree of freedom. For instance, two states with spin quantum number $j_z = \pm l/2$ with odd l have relative angular momentum l.

Similarly, by considering states with general spin quantum numbers $l_1/2$ and $l_2/2$ and engineering couplings between such states, it becomes possible to realize band inversions with angular momentum $(l_1 - l_2)/2$, where $l_{1,2}$ are both odd. In this subsection we follow this approach.

In the presence of a spin degree of freedom a minimal model describing a band inversion must have four bands. We therefore begin by considering a triangular lattice model with two spin $j_z = \pm\frac{3}{2}$ Kramers pairs. We introduce the electron operators $c_{\mathbf{k}\Uparrow,\Downarrow}$ for each Kramers pair, where $\Uparrow,\Downarrow \equiv \pm\frac{3}{2}$, and collect these in a vector $c_{\mathbf{k}}$ defined as

$$c_{\mathbf{k}} = \begin{pmatrix} c_{\mathbf{k}\Uparrow\alpha} \\ \\ c_{\mathbf{k}\Downarrow\alpha} \end{pmatrix}. \tag{5.3.19}$$

Here $\alpha = 1, 2$ is a flavor index which labels the two pairs. The Hamiltonian is then defined as $H = \sum_{\mathbf{k}} c^{\dagger}_{\mathbf{k}} h_{\mathbf{k}} c_{\mathbf{k}}$ with four-band matrix $h_{\mathbf{k}}$. To describe the couplings between spin states we introduce a set of spin Pauli matrices $\sigma_{x,y,z}$, where $\sigma_z = \pm 1$ corresponds to $\Uparrow,\Downarrow$; we use the Pauli matrices $\tau_{x,y,z}$ to describe couplings in flavor space.

The form of the Hamiltonian $h_{\mathbf{k}}$ can be determined using the same symmetry prescription as before. The symmetry of the spin matrices $\sigma_{x,y,z}$ follows from the transformation properties of the $j_z = \pm\frac{3}{2}$ spin states, which are different from the transformation properties of a more familiar $j_z = \pm\frac{1}{2}$ doublet. In particular, the spin matrices σ_x and σ_y do not transform as the x, y-components of an $S = 1$ angular momentum (which transform as $p_{x,y}$ waves) but instead transform as f

waves. This implies that a rotationally symmetric coupling of the spin states has f-wave symmetry. We again take $\varepsilon_{\mathbf{k}} = 3 - \lambda^s_{\mathbf{k}} - \delta$ and find that a minimal Hamiltonian with C_6 symmetry but broken T and M symmetry takes the form

$$h_{\mathbf{k}} = \varepsilon_{\mathbf{k}}\tau_z + b_z\sigma_z + \Delta_1\lambda^{f_1}_{\mathbf{k}}\tau_x\sigma_x + \Delta_2\lambda^{f_2}_{\mathbf{k}}\tau_x\sigma_y. \tag{5.3.20}$$

The first term describes the dispersion $\varepsilon_{\mathbf{k}}$ and energy difference δ of two spin-degenerate bands. Here, we are interested the regime where these bands remain uninverted and therefore set $\delta < 0$. The second term describes a Zeeman splitting of the $j_z = \pm\frac{3}{2}$ Kramers pair states in each band, and as such it breaks T, vertical reflections, and twofold rotations about in-plane axes; the Zeeman splitting preserves C_6. For Eq. (5.3.20) to describe a band inversion with angular momentum $l = \pm 3$, we consider the case $|b_z| > \delta$, which corresponds to an inversion of a $j_z = \frac{3}{2}$ and $j_z = -\frac{3}{2}$ band with different flavor index. The final two terms then describe an f-wave coupling between the spin species, which is off-diagonal in flavor space. This coupling gaps out the inverted bands and realizes a Chern insulating phase in the way described by Eq. (5.2.2). We note here that the f-wave coupling of Eq. (5.3.20) does not break T and can thus viewed as a form of spin-orbit coupling; we will return to this observation in Sec. 5.5. This remains true when considering a slightly more general coupling of the form $(\Delta_1\lambda^{f_1}_{\mathbf{k}} + \Delta_2\lambda^{f_2}_{\mathbf{k}})\tau_x\sigma_+ + \text{h.c.}$, where $\Delta_{1,2}$ are complex. The latter form should be viewed in the context of the discussion following Eqs. (5.3.17) and (5.3.18).

Next, consider the case of two Kramers pairs with $j_z = \pm\frac{3}{2}$ and $j_z = \pm\frac{1}{2}$,

respectively. Adopting the notation $\uparrow, \downarrow \equiv \pm\frac{1}{2}$ for the two $j_z = \pm\frac{1}{2}$ states, we can collect the electron operators in a vector $c_{\mathbf{k}}$ given by

$$c_{\mathbf{k}} = (c_{\mathbf{k}\Uparrow}, c_{\mathbf{k}\uparrow}, c_{\mathbf{k}\downarrow}, c_{\mathbf{k}\Downarrow})^T, \tag{5.3.21}$$

which has the structure of a $j = \frac{3}{2}$ quartet. Since the particle-hole pairs $c^\dagger_{\mathbf{k}\Uparrow} c_{\mathbf{k}\downarrow}$ and $c^\dagger_{\mathbf{k}\Downarrow} c_{\mathbf{k}\uparrow}$ have angular momentum $+2$ and -2, respectively, we can seek to engineer a band inversion between the corresponding bands and couple these with angular momentum $l = \pm 2$ lattice harmonics. The minimal Hamiltonian which achieves this has a structure similar to Eq. (5.3.20) and takes the form

$$h_{\mathbf{k}} = \varepsilon_{\mathbf{k}} \sigma_z \tau_z + b_z \sigma_z + \Delta(\lambda^{d_+}_{\mathbf{k}} \sigma_- + \lambda^{d_-}_{\mathbf{k}} \sigma_+). \tag{5.3.22}$$

Here $\tau_z = \pm 1$ still describes the two Kramers pairs but the basis is defined by Eq. (5.3.21). As in Eq. (5.3.20), the first two terms are responsible for the band inversion and the final two terms describe a d wave pairing of the inverted bands, which is responsible for the energy gap. Recall that the d waves are degenerate on the triangular lattice, leading to a single coupling parameter Δ. Due to the d-wave nature of the coupling, the ground state of (5.3.22) realizes a Chern insulator with $C = \pm 2$. A model related to Eq. (5.3.22) was considered in Ref. [193].

5.4 Interactions and Excitonic Pairing

In this section we turn to a more thorough study of the Chern insulator models introduced in the previous section. In particular, we address the effect of elec-

tronic correlations on the nature of the band inversion transition. As explained in Sec. 5.2, the Hamiltonian of Eq. (5.2.2) describes a band inversion transition of non-interacting fermions. Similarly, the lattice models introduced in the previous section are free fermion models. To see how interactions can affect the nature of the band inversion, consider the critical point defined by $\delta = 0$ where the two bands touch at $\mathbf{k} = 0$. First note that symmetry protects the quadratic dispersion of the bands at the touching point, which implies that the density of states does not vanish. This should be contrasted with a Dirac fermion transition, characterized by linear dispersion at the touching point, for which the density of states vanishes. Due to the nonzero density of states it is natural to expect that interactions give rise to correlated states with an energy gap.

Two different possibilities for correlated states can be distinguished. The first is the formation of an excitonic insulator defined by the condensation of (conduction band) electron and (valence band) hole bound states. The condensation of electron-hole excitons breaks rotational symmetry and is therefore associated with a spontaneously broken (discrete) symmetry. The second possibility is the formation of a correlated liquid of electrons and holes which does not break symmetries but instead has fractional quantum Hall topological order [194, 204]. This intriguing second scenario has motivated a previous study [194], in which we proposed and analyzed a wave function description for such correlated liquid of electrons and holes. In this work we focus on the first scenario and study the excitonic insulator

state in the vicinity of the band inversion. More precisely, we consider the mean field theory of the excitonic insulator.

We have argued in Sec. 5.2 that the description of the higher angular momentum band inversions is formally similar to the BCS theory for (higher angular momentum) pairing states of fermions. In case of the former, however, there is no notion of a broken symmetry in the absence of interactions. The interaction-driven excitonic insulator, on the other hand, does break a symmetry and its mean field theory (at low-energies) is an analog of BCS theory for s-wave pairing. As a result, the formation of excitons can be referred to as excitonic pairing of electrons and holes. As we will demonstrate, the development of a mean field theory for excitonic pairing, in close analogy with BCS theory, gives access to information about the structure of the ground state in the vicinity of the band inversion transition. Most importantly, this will lead us to the conclusion that the ground state in the band inverted regime can be viewed as a multicomponent $C = 1$ quantum Hall liquid of electrons and holes.

It is worth pointing out that the present case of quadratically crossing bands is different from previously studied quadratic band crossing models [186, 190–192]. In the latter, the degeneracy at the touching point is protected by point group and T symmetry. In contrast, in the present case the touching point is not symmetry-protected, but instead defines the critical point of the band inversion transition parametrized by δ; δ does not reflect a broken symmetry. A band inversion of this

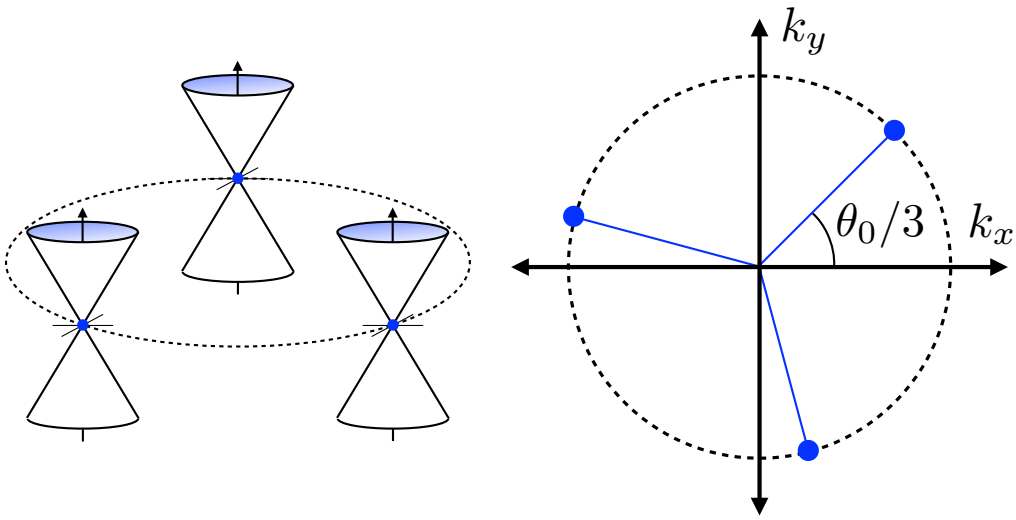

Figure 5.4.1: Dirac points at the topological phase transition. For the case $m = 3$ the transition from the topological Chern insulating phase to the excitonic insulator phase is marked by three Dirac points, as shown schematically on the left. This transition is described by Eq. 5.4.1 and occurs when $|\Delta_0| = |\Delta_{m=3}|(2\delta)^{3/2}$. The Dirac points are located on a circle with radius k_F and are related by threefold rotation symmetry, as shown on the right. Importantly, the angle at which the Dirac points are located is determined by the phase of Δ_0.

kind was considered in Ref. [193], which recognized the importance of interactions when symmetry protects the quadratic band dispersion and studied the implications for the topological transition.

5.4.1 Excitonic Insulator Mean Field Theory

General Analysis of the Continuum Model

To begin, consider the low-energy description of the square and triangular lattice models of Eqs. (5.3.6) and (5.3.11). In the analysis that follows we particularize to these models for illustrative purposes, without loss of generality. Consider furthermore the special case $\Delta_1 = \Delta_2 \equiv \Delta$; according to Eq. (5.3.16), for small momenta $\mathbf{k}$

this implies $\Delta_{\mathbf{k}} \sim \Delta_m(k_x - ik_y)^m$ with $m = 2, 3$. Based on Eq. (5.3.18), we promote Δ_m to a complex number with arbitrary phase. In addition, in the small momentum limit one has $\varepsilon_{\mathbf{k}} \simeq \mathbf{k}^2/2 - \delta$. As discussed, the form of $\Delta_{\mathbf{k}}$ (i.e., an eigenstate of L_z with angular momentum $l = -m$) is determined by the rotational symmetry of the system. Importantly, the formation of excitons, i.e., excitonic pairing, alters the form of $\Delta_{\mathbf{k}}$ and breaks rotational symmetry. Specifically, in a mean field description of excitonic pairing $\Delta_{\mathbf{k}}$ becomes

$$\Delta_{\mathbf{k}} = \Delta_0 + \Delta_m(k_x - ik_y)^m, \tag{5.4.1}$$

where $m = 2, 3$ and Δ_0 represents the formation of excitons. We observe that Δ_0 is an angular momentum $l = 0$ coupling of conduction and valence band, and since (5.4.1) is a superposition of terms with different angular momentum, rotational symmetry is broken. In the low-energy continuum limit the $l = 0$ angular momentum term breaks the emergent continuous rotation symmetry and lowers the symmetry to $\mathbb{Z}_m$. In particular, Δ_0 transforms as $\Delta_0 \to e^{-im\theta}\Delta_0$ under rotations by an angle θ. This establishes a link between the phase of Δ_0 and rotation symmetry breaking, which is analogous to the link between the superconducting phase and $U(1)$ charge conjugation.

On the lattice, in the case $m = 2$ the fourfold rotation C_4 is reduced to C_2; in the case $m = 3$ the rotational symmetry is lowered from C_6 to C_3. In both cases, $m = 2$ and $m = 3$, the form of (5.4.1) can be derived from a lattice model mean field Hamiltonian given by $h_{\mathbf{k}} \to h_{\mathbf{k}} + \Delta_0\tau_+ + \Delta_0^*\tau_-$.

To examine the implications of (5.4.1), in particular the excitonic term, it is useful to invoke the connection to the problem of pairing states. In the context of pairing states, Δ_0 can be interpreted as an s-wave pairing. Assuming one is in the band inverted regime, this implies a transition from a Chern insulating phase to a trivial insulator phase as function of the strength of Δ_0. This follows from the fact that s-wave pairing is topologically trivial. The transition occurs when $|\Delta_0| = |\Delta_m| k_F^m = |\Delta_m| (2\delta)^{m/2}$, where k_F is a momentum defined by the condition $\varepsilon_{\mathbf{k}} = 0$ (see Sec. 5.2). At the transition the system is gapless, with three ($m = 3$) or two ($m = 2$) Dirac points located on a circle in momentum space with radius k_F. Thus, the transition is marked by three (or two, in the case of $m = 2$) Dirac fermion mass inversions, which is consistent with the total change in the Chern number. This is shown schematically in Fig. 5.4.1 for the case $m = 3$. Note that the location of the Dirac points depends on the phase of Δ_0: assuming $\Delta_0 = |\Delta_0| e^{i\theta_0}$ and Δ_m real but negative, the Dirac points are located at angles $\theta_0/m + j2\pi/m$ with $j = 0, 1, 2$.

Mean Field Phase Diagram

Having discussed the qualitative features of the excitonic mean field theory, we now turn to a more quantitative analysis. To this end, we take the triangular lattice model of Eq. (5.3.11) (the analysis is similar for the $m = 2$ square lattice model), in which we set $\Delta_1 = \Delta_2 \equiv \Delta_{m=3}$, and add an onsite Hubbard repulsion of the form

$H_U = U \sum_j n_{js} n_{jf}$, where $n_{s,f}$ are the density operators of the s and f orbitals and the sum is over sites. A similar mean field theory for a many-body band inversion of spinful electrons was previously considered for a $C = \pm 2$ transition on the triangular lattice [193].

In momentum space the Hubbard repulsion takes the form

$$H_U = \frac{U}{N} \sum_{\mathbf{q}} \sum_{\mathbf{k}\mathbf{k}'} s^\dagger_{\mathbf{k}+\mathbf{q}} s_{\mathbf{k}} f^\dagger_{\mathbf{k}'} f_{\mathbf{k}'+\mathbf{q}}, \tag{5.4.2}$$

where N is the system size (i.e., total number of sites). By performing a mean field decoupling of (5.4.2) in the excitonic channel (see Appendix 5.B for details) one obtains a self-consistency condition for the excitonic order parameter Δ_0 given by

$$\Delta_0 = -\frac{U}{2N} \sum_{\mathbf{k}} \langle \varphi^\dagger_{\mathbf{k}} \tau_x \varphi_{\mathbf{k}} \rangle. \tag{5.4.3}$$

Here $\varphi_{\mathbf{k}}$ are the fermion operators defined in Eq. (5.3.7). At zero temperature Eq. (5.4.3) defines the stationary point of the free energy density

$$F[\Delta_0] = -\sum_{\mathbf{k}} E_{\mathbf{k}} + \frac{N}{U} \Delta_0^2, \quad E_{\mathbf{k}} = \sqrt{\varepsilon^2_{\mathbf{k}} + |\Sigma_{\mathbf{k}}|^2}, \tag{5.4.4}$$

where $\Sigma_{\mathbf{k}}$ is defined as $\Sigma_{\mathbf{k}} = \Delta_0 + \Delta_{\mathbf{k}}$ with $\Delta_{\mathbf{k}} = \Delta_3 (i\lambda^{f_1}_{\mathbf{k}} + \lambda^{f_2}_{\mathbf{k}})$.

Solving these equations at zero temperature, we obtain a phase diagram of excitonic pairing as function of the interaction strength U and the band inversion parameter δ. The results are presented in Fig. 5.4.2, which we now discuss. We first focus on the case $\delta = 0$. In this case, the non-interacting system is right at the topological transition and is gapless, with two quadratically dispersing bands

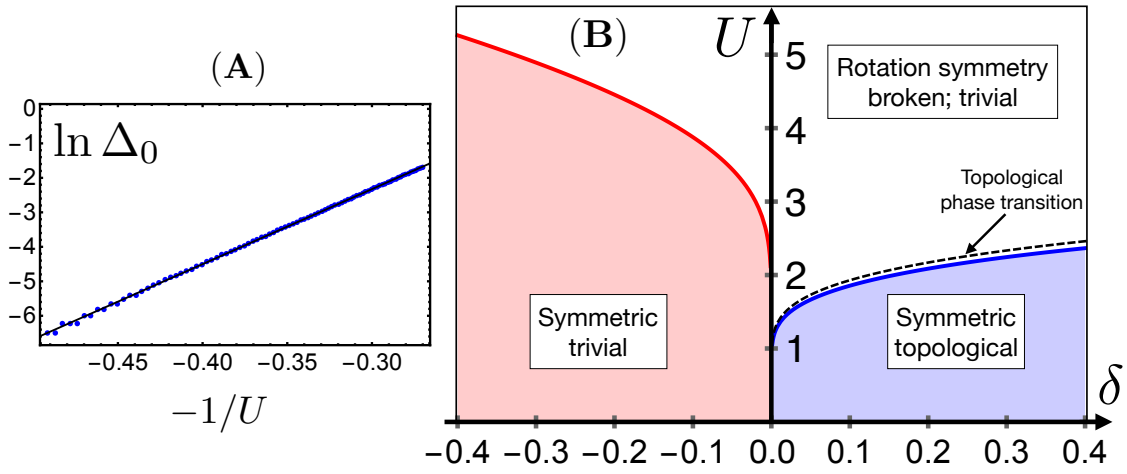

Figure 5.4.2: Excitonic mean-field theory. Panel (**A**) shows the dependence of Δ_0 on U at the band inversion transition defined by $\delta = 0$; since $\Delta_0 \sim \exp(-1/\alpha U)$, we plot $\ln \Delta_0$ as function of $-1/U$. Panel (**B**) shows the U–δ phase diagram obtained from the mean field theory of excitonic pairing at zero temperature. In the inverted regime ($\delta > 0$) the blue curve shows the phase boundary separating the rotation symmetric topological phase from the rotation symmetry broken phase with nonzero excitonic pairing. The critical interaction strength U_c, which defines this phase boundary, is obtained from (5.4.6). The dashed curve indicates the presence of a second transition in the vicinity of the symmetry breaking transition, at $U_c' > U_c$, which separates the symmetry broken topological phase from the trivial excitonic insulator. In all calculations the overall energy scale is fixed by setting $t = 1$ and Δ_3 is set to $\Delta_3 = 1.0$.

touching at $\mathbf{k} = 0$. As a consequence of the non-vanishing density of states at the gapless point, the susceptibility is divergent and one expects a rotation symmetry broken state with nonzero Δ_0 at infinitesimal U. More precisely, one expects $\Delta_0 \sim \exp(-1/\alpha U)$, where α is a constant reflecting the density of states [186]. This is confirmed in Fig. 5.4.2 (**A**), where we show $\ln \Delta_0$ as function of $-1/U$ for the case $\delta = 0$. (In all calculations we choose $\Delta_3 = 0.5t$.)

We then proceed to the case $\delta \neq 0$. For nonzero δ, when the non-interacting system given by $h_{\mathbf{k}}$ in Eq. (5.3.11) is gapped, one expects a transition to the rotation symmetry broken state at finite interaction strength U_c. The critical interaction strength as function of δ defines the phase boundary which separates the rotation symmetric phase from the rotation symmetry broken phase with nonzero excitonic pairing. Since the inverted regime ($\delta > 0$) and the uninverted regime ($\delta < 0$) have different dispersion, as is clear from Fig. 5.2.1 (**A**) and (**C**), the critical strength U_c is expected to be smaller in the inverted regime. We find that the transition to the symmetry broken phase is a second order transition in mean field theory, which implies that a closed form expression for U_c can be obtained by expanding F of Eq. (5.B.9) in powers of Δ_0. Such Landau-type expansion can only have even powers of Δ_0 and is valid in the vicinity of the transition when Δ_0 is small; specifically, one has up to fourth order

$$F[\Delta_0]/N = \left(U^{-1} - c_2\right) \Delta_0^2 + c_4 \Delta_0^4. \tag{5.4.5}$$

Then, U_c is defined by the condition that the coefficient of the quadratic term

vanishes and we find

$$U_c = \frac{1}{c_2}, \quad c_2 = \frac{1}{2N}\sum_{\mathbf{k}}\left[\frac{1}{E_{\mathbf{k}}} - \frac{(\mathrm{Re}\Delta_{\mathbf{k}})^2}{E_{\mathbf{k}}^3}\right], \tag{5.4.6}$$

where $E_{\mathbf{k}}$ defined in Eq. (5.B.9) is evaluated at $\Delta_0 = 0$. Figure 5.4.2 (**B**) shows the U–δ phase diagram obtained by evaluating U_c as function of δ. As expected, U_c is smaller in the inverted regime (blue curve) compared to the uninverted regime (red curve).

As discussed above in Sec. 5.4.1, in the inverted regime defined by $\delta > 0$ one expects a second transition as the interaction strength increases. This second transition is a topological phase transition described by three Dirac fermions and occurs when $|\Delta_0| \sim |\Delta_{\mathbf{k}=k_F}|$. One may thus identify a second U_c' associated with the topological phase transition and it is then natural to ask how U_c' differs from U_c. To get an understanding, we employ the Landau theory of Eq. (5.4.5) and solve for Δ_0. Minimization directly yields $|\Delta_0| = \sqrt{(c_2 - U^{-1})/2c_4}$. Within this approach the value of U_c' is determined by setting this result equal to the value of Δ_0 at which which the topological transition occurs. Defining the latter as $\tilde{\Delta}_0$, we find

$$\frac{U_c' - U_c}{U_c} = \frac{1}{(2c_4 U_c \tilde{\Delta}_0^2)^{-1} - 1}. \tag{5.4.7}$$

We have verified that this estimate based on (5.4.5) is in good agreement with the numerically exact result. Since $(2c_4 U_c \tilde{\Delta}_0^2)^{-1} \gg 1$, Eq. (5.4.7) implies that the transitions, i.e., the symmetry breaking transition and the topological transition, are in close proximity. This is indicated by the dashed line in Fig. 5.4.2 (**B**).

To understand why $(U_c' - U_c)/U_c$ is small, it is helpful to consider the continuum description discussed in Sec. 5.4.1, which is valid for small δ. In this case one has $\tilde{\Delta}_0^2 \sim \delta^3$ and $c_4 \sim \delta^{-2}$, from which one finds $(U_c' - U_c)/U_c \sim \delta/\ln\delta$. Note that in case of the square lattice one finds $(U_c' - U_c)/U_c \sim 1/\ln\delta$.

The close proximity of the two transitions is an interesting aspect of higher angular momentum band inversions. The fate of these two transitions in an interacting theory beyond mean field will be an interesting question to address. Such theory should be formulated in terms of three flavors of Dirac fermions coupled to a fluctuating phase of the excitonic order parameter Δ_0, as suggested by Fig. 5.4.1.

5.4.2 Structure of the Ground State

Having discussed the quantitative aspects of the excitonic pairing mean field theory, we return to a more conceptual analysis, which we develop within the low-energy continuum model. More specifically, we proceed to examine the structure of the ground state as defined in Eq. (5.2.4). As discussed in Sec. 5.2 (see also Appendix 5.A), the continuum model ground state is specified in terms of the function $g_{\mathbf{k}}$ and we demonstrate below that the excitonic pairing term Δ_0 plays a key role in the interpretation of its Fourier transform $g(\mathbf{r})$. This leads to the conclusion that a theory for the band inversion transition which includes the excitonic pairing term gives access to the structure of the electron-hole ground state.

To show this, it is useful to first consider the case $\Delta_0 = 0$, i.e., when rotation

symmetry is not broken, and obtain $g(\mathbf{r})$. We note that the form of $g_{\mathbf{k}}$, and thus $g(\mathbf{r})$, changes across the band inversion transition and thus depends on δ. We focus on two cases: the critical point of the transition when $\delta = 0$, and the Chern insulating phase when $\delta > 0$. Consider the former case first. Right at the transition and for small momentum $\mathbf{k} \to 0$ one finds that $g_{\mathbf{k}} \propto \mathbf{k}^2/\Delta(k_x - ik_y)^m$. Taking the Fourier transform to obtain $g(\mathbf{r})$ one obtains

$$g(\mathbf{r}) \propto 1/z^m, \tag{5.4.8}$$

where $z = x + iy$. Note that since $g_{\mathbf{k}}$ is considered in the small momentum limit, (5.4.8) describes the long-distance behavior of $g(\mathbf{r})$. In this limit $g(\mathbf{r})$ falls off as a power law as function of the distance between the electron and hole forming a pair, and this regard the interpretation of (5.4.8) as describing the pairing of electrons and holes with angular momentum $l = -m$ makes sense. Furthermore, in Ref. [194] wave argued that many-body Slater-determinant of (5.4.8), defined by (5.2.4), can be related to lowest Landau level wavefunctions at filling factor $\nu = 1/m$. This argument was based on a comparison of the number of zeros of the many-body wave function, viewed as a function of one of its variables.

Consider next the band-inverted regime $\delta > 0$ (still taking $\Delta_0 = 0$). In this case the small momentum limit of $g_{\mathbf{k}}$ is given by $g_{\mathbf{k}} \propto \delta/\Delta^*(k_x + ik_y)^m$, which implies that in the long-distance limit $g(\mathbf{r})$ has the form

$$g(\mathbf{r}) \propto (z^*)^{m-1}/z. \tag{5.4.9}$$

As a result, one has that $|g|$ is constant for $m = 2$ [177] and $|g| \sim |z|$ for $m = 3$ at

long distances. This long-distance behavior of $g(\mathbf{r})$ presents a puzzle, since it is not immediately clear how to reconcile it with the interpretation of $g(\mathbf{r})$ as describing the pairing of electrons and holes; the electrons and holes cannot be said to be bound into a pair in a meaningful sense. In contrast, this is different for the well-known case of an $l = -1$ band inversion transition described by a Dirac fermion, which corresponds to $m = 1$ in (5.4.9). In the case of the latter, (5.4.9) corresponds to the "weak-pairing phase" [177] and the many-body Slater determinant of the electron-hole paired state defines a many-body wavefunction for the $C = \pm 1$ Chern insulator.

To make progress in understanding the higher Chern number phases in the inverted-regime, we break rotation symmetry by introducing a nonzero Δ_0, such that Δ_k is given by (5.4.1). As explained earlier, the amplitude of Δ_0 controls a transition from a Chern insulating phase to a trivial insulator phase, while keeping δ fixed. As far as the topology of the two phases is concerned, this is same topological transition as the transition controlled by δ (while keeping $\Delta_0 = 0$). The former, however, is characterized by a critical gapless phase with three linearly dispersing Dirac points and as a result, the topological transition parametrized by Δ_0 is described by m simultaneous $l = -1$ band inversions, consistent with a total angular momentum $l = -m$ transition. Each of these $l = -1$ band inversions, which are described by a Dirac fermion theory, is well understood and has $g(\mathbf{r}) \propto 1/z$. Consequently, the band inversion via three Dirac points reveals that a higher angular

momentum band inversion has the generic structure of three $l = -1$ Dirac fermion transitions, with three flavors of electron-hole pairing states describing a $\nu = 1$ quantum Hall phase.

This argument can be put on a more precise footing by considering $g_{\mathbf{k}}$ for Δ_k given by (5.4.1). In this case one finds

$$g_{\mathbf{k}} \propto \frac{\delta}{k_+^m + \Delta_0/\Delta_m}, \tag{5.4.10}$$

which has m first order poles at k_n $(n = 1, \ldots, m)$ rather than one m-th order pole at $\mathbf{k} = 0$. Defining $k_1 = (\Delta_0/\Delta_m)^{1/m}$ one has $k_n = e^{i2\pi(n-1)/3}k_1$ and (5.4.10) can be written as a sum over the three poles $\sum_{n=1}^{m} \gamma_n/(k_+ - k_n)$, where γ_n are the residues. Fourier transforming then gives the expected form of $g(\mathbf{r})$ for three $l = -1$ transitions, with additional oscillatory factors originating from the nonzero momenta k_n.

A few comments are in order regarding the significance of rotational symmetry breaking. As explained, the existence of m Dirac points at three distinct nonzero momenta requires the breaking of rotation symmetry. When full rotation symmetry is present it forces the three transitions to all occur at $\mathbf{k} = 0$, which in a sense obscures the topological structure of the transition, as evidenced by (5.4.9). As far as the topological structure of the transition between the higher Chern number insulating phase and the trivial insulator is concerned, the presence of higher rotational symmetry is not required. In fact, from the perspective of topology the situation where the three $l = -1$ transitions occur at different momenta is more generic.

A similar reasoning relying on broken rotation symmetry has been presented by Read and Green in the context of chiral d-wave pairing [177], which may be compared to our $m = 2$ case. In the case of chiral d-wave pairing, Read and Green showed that by studying the transition to a trivial s-wave pairing state—in contrast to changing the chemical potential—the correct edge excitation spectrum and vortex states of a chiral d-wave superconductor can be obtained. Since both the edge and vortex modes are rooted in the topological structure of the phase, this is another instance where only the more generic transition described by multiple Dirac fermions (and with broken rotation symmetry) reveals the true nature of the phase.

5.4.3 m-component $C = 1$ Quantum Hall States

The previous analysis of band inversions with broken rotation symmetry, in particular the splitting into multiple $l = -1$ band inversions, leads to an important insight regarding the structure of the higher Chern number phase. It can be stated as follows: Since the transition is described by m flavors of Dirac fermions, the higher Chern number phase can be viewed as an m-component $C = 1$ phase, of which each component is characterized by a quantum Hall wavefunction for electron-hole pairs at the Dirac point.

It should be emphasized that here we reach this conclusion based on a theory for the band inversion transition and do not make reference to the notion of a full

Chern band. This approach is very different from—but may be compared to—an approach which explicitly addresses the structure of the Chern band by studying its Wannier state representation [205]. The latter approach clearly requires knowledge of the full Chern band, as the Wannier state representation is inaccessible within a (low-energy) continuum model for the band inversion. Using the Wannier state representation, Ref. [205] showed that a band with Chern number $C > 1$ can be mapped to C layers of Landau levels, each of which is equivalent to a $C = 1$ band. Even though the two approaches are different, we thus see that both point to a characteristic structural property of higher Chern number bands: they are intrinsically multi-component in nature, with the number of components given by the Chern number C.

The Wannier state representation of bands with higher Chern number leads to a further important observation regarding the action of translational symmetry on the multi-layer quantum Hall systems [205]. Due to the structure of the Wannier states, one of the two primitive translations acts as a permutation on the C layers and thus acts nontrivially on the layer degree of freedom. This was shown to have rather drastic consequences when lattice dislocations are present. In particular, dislocations give rise to an intricate interplay between geometry and topology, resulting in topological degeneracy even for Abelian states.

Within the framework of the continuum model for the band inversion transition, we can establish a connection to this result by considering the effect of the m-fold

rotations. As noted earlier, the m-fold rotations give rise to a residual $\mathbb{Z}_m$ symmetry. Furthermore, the m-fold rotations permute the m Dirac points and thus permute the m $C = 1$ components. As an example, consider $m = 3$ and let $\mathbf{k}_{0,1,2}$ denote the location of the three Dirac points at the transition, as shown in Fig. 5.4.1. The threefold rotation relates these as $\mathbf{k}_n = C_3^n \mathbf{k}_0$, where $n = 0, 1, 2$. As explained in Sec. 5.4.1, the three Dirac point momenta $\mathbf{k}_{0,1,2}$ are determined by the phase of Δ_0. A $U(1)$ vortex in the phase of Δ_0 is associated with a $2\pi/3$ rotation and permutes the Dirac points. This suggests an interesting field theoretic description of the band inversion transition in terms of an XY variable Δ_0 and three Dirac fermions, where proliferation of vortices in the phase of Δ_0 restores rotational symmetry and leaves the Dirac fermions ill-defined. We leave the systematic development and analysis of such field theoretic description of higher angular momentum band inversions for future studies.

5.5 Time-reversal Invariant Generalizations

5.5.1 Transition from Normal to Topological Insulator

Now that we have introduced a class of Chern insulator models based on the notion of higher angular momentum band inversions, both the theory and the historical development of topological insulators lead to a natural question: do there exist time-reversal invariant generalizations of such models? For the orbital models of

Sec. 5.3.1 the answer is clearly yes, since we may simply introduce a spin degree of freedom and build a T-invariant Hamiltonian by combining two copies of $h_{\mathbf{k}}$: one for the up spins and a time-reversed version of $h_{\mathbf{k}}$ for the down spins. In particular, in the spirit of BHZ [3, 206] one can define

$$\mathcal{H}_{\mathbf{k}} = \begin{pmatrix} h_{\mathbf{k}} & \\ & h^*_{-\mathbf{k}} \end{pmatrix}. \tag{5.5.1}$$

This Hamiltonian describes a transition between a trivial insulator and a Chern insulating phase in each spin sector, where the Chern numbers associated with the two spin species have opposite sign. This can be viewed as a transition between a normal insulator and a topological insulator characterized by an integer number of helical edge modes. The number of helical edge modes is equal to the angular momentum of the transition.

At low-energies, close to the band inversion transition, the coupling of the $|l = 0, \pm\frac{1}{2}\rangle$ and $|l = \pm m, \pm\frac{1}{2}\rangle$ bands is a diagonal matrix $\Delta_{\mathbf{k}}$ in spin space given by

$$\Delta_{\mathbf{k}} = \Delta \begin{pmatrix} k_{\pm}^m & \\ & (-k_{\mp})^m \end{pmatrix}, \tag{5.5.2}$$

with $m = 2, 3$ and $k_{\pm} = k_x \pm ik_y$. By construction, this implies that the transition from normal to topological insulator (or vice versa) is special in the sense that right at the critical point of the transition (i.e., when the bands touch) the bands disperse quadratically. As in Sec. 5.4, one then expects interaction effects to be important. In this time-reversal invariant case, the two possibilities for correlated states are

the excitonic insulator and the fractional topological insulator [44, 154, 207–213]. In particular the fractional topological insulator is an interesting possibility, and band inversions of the type described by (5.5.1) and (5.5.2) are a promising venue for their realization.

The Hamiltonian of Eq. (5.5.1) has the property that it commutes with spin rotations about the z-axis, i.e., $[\mathcal{H}_{\mathbf{k}}, \sigma_z] = 0$, which implies that S_z is conserved. This property, however, is not guaranteed unless it is mandated by appropriate physical symmetries of the system. For a given symmetry group, the most general Hamiltonian allowed by symmetry may have spin-orbit coupling terms which violate S_z conservation. Since such terms are likely to spoil the form of the coupling $\Delta_{\mathbf{k}}$ at low energies, and thus potentially destroy the preconditions for interactions to be important, it is necessary to determine under what conditions the form of (5.5.1) is enforced by symmetry.

5.5.2 Symmetry Protection

To examine the symmetry protection of the T-invariant band inversion, we consider the axial point groups of two-dimensional layer groups (as in Sec. 5.3) and determine the constraints each imposes. Importantly, whereas in Sec. 5.3 we only needed to consider symmetry groups compatible with nonzero chirality, here we must consider a more general class of axial symmetry groups. These groups are summarized in Table 5.5.1, organized by crystal system and the presence of inversion symmetry.

We start by examining systems with orbital (l) and spin (j_z) degrees of freedom given by $(l, j_z) = (m, \pm\frac{1}{2})$, with $m = 2, 3$, which are simple spinful generalizations of the models introduced in Sec. 5.3.1. We then consider T-invariant generalizations of the models introduced in Sec. 5.3.2, which are constructed from two $j_z = \pm\frac{3}{2}$ Kramers pairs. We conclude by discussing a generalized Kane-Mele model [42] based on Sec. 5.3.1.

Systems with $(l, j_z) = (m, \pm\frac{1}{2})$ States

Consider the triangular lattice with s and f states (i.e., $m = 3$). We introduce the spin degree of freedom by defining

$$H = \sum_{\mathbf{k}} \Phi_{\mathbf{k}}^{\dagger} \mathcal{H}_{\mathbf{k}} \Phi_{\mathbf{k}}, \quad \Phi_{\mathbf{k}} = \begin{pmatrix} s_{\mathbf{k}\uparrow,\downarrow} \\ \\ f_{\mathbf{k}\uparrow,\downarrow} \end{pmatrix}, \tag{5.5.3}$$

such that $\mathcal{H}_{\mathbf{k}}$ is matrix in orbital and spin space; $\sigma_z = \pm 1$ denotes $\uparrow, \downarrow$. A T-invariant version of Eq. (5.3.11) is given by

$$\mathcal{H}_{\mathbf{k}} = \varepsilon_{\mathbf{k}} \tau_z + \Delta_1 \lambda_{\mathbf{k}}^{f_1} \tau_y + \Delta_2 \lambda_{\mathbf{k}}^{f_2} \tau_x \sigma_z, \tag{5.5.4}$$

which is clearly of the form (5.5.1). To determine what symmetries are sufficient to protect the structure of the Hamiltonian, we begin by examining the hexagonal and trigonal symmetry groups of Table 5.5.1 with inversion symmetry. In the presence of both T and inversion symmetry all bands are necessarily twofold degenerate, imposing a strong constraint on the Hamiltonian.

We first observe that (5.5.4) is invariant under all symmetries of the hexagonal

group D_{6h}. In fact, if D_{6h} is imposed (5.5.4) exhausts all symmetry-allowed terms, which implies that the full group D_{6h} is sufficient to protect the band inversion transition. The same is true for the trigonal group D_{3d}, which is a subgroup of D_{6h}. We conclude that both D_{6h} and D_{3d} protect a T-invariant band inversion of spinful s and f bands.

Next, consider the symmetry groups C_{6h} and S_6. These differ from the previous two groups by the absence of twofold rotations about axes in the plane. As a result of the lower symmetry, the Hamiltonian takes a more general form given by

$$\mathcal{H}_{\mathbf{k}} = \varepsilon_{\mathbf{k}}\tau_z + (\Delta_1\lambda_{\mathbf{k}}^{f_+} + \Delta_1^*\lambda_{\mathbf{k}}^{f_-})\tau_y + (\Delta_2\lambda_{\mathbf{k}}^{f_+} + \Delta_2^*\lambda_{\mathbf{k}}^{f_-})\tau_x\sigma_z, \quad (5.5.5)$$

where now $\Delta_{1,2}$ are complex and we have defined $\lambda_{\mathbf{k}}^{f_\pm} = \lambda_{\mathbf{k}}^{f_1} \pm i\lambda_{\mathbf{k}}^{f_2}$. Since (5.5.5) still commutes with σ_z, the Hamiltonian is of the form (5.5.1). The effect the of the more general coupling can be understood by expanding around the band inversion transition at $\mathbf{k} = 0$. We find

$$\Delta_{\mathbf{k}} = (-i\Delta_1 \pm \Delta_2)k_+^3 + (-i\Delta_1^* \pm \Delta_2^*)k_-^3, \quad (5.5.6)$$

which should be compared to the discussion in Sec. 5.3.1. We see that the additional couplings only have an effect on the phase and amplitude of the cubic terms and therefore do not fundamentally alter the structure of the band inversion. As a result, all symmetry groups which possess an inversion symmetry provide sufficient protection for a T-invariant band inversion with higher angular momentum.

We then proceed to the point groups listed in Table 5.5.1 which do not have an

	Hexagonal	Trigonal	Tetragonal
Inversion	D_{6h}	D_{3d}	D_{4h}
	C_{6h}	S_6	C_{4h}
No Inversion	D_6, C_{6v}, D_{3h}	D_3, C_{3v}	D_4, C_{4v}, D_{2d}
	C_6, C_{3h}	C_3	C_4, S_4

Table 5.5.1: Classification of axial point groups. Table summarizing the basic symmetry properties of the axial point groups. The point groups with an inversion symmetry can protect the structure of the band inversion given by Eqs. (5.5.1) and (5.5.2). Point groups on the second row differ from the first row by the lack of a twofold rotation perpendicular to the principal rotation axis; point groups on the fourth row differ from the third row by the lack of a perpendicular twofold rotation or a vertical mirror plane.

inversion symmetry. Owing to the absence of inversion symmetry, additional spin-orbit coupling terms can be symmetry-allowed. For instance, in the case of C_{6v} the following two spin-orbit coupling terms are generically present in the Hamiltonian:

$$\mathcal{H}'_{\mathbf{k}} = t_1(\lambda_{\mathbf{k}}^{p_1}\sigma_y - \lambda_{\mathbf{k}}^{p_2}\sigma_x) + t_2\tau_y(\lambda_{\mathbf{k}}^{d_1}\sigma_y - \lambda_{\mathbf{k}}^{d_2}\sigma_x). \tag{5.5.7}$$

These terms do not commute with σ_z and, furthermore, when expanded in small momenta $\mathbf{k}$ the first term describes a linear splitting of the spin species. Such linear coupling changes the nature of the band inversion, as it causes the density of states to vanish at the transition. A similar result is obtained for the symmetry groups D_6 and C_6, which leads to the conclusion that systems governed by these groups cannot have symmetry-protected higher angular momentum band inversions.

The point group D_{3h} is similar to D_6 and C_{6v} but differs in an essential way:

instead of a twofold rotation about the principal axis it contains a horizontal reflection. Since under the latter reflection $(\sigma_x, \sigma_y, \sigma_z) \to (-\sigma_x, -\sigma_y, \sigma_z)$ the terms of Eq. (5.5.7) are symmetry-forbidden. We therefore find that D_{3h} imposes sufficient constraints for the protection of the band inversion. This is not true for the point group C_{3h}, as its admits the coupling $\Delta_0 \tau_x$, which changes the nature of the band inversion transition.

Finally, since the trigonal groups without inversion are all subgroups of symmetry groups for which protection is lost, these do not protect the T-invariant higher angular momentum band inversion.

We conclude this part by noting that a similar analysis applies to the square lattice Hamiltonian of Eq. (5.3.6). Its T-invariant generalization based on (5.5.1) is given by

$$\mathcal{H}_{\mathbf{k}} = \varepsilon_{\mathbf{k}} \tau_z + \Delta_1 \lambda_{\mathbf{k}}^{d_1} \tau_y + \Delta_2 \lambda_{\mathbf{k}}^{d_2} \tau_x \sigma_z. \tag{5.5.8}$$

The form of this Hamiltonian is protected by tetragonal D_{4h} symmetry. Lowering the symmetry to C_{4h} allows for the additional couplings $\Delta_2' \lambda_{\mathbf{k}}^{d_2} \tau_y + \Delta_1' \lambda_{\mathbf{k}}^{d_1} \tau_x \sigma_z$, which have an effect similar to that described by Eq. (5.5.6). When inversion symmetry is lacking, as is the case for symmetry groups D_4 and C_{4v}, the additional spin-orbit coupling term $\lambda_{\mathbf{k}}^{p_1} \sigma_y - \lambda_{\mathbf{k}}^{p_2} \sigma_x$ is activated.

Systems with $j_z = \pm\frac{3}{2}$ Doublets

In Sec. 5.3.2 we introduced models for higher angular momentum inversions of $j_z = \pm\frac{3}{2}$ states. To describe such band inversions, it is necessary to consider two $j_z = \pm\frac{3}{2}$ Kramers pairs, see Eq. (5.3.19). As a result, a T-invariant generalization can be obtained by imposing T symmetry on the Hamiltonian defined in Eq. (5.3.20), which yields

$$h_{\mathbf{k}} = \varepsilon_{\mathbf{k}}\tau_z + \tau_x(\Delta\lambda_{\mathbf{k}}^{f_+}\sigma_+ + \Delta^*\lambda_{\mathbf{k}}^{f_-}\sigma_-), \tag{5.5.9}$$

where Δ is complex and $\lambda_{\mathbf{k}}^{f_\pm} = \lambda_{\mathbf{k}}^{f_1} \pm i\lambda_{\mathbf{k}}^{f_2}$ as before. Close to $\mathbf{k} = 0$ the coupling between the bands is a matrix in spin space and reads as

$$\Delta_{\mathbf{k}} = \begin{pmatrix} & \Delta k_\pm^3 \\ \Delta^* k_\mp^3 & \end{pmatrix}. \tag{5.5.10}$$

To determine the symmetry protection it is necessary to specify the symmetry quantum numbers more precisely. Here we first assume the presence of inversion symmetry and focus on the case where one of Kramers pairs is inversion even and one is odd. This implies that (5.5.9) is invariant under inversion. More specifically, (5.5.9) is invariant under all symmetries of D_{6h} and represents the most general form of the Hamiltonian with this symmetry. Furthermore, lowering the symmetry to D_{3d}, C_{6h}, or S_6 does not give rise to additional terms in the Hamiltonian and a result, all symmetry groups with inversion symmetry protect the structure of the T-invariant band inversion.

Generalized Kane-Mele Model

We conclude this section by discussing the time-reversal invariant generalization of the honeycomb lattice model defined in Eq. (5.3.15). As discussed, the honeycomb lattice model can be viewed as the Haldane model with third-nearest neighbor hopping across the hexagon. This immediately suggests that a time-reversal invariant version is obtained by replacing the Haldane term with the Kane-Mele spin-orbit coupling term [42]. The Hamiltonian then becomes [see Eq. (5.3.15)]

$$\mathcal{H}_{\mathbf{k}} = (\phi_{\mathbf{k}} - t'\phi'_{\mathbf{k}})\tau_+ + (\phi^*_{\mathbf{k}} - t'\phi'^*_{\mathbf{k}})\tau_- + t_{\mathrm{soc}}\lambda^{f_1}_{\mathbf{k}}\tau_z\sigma_z. \tag{5.5.11}$$

The structure of this Hamiltonian is symmetry-protected as long as the symmetry group of the systems is D_{6h} or C_{6h}.

Appendix

5.A Ground State of Hamiltonian (5.2.2)

The Hamiltonian $h_{\mathbf{k}}$ of Eq. (5.2.2) is diagonalized with the help of the unitary matrix $U_{\mathbf{k}}$, which contains the eigenvectors as its columns, and one has

$$U_{\mathbf{k}}^{\dagger} h_{\mathbf{k}} U_{\mathbf{k}} = \begin{pmatrix} E_{\mathbf{k}} & \\ & -E_{\mathbf{k}} \end{pmatrix}, \quad U_{\mathbf{k}} = \begin{pmatrix} -u_{\mathbf{k}}^{*} & v_{\mathbf{k}} \\ v_{\mathbf{k}}^{*} & u_{\mathbf{k}} \end{pmatrix} \tag{5.A.1}$$

where $E_{\mathbf{k}} = \sqrt{\varepsilon_{\mathbf{k}}^2 + |\Delta_{\mathbf{k}}|^2}$ is the energy. The matrix $U_{\mathbf{k}}$ must satisfy $U_{\mathbf{k}}^{\dagger} U_{\mathbf{k}} = 1$, which implies $|u_{\mathbf{k}}|^2 + |v_{\mathbf{k}}|^2 = 1$. The ratio of $u_{\mathbf{k}}$ and $v_{\mathbf{k}}$ is independent of the $U(1)$ phase degree of freedom associated with the eigenvectors and is given by

$$v_{\mathbf{k}}/u_{\mathbf{k}} = -(E_{\mathbf{k}} - \xi_{\mathbf{k}})/\Delta_{\mathbf{k}}^{*}. \tag{5.A.2}$$

We define normal mode operators $\gamma_{\mathbf{k}e}$ and $\gamma_{\mathbf{k}h}$ corresponding to the energy eigenvalues $\pm E_{\mathbf{k}}$ as

$$\gamma_{\mathbf{k}} = \begin{pmatrix} \gamma_{\mathbf{k}e} \\ \gamma_{\mathbf{k}h} \end{pmatrix} = U^{\dagger} \psi_{\mathbf{k}}. \tag{5.A.3}$$

The normal mode operators for the negative energy states are given by

$$\gamma^{\dagger}_{\mathbf{k}h} = v_{\mathbf{k}} c^{\dagger}_{\mathbf{k}e} + u_{\mathbf{k}} c^{\dagger}_{\mathbf{k}h}. \tag{5.A.4}$$

The mean-field ground state $|\mathrm{GS}\rangle$ is given by filling all the negative energy states, i.e., $|\mathrm{GS}\rangle = \prod_{\mathbf{k}} \gamma^{\dagger}_{\mathbf{k}h} |0\rangle$. Substituting Eq. (5.A.4) and using the identity $c_{\mathbf{k}h} c^{\dagger}_{\mathbf{k}h} |0\rangle = |0\rangle$, the ground state can be written in the following form

$$|\mathrm{GS}\rangle = \prod_{\mathbf{k}} (u_{\mathbf{k}} + v_{\mathbf{k}} c^{\dagger}_{\mathbf{k}e} c_{\mathbf{k}h}) |\Omega\rangle \,. \tag{5.A.5}$$

Here $|\Omega\rangle$ defines a vacuum state obtained by filling all valence band states: $|\Omega\rangle = \prod_{\mathbf{k}} c^{\dagger}_{\mathbf{k}h} |0\rangle$. Since $c_{\mathbf{k}h}$ creates holes in the vacuum defined by $|\Omega\rangle$, it is natural to perform a particle-hole transformation on the hole operators given by

$$c_{\mathbf{k}h} \to c^{\dagger}_{-\mathbf{k}h}, \quad \gamma_{\mathbf{k}h} \to \gamma^{\dagger}_{-\mathbf{k}h}. \tag{5.A.6}$$

After particle-hole transformation the normal mode annihilation operators take the form

$$\gamma_{\mathbf{k}e} = v_{\mathbf{k}} c^{\dagger}_{-\mathbf{k}h} - u_{\mathbf{k}} c_{\mathbf{k}e} \tag{5.A.7}$$

$$\gamma_{-\mathbf{k}h} = v_{\mathbf{k}} c^{\dagger}_{\mathbf{k}e} + u_{\mathbf{k}} c_{-\mathbf{k}h} \tag{5.A.8}$$

and in full analogy with BCS theory one obtains the ground state by determining the state which is annihilated by all such normal mode operators. A state which clearly has this property is $\prod_{\mathbf{k}} \gamma_{\mathbf{k}e} \gamma_{-\mathbf{k}h} |\Omega\rangle$ and one thus finds the ground state as

$$|\mathrm{GS}\rangle = \prod_{\mathbf{k}} (u_{\mathbf{k}} + v_{\mathbf{k}} c^{\dagger}_{\mathbf{k}e} c^{\dagger}_{-\mathbf{k}h}) |\Omega\rangle \,, \tag{5.A.9}$$

which is precisely (5.A.5) with $c_{\mathbf{k}h} \to c^{\dagger}_{-\mathbf{k}h}$.

5.B Excitonic Insulator Mean Field Theory

For the purpose of a mean field analysis it is useful to express interacting Hamiltonian H_U of Eq. (5.4.2) in a form which can decoupled. To this end we rewrite the interacting Hamiltonian as

$$H_U = -\frac{U}{4N}\sum_{\mathbf{k}\mathbf{k}'}(\varphi^\dagger_{\mathbf{k}}\tau_x\varphi_{\mathbf{k}})(\varphi^\dagger_{\mathbf{k}'}\tau_x\varphi_{\mathbf{k}'}), \tag{5.B.1}$$

with $\varphi_{\mathbf{k}}$ as defined in Eq. (5.3.7). Here N is the system size. To perform the mean field decoupling of the interaction, we write the action of interacting system as $S = S_0 + S_U$ with $S_0 = \int_0^\beta d\tau \sum_{\mathbf{k}} \varphi^\dagger_{\mathbf{k}}(\partial_\tau + h_{\mathbf{k}})\varphi_{\mathbf{k}}$ and $S_U = \int_0^\beta d\tau H_U$. The interacting part of the action is decoupled in terms of the field Δ_0 as $\exp(-S_U) = \int \mathcal{D}\Delta_0 \exp(-S'_U[\Delta_0])$, where $S'_U[\Delta_0]$ is now bilinear in the fermions and given by $S'_U[\Delta_0] = \int_0^\beta d\tau H'_U[\Delta_0]$ with

$$H'[\Delta_0] = 2\Delta_0 \sum_{\mathbf{k}} \varphi^\dagger_{\mathbf{k}}\tau_x\varphi_{\mathbf{k}} + 4N\Delta_0^2/U. \tag{5.B.2}$$

For the subsequent analysis it is convenient to redefine the mean field as $2\Delta_0 \to \Delta_0$.

5.B.1 Mean Field Solution

Integrating out the fermions one obtains the free energy as a functional of Δ_0; the saddle-point of this free energy defines the mean field self-consistency equation, which is given by

$$\frac{\delta F}{\delta \Delta_0} = 0 \;\Rightarrow\; \Delta_0 = -\frac{U}{2N}\sum_{\mathbf{k}}\langle\varphi^\dagger_{\mathbf{k}}\tau_x\varphi_{\mathbf{k}}\rangle. \tag{5.B.3}$$

The expectation value is defined with respect to the ground state of the mean field Hamiltonian

$$h_{\mathbf{k}}^{\mathrm{MF}} = \begin{pmatrix} \varepsilon_{\mathbf{k}} & \Sigma_{\mathbf{k}} \\ \Sigma_{\mathbf{k}}^{*} & -\varepsilon_{\mathbf{k}} \end{pmatrix}, \quad \Sigma_{\mathbf{k}} = \Delta_0 + \Delta_{\mathbf{k}}, \tag{5.B.4}$$

where $\Delta_{\mathbf{k}} = \Delta_3(i\lambda_{\mathbf{k}}^{f_1} + \lambda_{\mathbf{k}}^{f_2})$. Here we have taken $\Delta_1 = \Delta_2$ in Eq. (5.3.11) and redefined it as $\Delta_{m=3}$. The energies of the mean field Hamiltonian are given by $\pm E_{\mathbf{k}} = \pm\sqrt{\varepsilon_{\mathbf{k}}^2 + |\Sigma_{\mathbf{k}}|^2}$ and the matrix $U_{\mathbf{k}}$ which diagonalizes the mean field Hamiltonian is given by

$$U_{\mathbf{k}} = \frac{1}{\sqrt{2E_{\mathbf{k}}(E_{\mathbf{k}} - \varepsilon_{\mathbf{k}})}} \begin{pmatrix} -\Sigma_{\mathbf{k}}^{*} & \varepsilon_{\mathbf{k}} - E_{\mathbf{k}} \\ \varepsilon_{\mathbf{k}} - E_{\mathbf{k}} & \Sigma_{\mathbf{k}} \end{pmatrix}. \tag{5.B.5}$$

Substituting this into the self-consistency condition (5.B.3) one finds

$$\Delta_0 = \frac{U}{2N} \sum_{\mathbf{k}} \frac{\mathrm{Re}[\Sigma_{\mathbf{k}}]}{E_{\mathbf{k}}} [f(-E_{\mathbf{k}}) - f(E_{\mathbf{k}})]. \tag{5.B.6}$$

where $f(\varepsilon) = (1 + e^{\beta\varepsilon})^{-1}$ is the Fermi function. At zero temperature the self-consistency condition reduces to $\Delta_0 = \frac{U}{2N} \sum_{\mathbf{k}} \mathrm{Re}[\Sigma_{\mathbf{k}}]/E_{\mathbf{k}}$.

5.B.2 Free Energy

The free energy itself can be directly evaluated and at finite temperature T

$$F[\Delta_0] = -\frac{2}{\beta} \sum_{\mathbf{k}} \ln\cosh\left(\frac{\beta E_{\mathbf{k}}}{2}\right) + \frac{N}{U}\Delta_0^2, \tag{5.B.7}$$

where we have ignored the constant contribution $-(N/\beta)\ln 4$. By taking the derivative with respect to Δ_0 and setting it equal to zero one recovers the saddle-point equation (5.B.6).

At zero temperature the free energy takes the simple form

$$F[\Delta_0] = -\sum_{\mathbf{k}} E_{\mathbf{k}} + N\Delta_0^2/U. \tag{5.B.8}$$

5.B.3 Expansion of Free Energy in Δ_0

To study the phase transition to the rotation symmetry broken state one may expand the free energy powers of the order parameter Δ_0 to obtain a simple Landau theory for the transition. At zero temperature, the free energy (5.B.8) can be expanded as

$$F[\Delta_0]/N = \left(U^{-1} - c_2\right)\Delta_0^2 + c_4\Delta_0^4, \tag{5.B.9}$$

where the expansion coefficients are given by

$$c_2 = \frac{1}{2N}\sum_{\mathbf{k}}\left(\frac{1}{E_{\mathbf{k}}} - \frac{(\mathrm{Re}\Delta_{\mathbf{k}})^2}{E_{\mathbf{k}}^3}\right), \tag{5.B.10}$$

$$c_4 = \frac{1}{8N}\sum_{\mathbf{k}}\left(\frac{1}{E_{\mathbf{k}}^3} - 6\frac{(\mathrm{Re}\Delta_{\mathbf{k}})^2}{E_{\mathbf{k}}^5} + 5\frac{(\mathrm{Re}\Delta_{\mathbf{k}})^4}{E_{\mathbf{k}}^7}\right). \tag{5.B.11}$$

Note that since we are expanding around $\Delta_0 = 0$, in these expressions the energy $E_{\mathbf{k}}$ is evaluated at Δ_0, i.e., $E_{\mathbf{k}} = \sqrt{\varepsilon_{\mathbf{k}}^2 + |\Delta_{\mathbf{k}}|^2}$.

Chapter 6

Future Directions

"*A prudent question is one-half of wisdom.*" Following the wisdom of Francis Bacon, we present questions arise from all three parts of this dissertation. Hopefully, this would serve partially as a guide for future directions of research and partially a fun read composing some of my wild speculations.

A small plateau is found in quantum point contact experiments to exist at 0.7 e^2/h[216, 217]. Its origin is still far from clear, despite many proposed explanations from smeared van Hove singularity[218] to exchange interaction induced spin fluctuations[219]. It is suggested that this phenomenon could be associated with a Kondo problem[220] and reflects the existence of an intermediate fixed point. Then one may wonder if 0.7 anomaly could be analyzed using methods developed in Chapter 2? Quantum Brownian motion picture is a powerful tool for studying lower dimension electron transport problems. It recently has found applications in

electron teleportation problems[221] and localization problems of electrons moving in quasiperiodic potential[222]. It would be interesting to extend discussions along this line of research.

G_2 is the first of five exceptional Lie group. What most interesting about it is that it is the automorphic group of the octonions[126]. For octonions, its algebra even breaks associativity[126]. This is originally seen as problematic when particle physicists tried to use them to build GUT based on G_2 as the non-associativity is in conflict with quantum mechanics. It would be interesting to ask if this non-associativity turns out to be related to something interesting in our condensed matter settings. Another aspect differentiates particle physic/string theory's view towards G_2 compared to our case is that they are really thinking of G_2 as a larger group that contains $SU(3)$. For them, having $SU(3)$ guarantees that the physics of quarks can be reproduced[223]. Would this particular structure be useful for condensed matter physics? Apart from the peculiar mathematics of G_2, physically it would be very useful if a field theoretical description could be developed starting from our topological superconductor system. In this way, a complete phase diagram relating the Fibonacci phase and topological superconductor systems can be worked out and tell us where to look for this exotic phase.

Understanding the role of electron interactions starting with a higher angular momentum paired gapless state is crucial for the fractional excitonic phase. Our presented arguments would come short moving away from the long-wavelength limit.

Therefore, it is desirable to numerically test the effect of turning on some short-ranged repulsive interactions between same charged particles. Another avenue to explore is d-wave paired states($m = 2$). Are they gapless Fermi liquids or would develop some topological order under electron interactions? Would our composite fermion theory with both electrons and holes provide any insight? Also, since our system is equipped with particle-hole symmetry to begin with, would it have any connection to the recently proposed particle-hole Pfaffian topological order[169]?

Bibliography

[1] L. D. Landau, Phys. Z. Soviet II **26**, 545 (1937).

[2] K. v. Klitzing, G. Dorda, and M. Pepper, Phys. Rev. Lett. **45**, 494 (1980).

[3] B. A. Bernevig, T. L. Hughes, and S.-C. Zhang, Science **314**, 1757 (2006).

[4] L. Fu, C. L. Kane, and E. J. Mele, Phys. Rev. Lett. **98**, 106803 (2007).

[5] D. C. Tsui, H. L. Stormer and A. C. Gossard, Phys. Rev. Lett. **48**, 1559 (1982).

[6] G. R. Stewart, Rev. Mod. Phys. **56**, 755 (1984).

[7] P. A. Lee, N. Nagaosa and X. Wen, Rev. Mod. Phys. **78**, 17 (2006).

[8] J. Bardeen, L. N. Cooper and J. R. Schrieffer, Phys. Rev. **108**, 1175 (1957).

[9] L. D. Landau, JETP-USSR 3 (6) (1957) 920–925.

[10] L. D. Landau, JETP-USSR 5 (1) (1957) 101–108.

[11] U. Meirav, M. A. Kastner and S. J. Wind, Phys. Rev. Lett. **65**, 771 (1990).

[12] A. A. M. Staring, J. G. Williamson, H. van Houten, C. W. J. Beenakker and L. P. Kouwenhoven, Physica B: Condensed Matter **175**, 226 (1991).

[13] L. Fu, Phys. Rev. Lett. **104**, 056402 (2010).

[14] V. E. Manucharyan, J. Koch, L. Glazman and M. H. Devoret, Science **326**, 113 (2009).

[15] D. Supriyo, *Electronic Transport in Mesoscopic Systems*, (Cambridge University Press, 1995).

[16] C. Bauerle, D. C. Glattli, T. Meunier, F. Portier, P. Roche, S. Takada and X. Waintal, Reports on Progress in Physics **81**, 503 (2018).

[17] F. D. M. Haldane, Journal of Physics C: Solid State Physics **14**, 2585 (1981).

[18] F. D. M. Haldane, Phys. Rev. Lett. **47**, 1840 (1981).

[19] C. L. Kane and M. P. A. Fisher, Phys. Rev. Lett. **68**, 1220 (1992).

[20] C. L. Kane and M. P. A. Fisher, Phys. Rev. B **46**, 15233 (1992).

[21] E. Majorana, Nuovo Cimento **5**, 171 (1938).

[22] C. E. Aslseth, F. T. Avignone III, *et al.*, Mod. Phys. Lett. A **16**, 2409 (2001).

[23] F. T. Avignone, S. R. Elliott and J. Engel, Rev. Mod. Phys. **80**, 481 (2008).

[24] N. B. Kopnin, and M. M. Salomaa, Phys. Rev. B **44**, 9667 (1991).

[25] G. E. Volovik, *The Universe in a Helium Droplet*, (Oxford, 2003).

[26] G. Moore and N. Read, Nuclear Physics B **360**, 362 (1991).

[27] N. Read and D. Green, Phys. Rev. B **61**, 10267 (2000).

[28] L. Fu and C. L. Kane, Phys. Rev. Lett. **100**, 096407 (2008).

[29] A. Kitaev, Phys. Usp. (suppl.) **44**, 131 (2001).

[30] D. A. Ivanov, Phys. Rev. Lett. **86**, 268 (2001).

[31] V. Mourik, K. Zou, S. M. Frolov, S. R. Plissard, E. P. A. M. Bakkers, and L. P. Kouwenhoven, Science **336**, 1003 (2012).

[32] S. Nadj-Perge, I. K. Drozdov, J. Li, H. Chen, S. Jeon, J. Seo, A. H. MacDonald, B. A. Bernevig, and A. Yazdani, Science **346**, 602 (2014).

[33] Q. L. He, L. Pan, A. L. Stern, E. C. Burks, X. Che, and J. Wang, *et al.*, Science **357**, 294 (2017).

[34] M. Banerjee, M. Heiblum, V. Umansky, D. Feldman, Y. Oreg, and A. Stern, Nature **559**, 205 (2018).

[35] F. D. M. Haldane, Phys. Rev. Lett. **61**, 2015 (1988).

[36] C. Chang, J. Zhang, X. Feng, J. Shen, Z. Zhang, and M. Guo, et al., Science **340**, 167 (2013).

[37] N. R. Cooper, and J. Dalibard, Phys. Rev. Lett. **110**, 185301 (2013).

[38] G. Jotzu *et al.*, Nature **515**, 237 (2015).

[39] N. Y. Yao *et al.*, Phys. Rev. Lett. **110**, 185302 (2013).

[40] M. Z. Hasan and C. L. Kane, Rev. Mod. Phys. **82**, 3045 (2010).

[41] X.-L. Qi and S.-C. Zhang, Rev. Mod. Phys. **83**, 1057 (2011).

[42] C. L. Kane and E. J. Mele, Phys. Rev. Lett. **95**, 226801 (2005).

[43] C. L. Kane and E. J. Mele, Phys. Rev. Lett. **95**, 146802 (2005).

[44] B. A. Bernevig and S.-C. Zhang, Phys. Rev. Lett. **96**, 106802 (2006).

[45] L. Fu, Phys. Rev. Lett. **106**, 106802 (2011).

[46] X. Chen, Z.-C. Gu, and X.-G. Wen, Phys. Rev. B **83**, 035107 (2011).

[47] Z.-X. Liu and X.-G. Wen, Phys. Rev. Lett. **110**, 067205 (2013).

[48] X. Chen, Z.-C. Gu, Z.-X. Liu, and X.-G. Wen, Phys. Rev. B **87**, 155114 (2013).

[49] J. Kondo, Progress of theoretical physics **32**, 37 (1964).

[50] P. Nozières and A. Blandin, Journal de Physique **41**, 193 (1980).

[51] G. A. Fiete, W. Bishara, and C. Nayak, Phys. Rev. B **82**, 035301 (2010).

[52] G. A. Fiete, W. Bishara, and C. Nayak, Phys. Rev. Lett. **101**, 176801 (2008).

[53] P. Fendley, M. P. A. Fisher, and C. Nayak, Phys. Rev. B **75**, 045317 (2007).

[54] P. Fendley, M. P. Fisher, and C. Nayak, Annals of Physics **324**, 1547 (2009), july 2009 Special Issue.

[55] N. P. Sandler and E. Fradkin, Phys. Rev. B **63**, 235301 (2001).

[56] O. M. Auslaender, A. Yacoby, R. de Picciotto, K. W. Baldwin, L. N. Pfeiffer, and K. W. West, Phys. Rev. Lett. **84**, 1764 (2000).

[57] F. Milliken, C. Umbach, and R. Webb, Solid State Communications **97**, 309 (1996).

[58] A. Furusaki and N. Nagaosa, Phys. Rev. B **47**, 4631 (1993).

[59] T. L. Hughes, E. Prodan, and B. A. Bernevig, Phys. Rev. B **83**, 245132 (2011).

[60] I. Affleck, Nuclear Physics B **336**, 517 (1990).

[61] I. Affleck and A. W. Ludwig, Nuclear Physics B **352**, 849 (1991).

[62] The value of Luttinger parameters g_ρ and g_σ is set to 2 for noninteracting electrons in spinful Luttinger liquid in Ref. KF2,KF.

[63] H. Yi and C. L. Kane, Phys. Rev. B **57**, R5579 (1998).

[64] H. Yi, Phys. Rev. B **65**, 195101 (2002).

[65] I. Affleck, M. Oshikawa, and H. Saleur, Journal of Physics A: Mathematical and General **34**, 1073 (2001).

[66] I. Affleck, M. Oshikawa, and H. Saleur, Nuclear Physics B **594**, 535 (2001).

[67] C. L. Kane, M. P. A. Fisher, and J. Polchinski, Phys. Rev. Lett. **72**, 4129 (1994).

[68] K. Moon, H. Yi, C. Kane, S. Girvin, and M. P. Fisher, Phys. Rev. Lett. **71**, 4381 (1993).

[69] A. Caldeira and A. Leggett, Annals of Physics **149**, 374 (1983).

[70] M. P. A. Fisher and W. Zwerger, Phys. Rev. B **32**, 6190 (1985).

[71] A. Schmid, Phys. Rev. Lett. **51**, 1506 (1983).

[72] F. Guinea, V. Hakim, and A. Muramatsu, Phys. Rev. Lett. **54**, 263 (1985).

[73] G. Toulouse, Phys. Rev. B **2**, 270 (1970).

[74] A. Komnik and A. O. Gogolin, Phys. Rev. Lett. **90**, 246403 (2003).

[75] V. J. Emery and S. Kivelson, Phys. Rev. B **46**, 10812 (1992).

[76] K. Itai, Phys. Rev. Lett. **58**, 602 (1987).

[77] G. T. Zimányi, K. Vladár, and A. Zawadowski, Phys. Rev. B **36**, 3186 (1987).

[78] A. W. Ludwig and I. Affleck, Nuclear Physics B **428**, 545 (1994).

[79] J. C. Y. Teo and C. L. Kane, Phys. Rev. B **79**, 235321 (2009).

[80] A. W. Ludwig, International Journal of Modern Physics B **8**, 347 (1994).

[81] J. L. Cardy, Nuclear Physics B **275**, 200 (1986).

[82] P. Francesco, P. Mathieu, and D. Sénéchal, *Conformal field theory* (Springer Science & Business Media, 2012).

[83] I. Affleck, A. W. W. Ludwig, H.-B. Pang, and D. L. Cox, Phys. Rev. B **45**, 7918 (1992).

[84] P. W. Anderson, G. Yuval, and D. R. Hamann, Phys. Rev. B **1**, 4464 (1970).

[85] I. Safi and H. J. Schulz, Phys. Rev. B **52**, R17040 (1995).

[86] D. L. Maslov and M. Stone, Phys. Rev. B **52**, R5539 (1995).

[87] V. V. Ponomarenko, Phys. Rev. B **52**, R8666 (1995).

[88] A. Kawabata, Journal of the Physical Society of Japan **65**, 30 (1996), http://dx.doi.org/10.1143/JPSJ.65.30 .

[89] C. Chamon, M. Oshikawa, and I. Affleck, Phys. Rev. Lett. **91**, 206403 (2003).

[90] M. Oshikawa, C. Chamon, and I. Affleck, Journal of Statistical Mechanics: Theory and Experiment **2006**, P02008 (2006).

[91] C. de C. Chamon and E. Fradkin, Phys. Rev. B **56**, 2012 (1997).

[92] A. Kitaev, Annals of Physics **321**, 2 (2006).

[93] C. Nayak, S. H. Simon, A. Stern, M. Freedman, and S. Das Sarma, Rev. Mod. Phys. **80**, 1083 (2008).

[94] I. P. Radu, J. B. Miller, C. M. Marcus, M. A. Kastner, L. N. Pfeiffer, and K. W. West, Science **320**, 899 (2008).

[95] M. Dolev, M. Heiblum, V. Umansky, A. Stern, and D. Mahalu, Nature **452**, 829 (2008).

[96] R. L. Willett, L. N. Pfeiffer, and K. W. West, Proceedings of the National Academy of Sciences **106**, 8853 (2009).

[97] L. Fu and C. L. Kane, Phys. Rev. B **79**, 161408 (2009).

[98] R. M. Lutchyn, J. D. Sau, and S. Das Sarma, Phys. Rev. Lett. **105**, 077001 (2010).

[99] Y. Oreg, G. Refael, and F. von Oppen, Phys. Rev. Lett. **105**, 177002 (2010).

[100] X.-L. Qi, T. L. Hughes, and S.-C. Zhang, Phys. Rev. B **82**, 184516 (2010).

[101] V. Mourik, K. Zuo, S. M. Frolov, S. R. Plissard, E. P. A. M. Bakkers, and L. P. Kouwenhoven, Science **336**, 1003 (2012).

[102] Q. L. He, L. Pan, A. L. Stern, E. C. Burks, X. Che, G. Yin, J. Wang, B. Lian, Q. Zhou, E. S. Choi, K. Murata, X. Kou, Z. Chen, T. Nie, Q. Shao, Y. Fan, S.-C. Zhang, K. Liu, J. Xia, and K. L. Wang, Science **357**, 294 (2017).

[103] M. H. Freedman, M. Larsen, and Z. Wang, Communications in Mathematical Physics **227**, 605 (2002).

[104] N. Read and E. Rezayi, Phys. Rev. B **59**, 8084 (1999).

[105] M. Barkeshli and X.-L. Qi, Phys. Rev. X **2**, 031013 (2012).

[106] N. H. Lindner, E. Berg, G. Refael, and A. Stern, Phys. Rev. X **2**, 041002 (2012).

[107] M. Cheng, Phys. Rev. B **86**, 195126 (2012).

[108] D. J Clarke, J. Alicea, and K. Shtengel, Nature communications **4**, 1348 (2013).

[109] A. Vaezi, Phys. Rev. B **87**, 035132 (2013).

[110] R. S. K. Mong, D. J. Clarke, J. Alicea, N. H. Lindner, P. Fendley, C. Nayak, Y. Oreg, A. Stern, E. Berg, K. Shtengel, and M. P. A. Fisher, Phys. Rev. X **4**, 011036 (2014).

[111] A. Vaezi, Phys. Rev. X **4**, 031009 (2014).

[112] A. R. Akhmerov, J. Nilsson, and C. W. J. Beenakker, Phys. Rev. Lett. **102**, 216404 (2009).

[113] L. Fu and C. L. Kane, Phys. Rev. Lett. **102**, 216403 (2009).

[114] A. Rahmani, X. Zhu, M. Franz, and I. Affleck, Phys. Rev. Lett. **115**, 166401 (2015).

[115] A. Feiguin, S. Trebst, A. W. W. Ludwig, M. Troyer, A. Kitaev, Z. Wang, and M. H. Freedman, Phys. Rev. Lett. **98**, 160409 (2007).

[116] E. Grosfeld and K. Schoutens, Phys. Rev. Lett. **103**, 076803 (2009).

[117] C. L. Kane, R. Mukhopadhyay, and T. C. Lubensky, Phys. Rev. Lett. **88**, 036401 (2002).

[118] J. C. Y. Teo and C. L. Kane, Phys. Rev. B **89**, 085101 (2014).

[119] P. Goddard, A. Kent, and D. Olive, Physics Letters B **152**, 88 (1985).

[120] E. Fradkin, C. Nayak, and K. Schoutens, Nuclear Physics B **546**, 711 (1999).

[121] P. Di Francesco, P. Mathieu, and D. Sénéchal, *Conformal field theory*, Graduate texts in contemporary physics (Springer, New York, NY, 1997).

[122] S. Sahoo, Z. Zhang, and J. C. Y. Teo, Phys. Rev. B **94**, 165142 (2016).

[123] S. Shatashvili and C. Vafa, Selecta Mathematica **1**, 347 (1995).

[124] P. Bonderson, *Non-Abelian Anyons and Interferometry*, Ph.D. thesis, California Institute of Technology (2007).

[125] M. Günaydin and S. V. Ketov, Nuclear Physics B **467**, 215 (1996).

[126] J. C. Baez, Bull. Amer. Math. Soc. **39**, 145 (2002).

[127] The Hamiltonian density is equivalent to the CFT energy momentum tensor on a cylinder: $H_0 = vT_{\text{cyl}}/2\pi$.

[128] In addition to [127], J^A differs in normalization from the WZW current defined in Ref. [121], which is $2\pi J^A$.

[129] Note that $\langle \gamma_a(x)\gamma_b(0)\rangle = \delta_{ab}/2\pi ix$ and $\sum *C^2_{abcd} = 168$.

[130] J. T. Chalker and P. D. Coddington, Journal of Physics C: Solid State Physics **21**, 2665 (1988).

[131] M. Levin, B. I. Halperin, and B. Rosenow, Phys. Rev. Lett. **99**, 236806 (2007).

[132] S.-S. Lee, S. Ryu, C. Nayak, and M. P. A. Fisher, Phys. Rev. Lett. **99**, 236807 (2007).

[133] F. Amet, C. T. Ke, I. V. Borzenets, J. Wang, K. Watanabe, T. Taniguchi, R. S. Deacon, M. Yamamoto, Y. Bomze, S. Tarucha, and G. Finkelstein, Science **352**, 966 (2016).

[134] G.-H. Lee, K.-F. Huang, D. K. Efetov, D. S. Wei, S. Hart, T. Taniguchi, K. Watanabe, A. Yacoby, and P. Kim, Nature Physics **13**, 693–698 (2017).

[135] C. L. Kane and M. P. A. Fisher, Phys. Rev. B **55**, 15832 (1997).

[136] M. Banerjee, M. Heiblum, A. Rosenblatt, Y. Oreg, D. E. Feldman, A. Stern, and V. Umansky, Nature **545**, 75 (2016).

[137] A. Stern and B. I. Halperin, Phys. Rev. Lett. **96**, 016802 (2006).

[138] P. Bonderson, A. Kitaev, and K. Shtengel, Phys. Rev. Lett. **96**, 016803 (2006).

[139] P. Bonderson, K. Shtengel, and J. K. Slingerland, Phys. Rev. Lett. **97**, 016401 (2006).

[140] D. E. Feldman and A. Kitaev, Phys. Rev. Lett. **97**, 186803 (2006).

[141] K. T. Law, Phys. Rev. B **77**, 205310 (2008).

[142] M. Büttiker, Phys. Rev. B **38**, 9375 (1988).

[143] C. L. Kane, Phys. Rev. Lett. **90**, 226802 (2003).

[144] D. J. Thouless, M. Kohmoto, M. P. Nightingale, and M. den Nijs, Phys. Rev. Lett. **49**, 405 (1982).

[145] D. R. Hofstadter, Phys. Rev. B **14**, 2239 (1976).

[146] A. W. W. Ludwig, M. P. A. Fisher, R. Shankar, and G. Grinstein, Phys. Rev. B **50**, 7526 (1994).

[147] L. Fu and C. L. Kane, Phys. Rev. B **76**, 045302 (2007).

[148] R. Yu, W. Zhang, H.-J. Zhang, S.-C. Zhang, X. Dai, and Z. Fang, Science **329**, 61 (2010).

[149] E. Tang, J.-W. Mei, and X.-G. Wen, Phys. Rev. Lett. **106**, 236802 (2011).

[150] T. Neupert, L. Santos, S. Ryu, C. Chamon, and C. Mudry, Phys. Rev. B **84**, 165107 (2011).

[151] K. Sun, Z. Gu, H. Katsura, and S. Das Sarma, Phys. Rev. Lett. **106**, 236803 (2011).

[152] N. Regnault and B. A. Bernevig, Phys. Rev. X **1**, 021014 (2011).

[153] S. A. Parameswaran, R. Roy, and S. L. Sondhi, Comptes Rendus Physique **14**, 816 (2013).

[154] T. Neupert, C. Chamon, T. Iadecola, L. H. Santos, and C. Mudry, Physica Scripta **2015**, 014005 (2015).

[155] Z. Liu and E. J. Bergholtz, Int. J. Mod. Phys. B **27**, 1330017 (2013).

[156] E. M. Spanton, A. A. Zibrov, H. Zhou, T. Taniguchi, K. Watanabe, M. P. Zaletel, and A. F. Young, Science **360**, 62 (2018).

[157] R. B. Laughlin, Phys. Rev. Lett. **50**, 1395 (1983).

[158] B. I. Halperin, Helv. Phys. Acta **56**, 75 (1983).

[159] Y. B. Kim, C. Nayak, E. Demler, N. Read, and S. Das Sarma, Phys. Rev. B **63**, 205315 (2001).

[160] The phase of $\Delta_{\mathbf{k}}$ can be chosen by defining the phase of $c_{h\mathbf{k}}$. The choice in (4.2.2) makes f in (4.1.1) real.

[161] X.-J. Liu, X. Liu, C. Wu, and J. Sinova, Phys. Rev. A **81**, 033622 (2010).

[162] X. Liu, Z. Wang, X. C. Xie, and Y. Yu, Phys. Rev. B **83**, 125105 (2011).

[163] M. Milovanović and N. Read, Phys. Rev. B **53**, 13559 (1996).

[164] K. Yang, Phys. Rev. Lett. **87**, 056802 (2001).

[195] D. Jérome, T. M. Rice, and W. Kohn, Phys. Rev. **158**, 462 (1967).

[166] B. I. Halperin and T. M. Rice, Rev. Mod. Phys. **40**, 755 (1968).

[167] B. I. Halperin, P. A. Lee, and N. Read, Phys. Rev. B **47**, 7312 (1993).

[168] S. C. Zhang, T. H. Hansson, and S. Kivelson, Phys. Rev. Lett. **62**, 82 (1989).

[169] D. T. Son, Phys. Rev. X **5**, 031027 (2015).

[170] J. M. Kosterlitz and D. J. Thouless, Journal of Physics C: Solid State Physics **6**, 1181 (1973).

[171] F. D. M. Haldane and E. H. Rezayi, Phys. Rev. B **31**, 2529 (1985).

[172] I. S. Gradshteyn and I. M. Ryzhik, *Table of integrals, series, and products* (Academic Press, New York, 1980) p. 921.

[173] E. Verlinde and H. Verlinde, Nuclear Physics B **288**, 357 (1987).

[174] D. P. Arovas and S. M. Girvin, in *Recent Progress in Many-Body Theories*, Vol. 3, edited by T. L. Ainsworth, C. E. Campbel, B. E. Clements, and E. Krotscheck (Plenum Press, New York, 1992) pp. 315–344.

[175] S. A. Trugman and S. Kivelson, Phys. Rev. B **31**, 5280 (1985).

[176] C. L. Kane, S. Kivelson, D. H. Lee, and S. C. Zhang, Phys. Rev. B **43**, 3255 (1991).

[177] N. Read and D. Green, Phys. Rev. B **61**, 10267 (2000).

[178] A. P. Schnyder, S. Ryu, A. Furusaki, and A. W. W. Ludwig, Phys. Rev. B **78**, 195125 (2008).

[179] C.-K. Chiu, J. C. Y. Teo, A. P. Schnyder, and S. Ryu, Rev. Mod. Phys. **88**, 035005 (2016).

[180] C. Fang, M. J. Gilbert, X. Dai, and B. A. Bernevig, Phys. Rev. Lett. **108**, 266802 (2012).

[181] B. Bradlyn, L. Elcoro, J. Cano, M. G. Vergniory, Z. Wang, C. Felser, M. I. Aroyo, and B. A. Bernevig, Nature **547**, 298 (2017).

[182] H. C. Po, A. Vishwanath, and H. Watanabe, Nat. Commun. **8**, 50 (2017).

[183] J. Kruthoff, J. de Boer, J. van Wezel, C. L. Kane, and R.-J. Slager, Phys. Rev. X **7**, 041069 (2017).

[184] T. L. Hughes, E. Prodan, and B. A. Bernevig, Phys. Rev. B **83**, 245132 (2011).

[185] C. Fang, M. J. Gilbert, and B. A. Bernevig, Phys. Rev. B **86**, 115112 (2012).

[186] K. Sun, H. Yao, E. Fradkin, and S. A. Kivelson, Phys. Rev. Lett. **103**, 046811 (2009).

[187] F. Zhang, H. Min, M. Polini, and A. H. MacDonald, Phys. Rev. B **81**, 041402 (2010).

[188] O. Vafek and K. Yang, Phys. Rev. B **81**, 041401 (2010).

[189] R. Nandkishore and L. Levitov, Phys. Rev. B **82**, 115124 (2010).

[190] S. Uebelacker and C. Honerkamp, Phys. Rev. B **84**, 205122 (2011).

[191] J. M. Murray and O. Vafek, Phys. Rev. B **89**, 201110 (2014).

[192] B. Dóra, I. F. Herbut, and R. Moessner, Phys. Rev. B **90**, 045310 (2014).

[193] A. M. Cook, C. Hickey, and A. Paramekanti, Phys. Rev. B **90**, 085145 (2014).

[194] Y. Hu, J. W. F. Venderbos, and C. L. Kane, Phys. Rev. Lett. **121**, 126601 (2018).

[195] D. Jérome, T. M. Rice, and W. Kohn, Phys. Rev. **158**, 462 (1967).

[196] F. Wang and Y. Ran, Phys. Rev. B **84**, 241103 (2011).

[197] Y.-F. Wang, H. Yao, C.-D. Gong, and D. N. Sheng, Phys. Rev. B **86**, 201101 (2012).

[198] S. Yang, Z.-C. Gu, K. Sun, and S. Das Sarma, Phys. Rev. B **86**, 241112 (2012).

[199] M. Trescher and E. J. Bergholtz, Phys. Rev. B **86**, 241111 (2012).

[200] S. Kourtis, Phys. Rev. B **97**, 085108 (2018).

[201] C. Nayak, Phys. Rev. B **62**, 4880 (2000).

[202] F. D. M. Haldane, Phys. Rev. Lett. **93**, 206602 (2004).

[203] N. Nagaosa, J. Sinova, S. Onoda, A. H. MacDonald, and N. P. Ong, Rev. Mod. Phys. **82**, 1539 (2010).

[204] J. Dubail and N. Read, Phys. Rev. B **92**, 205307 (2015).

[205] M. Barkeshli and X.-L. Qi, Phys. Rev. X **2**, 031013 (2012).

[206] R.-J. Slager, A. Mesaros, V. Juričić, and J. Zaanen, Nat. Phys. **9**, 98 (2012).

[207] M. Levin and A. Stern, Phys. Rev. Lett. **103**, 196803 (2009).

[208] A. Karch, J. Maciejko, and T. Takayanagi, Phys. Rev. D **82**, 126003 (2010).

[209] Y.-M. Lu and Y. Ran, Phys. Rev. B **85**, 165134 (2012).

[210] A. Chan, T. L. Hughes, S. Ryu, and E. Fradkin, Phys. Rev. B **87**, 085132 (2013).

[211] J. Maciejko and G. A. Fiete, Nature Physics **11**, 385 (2015).

[212] T. Neupert, L. Santos, S. Ryu, C. Chamon, and C. Mudry, Phys. Rev. B **84**, 165107 (2011).

[213] C. Repellin, B. A. Bernevig, and N. Regnault, Phys. Rev. B **90**, 245401 (2014).

[214] H. Shapourian and T. L. Hughes, Phys. Rev. B **93**, 075108 (2016).

[215] B.-J. Yang and N. Nagaosa, Nat. Commun. **5**, 4898 (2014).

[216] K. J. Thomas, J. T. Nicolls, Simmons M. Z. Simmons, *et al.*, Phys. Rev. Lett. **77**, 135 (1996).

[217] K. J. Thomas, J. T. Nicolls, Simmons N. J. Appleyard, *et al.*, Phys. Rev. B **58**, 4846 (1998).

[218] F. Bauer, J. Heyder, E. Schubert, *et al.*, Nature **501**, 73 (2013).

[219] Y. Tokura and A. Khaetskii, Physica E: Low-dimensional Systems and Nanostructures **12**, 711 (2002).

[220] Y. Meir, K. Hirose and N. S. Wingreen, Phys. Rev. Lett. **89**, 196802 (2002).

[221] K. Karen, L. A. Landau, E. Sela and L. Fu, Phys. Rev. B **96**, 205403 (2017).

[222] A. Friedman, R. Vasseur, A. Lamacraft and S. A. Parameswaran, arXiv:1901.02939 .

[223] M. Günaydin and F. Gürsey, Journal of Mathematical Physics **14**, 1651 (1973).